SANDIA REPORT

SAND2008-3111
Unlimited Release
Printed May 2008

West Pearl Queen CO_2 Sequestration Pilot Test and Modeling Project to 2006

Scott P. Cooper, Norman R. Warpinski, Rajesh J. Pawar, Bruce A. Stubbs, Robert D. Benson, Reid B. Grigg, Robert K. Svec, John C. Lorenz, Lewis C. Bartel, James L. Krumhansl, David F. Aldridge, David J. Holcomb, Carlos F. Jove-Colon, Charles Byrer, Andrea McNemar, Henry R. Westrich, Gregory J. Elbring

Prepared by
Sandia National Laboratories
Albuquerque, New Mexico 87185 and Livermore, California 94550

Sandia is a multiprogram laboratory operated by Sandia Corporation,
a Lockheed Martin Company, for the United States Department of Energy's
National Nuclear Security Administration under Contract DE-AC04-94AL85000.

Sandia National Laboratories

Issued by Sandia National Laboratories, operated for the United States Department of Energy by Sandia Corporation.

Printed in the United States of America. This report has been reproduced directly from the best available copy.

Available to DOE and DOE contractors from
U.S. Department of Energy
Office of Scientific and Technical Information
P.O. Box 62
Oak Ridge, TN 37831

Telephone:	(865) 576-8401
Facsimile:	(865) 576-5728
E-Mail:	reports@adonis.osti.gov
Online ordering:	http://www.osti.gov/bridge

Available to the public from
U.S. Department of Commerce
National Technical Information Service
5285 Port Royal Rd.
Springfield, VA 22161

Telephone:	(800) 553-6847
Facsimile:	(703) 605-6900
E-Mail:	orders@ntis.fedworld.gov
Online order:	http://www.ntis.gov/help/ordermethods.asp?loc=7-4-0#online

SAND2008-3111
Unlimited Release
Printed May 2008

West Pearl Queen CO_2 Sequestration Pilot Test and Modeling Project to 2007

Scott P. Cooper, Norman R. Warpinski, John C. Lorenz, Lewis C. Bartel, David F. Aldridge, James L. Krumhansl, David J. Holcomb, Carlos F. Jove-Colon, Gregory J. Elbring
Geoscience and Environment Center
Sandia National Laboratories
P.O. Box 5800
Albuquerque, New Mexico 87185

Robert D. Benson
Department of Geophysics
Colorado School of Mines
Golden Colorado, 80401-1887

Reid B. Grigg, Robert K. Svec
Petroleum Recovery Research Center
New Mexico Institute of Mining and Technology
Socorro, NM 87801

Rajesh J. Pawar
Earth and Environmental Sciences Division
Los Alamos National Laboratory
Los Alamos, NM 87545

Charles Byrer, Andrea McNemar
Fuel Resources Division
National Energy Laboratory
Morgantown, WV 26507

Bruce A. Stubbs
Pecos Petroleum Engineering, Inc.
Roswell, NM 88202

Abstract

The West Pearl Queen is a depleted oil reservoir that has produced approximately 250,000 bbl of oil since 1984. Production had slowed prior to CO_2 injection, but no previous secondary or tertiary recovery methods had been applied. The initial project involved reservoir characterization and field response to injection of CO_2; the field experiment consisted of injection, soak, and venting. For fifty days (December 20, 2002, to February 11, 2003) 2090 tons of CO_2 were injected into the Shattuck Sandstone Member of the Queen Formation at the West Pearl Queen site. This technical report highlights the test results of the numerous research participants and technical areas. The report discusses both pre- and post-test data at the West Pearl Queen site.

Acknowledgments

This work is sponsored by the U.S. Department of Energy, Office of Fossil Energy, with thanks to Charles Byrer and Andrea McNemar, contract managers for this project. The authors also thank Kinder Morgan for donating the CO_2 used for injection during the field test. The authors also gratefully acknowledge their home organizations and each other for their collaboration and support of this research (Sandia National Laboratories, Colorado School of Mines, Los Alamos National Laboratories, New Mexico Tech, Strata Production Company, and the National Energy Technology Laboratory). The authors thank Landmark Graphics Corporation and Hampson-Russell Software Services for the use of their software.

Contents

1.0 INTRODUCTION 11

2.0 GEOLOGIC ANALYSES 15
2.1 Core Studies 15
2.1.1 Previous Work 16
2.1.2 Stivason Federal #1 Core Description 19
2.1.3 Comparison with the Sulimar Queen #116 Slabbed Core 28
2.1.4 Conclusions from Core Analysis 30
2.1.5 Detailed Core Information 30
2.1.6 Acoustic Velocity Anisotropy of the Stivason #1 core 30
2.2 Shattuck Outcrop Studies 31
2.2.1 Fracture Descriptions 32
2.2.2 Fracturing in the Overlying, Reservoir-Seal Formation and Associated Strata 33
2.2.3 Conclusions from Outcrop Studies 34

3.0 GEOCHEMICAL STUDIES 53
3.1 Experimental Studies 53
3.2 Geochemical Modeling 54
3.3 Discussion of Results 56

4.0 PRE-INJECTION BOREHOLE GEOPHYSICS 61
4.1 Deviation Surveys 61
4.2 Dipole Sonic Logs 61
4.3 Crosswell Survey 61
4.4 Processing 61
4.5 Tomographic Inversion 63
4.6 Reflection Images 65

5.0 INJECTION TEST 77
5.1 Injection and Blowdown 77
5.2 Microseismic Monitoring 77
5.3 Final Build-Up 78

6.0 4D/9C SEISMIC ANALYSES 85
6.1 Design and Acquisition 85
6.2 Baseline Results 85
6.3 Comparison of Baseline and Post-Injection P-Wave Surveys 86

7.0 SUMMARY 97

8.0 REFERENCES 98

APPENDIX A 99

APPENDIX B 118

APPENDIX C 124

FIGURES

Figure 1.1. Location of Sequestration Project near Hobbs, NM. 13
Figure 1.2. Location of Strata West Pearl Queen Wells Relative to Sections and Structural Contours. 13
Figure 2.1. Entire core available for study from the Stivason Federal #1 Well. 15
Figure 2.2. Digital wire-line gamma ray log (black line) of the Stivason Federal #1 Well. 17
Figure 2.5. Photographs illustrating the thinly bedded nature of Lithology A. 20
Figure 2.6. Poorly sorted and fine grained sandstones of lithology A near the top of the reservoir (4500.5 ft depth) – ½ mm wide pencil point for scale. 21
Figure 2.7. Layer of silty mudstone surrounded by sandstones of lithology A that is probably a large-scale permeability barrier (core section 17A, 4549 ft depth). 21
Figure 2.8. The laminated to massive bedding character of lithology B (at a depth of 4507.1 ft – 4507.8 ft). 22
Figure 2.9. The massive and irregularly oil-stained nature of lithology C (core sections 4C, 4D, 4E, 4F, 4G, 4510.5 ft depth). 23
Figure 2.10. Portions of lithology C that are poorly cemented and friable —the rock disintegrates under minimum pressure. 24
Figure 2.11. Core interval with numerous areas of oil stain. 24
Figure 2.12. A heavily oil stained zone within lithology C near the 4513 ft mark. 25
Figure 2.13. Chart showing the three generalized lithologies present in the Stivason Federal #1 well core with depth, and correlated to permeability and porosity data provided by Core Labs and to the core gamma ray log. 26
Figure 2.14. An abrupt color change between core section 4J (lower right hand corner of photo A) and the adjacent sections suggests invasive testing may have altered this section. 27
Figure 2.15. Abrupt changes in oil staining are observed at bed boundaries. 27
Figure 2.16. Oil stain is confined to the area below a small bedding plane even though the grain size across this plane is essentially unchanged (core section 5D, 4512.8 ft depth). 28
Figure 2.17. Laminated carbonate lithologies within the Sulimar Queen #116 core. 29
Figure 2.18. White circles denote areas where fractures within the Sulimar Queen core terminate at bedding intervals that contain vugs (i.e., intervals with vuggy porosity). 29
Figure 2.19. Core box #1. 35
Figure 2.20. Core box #2. 36
Figure 2.21. Core box #3. 37
Figure 2.22. Core box #4. 38
Figure 2.23. Core box #5. 39
Figure 2.24. Core box #6. 40
Figure 2.25. Core box #7. 41
Figure 2.26. Core box #8. 42
Figure 2.27. Lithologic description of core. 43
Figure 2.28. Lithologic description of core. 44
Figure 2.29. Lithologic description of core. 45
Figure 2.30. Lithologic description of core. 46
Figure 2.31. Lithologic description of core. 47
Figure 2.32. Lithologic description of core. 48
Figure 2.33. Fracture strikes in theupper Shattuck sandstone along County Route 540: n = 25, ring = 15%. 49

Figure 2.34. Fracture strikes in outcrops of the lower Shattuck Sandstone along County Route 540: n = 22, ring = 15%. 49
Figure 2.35. Fracture strikes within the Shattuck Sandstone, Rocky Arroyo roadcut: n =25, ring = 10%. Bed thickness 1.2 m. 49
Figure 2.36. Fracture strikes in the Shattuck Sandstone, Rocky Arroyo riverbed: n = 10, ring = 25%. 50
Figure 2.37. Fracture strikes in the unnamed sandstone below the Queen Dolomite, Rocky Arroyo: n = 20, ring = 15%. 50
Figure 2.38. High angle, bed-normal fractures near Sitting Bull Falls, sandstone tongue of the Cherry Canyon Fm: n = 21, ring = 45%. 51
Figure 2.39. Fracture strikes in the Queen Dolomite (immediately underlying the Shattuck Sandstone Member), Rocky Arroyo: n = 22, Ring = 15%. 51
Figure 2.40. Map-view presentation of natural fracture spacings in the Shattuck Sandstone at the bottom of Rocky Arroyo (same outcrop as Figure 4). 51
Figure 2.41. Fractured carbonate beds of the Seven Rivers Fm, overlying the Shattuck Sandstone Member of the Queen Fm. 52
Figure 2.42. Natural fractures near Sitting Bull Falls have vertical extents in the tens of meters range within sandstones of the Cherry Canyon Fm (scale is approximate). 52
Figure 3.1. Left (a) – Pre-test sample not exposed to CO_2. Right (b) – Appearance after being exposed to 700 psi CO_2 for 6.5 months. 58
Figure 3.2. Left (a) – 6.5 months CO_2 exposure, Note high-Mg carbonate crystal at top of the picture and incipient clay growth on the edge of the grain. Right (b) – Well developed clays formedafter 19 months exposure to 700 psi CO_2. 58
Figure 3.3. Left (a) – Etched plagioclase grain formed after 19 months exposure to 700 psi CO_2. Right (b) – Post-test sample from flow-through experiment. 59
Figure 3.5. Impact of reacting CO_2 with Pearl Queen brine plus minerals. 60
Figure 3.6. Effect of reacting CO_2 with Pearl Queen brine plus minerals while suppressing the appearance of all clays. 60
Figure 4.1. Trajectories of wells 4 and 5 from deviation survey. 66
Figure 4.2. Variation of well separation with depth. 66
Figure 4.3. Deviation trajectory of well #4. 67
Figure 4.4. Deviation trajectory of well #5. 67
Figure 4.5. Dipole sonic log velocities for well #4. 68
Figure 4.6. Dipole sonic log velocities for well #5. 68
Figure 4.7. Geometry of sources and receivers for crosswell survey. 69
Figure 4.8. Unprocessed traces from 4697-ft common receiver gather. 70
Figure 4.9. Traces from 4697-ft common receiver gather after signal processing. 70
Figure 4.10. Enlarged view of the vertical component of the 4697-ft common receiver gather. 71
Figure 4.11. Up-going P-wave reflections from the 4415 common-shot gather. 71
Figure 4.12. Down-going P-wave reflections from 4415 common shot gather. 72
Figure 4.13. Up-going shear wave reflections from the 4415 common shot gather. 72
Figure 4.14. Down-going shear wave reflections from the 4415 common shot gather. 73
Figure 4.15. Tomogram of P wave (center) and derived and measured log velocities. 73
Figure 4.16. Tomogram of S wave (center) and derived and measured log velocities (sides) for pre-injection crosswell survey between wells #4 and #5. 74
Figure 4.17. Reflection image for P waves constructed from crosswell survey data (center) and compared with synthetic reflection images at the wells (sides). 74
Figure 4.18. Reflection image for S waves constructed from crosswell survey data (center) and compared with synthetic reflection images at the wells (sides). 75
Figure 5.1. CO_2 injection history for West Pearl Queen reservoir. 78

Figure 5.2. Pressure bleed off after injection in days since shut-in. 79
Figure 5.3. Bottom-hole pressure drop during initial part of blow down. 79
Figure 5.4. Bottom-hole temperature during initial part of blow down 80
Figure 5.5. CO_2 flow rate during blow down. 80
Figure 5.6. Horner plot of soak pressure decay. 81
Figure 5.7. Waveforms of tube-wave generating event located near bottom of array. 81
Figure 5.8. Waveforms of tube-wave generating event located near center of array 82
Figure 5.9. Location of origin of tube-wave generating events as a function of time. 83
Figure 5.10. Pressure buildup after ~1.5 years of production. 83
Figure 5.11. Horner plot of final pressure build up 84
Figure 6.1. Aerial coverage for 4D, 9C seismic survey. 87
Figure 6.2. Operational parameters for 4D, 9C seismic survey. 87
Figure 6.3. Source and receiver points for 4D, 9C seismic survey. 88
Figure 6.4. Fold coverage for 4D, 9C seismic survey. 88
Figure 6.5. Site with acquisition trucks at left. 89
Figure 6.6. Industrial Vehicles TRI-AX source truck. 89
Figure 6.7. Input/Output Sidewinder source truck. 89
Figure 6.8. Close-up of TRI-AX hydraulic foot. 90
Figure 6.9. Observed reflections on east-west line through the Stivason #4 Well – P wave. 90
Figure 6.10. Time structure map on Queen Sandstone – P wave. 91
Figure 6.11. Depth structure map on Queen Sandstone – P wave. 91
Figure 6.12. Observed reflections on east-west line through the Stivason #4 well – S wave. 92
Figure 6.13. Comparison of east-west, P-wave, reflection traverses for matched and unmatched data. 92
Figure 6.14. RMS reflection amplitude for baseline survey – P wave. 93
Figure 6.15. RMS reflection amplitude for monitor survey – P wave. 93
Figure 6.16. RMS reflection amplitude differences – P wave. 94
Figure 6.17. RMS reflection amplitude differences – P wave – along with depth structure contours and assume CO_2 plume. 94
Figure 6.18. Comparison of the reflection amplitudes for unmatched traverses of the S1 waves 95
Figure 6.19. Comparison of the reflection amplitudes for unmatched traverses of the S2 waves 95
Figure 6.20. Baseline RMS amplitude plot for S1 waves 96

TABLES

Table 1.1. Characteristics of West Pearl Queen Reservoir 12
Table 3.1. Pre- and post-test brine chemistry 57
Table 3.2. Comparison of activity coefficients from REACT and EQ3/6 using a Pitzer database: 57
EQ3/6 (top) and REACT (bottom) 57
Table 4.1. Differential deviation-survey data 65

NOMENCLATURE

bbl	Barrels
EDS	Energy Dispersive Spectrometer
EOR	Enhanced Oil Recovery
Fm	Formation
FY	Fiscal Year
HT/HP	High Temperature/High Pressure
LANL	Los Alamos National Laboratory
PRRC	Petroleum Research and Recovery Center
psi	Pounds per Square Inch
SEM	Scanning Electron Microscopy
SNL	Sandia National Laboratories

1.0 INTRODUCTION

Because anthropogenic release of carbon dioxide (CO_2) may cause atmospheric concentrations of this gas to reach levels that are unaccommodating to certain facets of current human civilization, it is prudent to investigate methods for capturing, separating, and sequestering large volumes of CO_2 The strategy of injecting the gas into geologic formations is currently the most direct method for preventing escape of CO_2 into the atmosphere while also avoiding potential deleterious effects of other sequestration schemes. Although saline reservoirs, coalbed methane deposits, depleted gas reservoirs, and several other potential reservoirs are available, depleted oil reservoirs are especially attractive because of economic, infra-structure, and site-characterization advantages. Specifically, many wells have already been drilled in these fields, and CO_2 pipelines may be in place for use in ongoing enhanced oil recovery projects. The economics can be improved considerably if the CO_2 is simultaneously used for oil production enhancement and sequestration. It is also likely that the reservoirs and the CO_2/rock/reservoir interactions in these reservoirs have been studied. Evaluating the differing economics of a working field versus a start from scratch site could be a future area of study.

Nevertheless, because long-term effects of CO_2 injection are not well understood, a regulatory apparatus needs to be developed (using concrete technological guidelines), safety issues must be addressed, and overall economics of such projects need to be better characterized. Thus, it is necessary that specific projects be undertaken to examine some of these issues in an environment that is conducive to such studies, rather than in typical enhanced-oil-recovery tests where projects are driven by oil production factors. This sequestration project is one such test to evaluate sequestration phenomena without the need to adhere to production related schedules, economics, or other direct business factors.

As indicated above, the objective of this project is to provide important elements of the science and technology base to properly evaluate the safety and efficacy of long-term CO_2 sequestration in a depleted oil reservoir in particular and in any geologic reservoir in general. Understanding the sequestration mechanisms (trapping, solubility, or mineralization) and associated reservoir processes (diffusion, fingering, gravity separation, miscibility, reaction kinetics and others) is an ultimate goal of such studies, although a complete assessment will eventually require a number of test programs to assess different geologic settings. In this project, a pilot field-injection experiment is combined with computer simulations of the expected and measured results and laboratory evaluations of the fluid flow and reaction behavior. The ultimate goal of the project is to predict the migration and interactions of the multi-phase fluids, to assess the ability of geophysical techniques to monitor the process, and to determine the reservoir reactions driven by the CO_2 injection.

The West Pearl Queen Field, which is owned and operated by Strata Production Company, of Roswell, NM, was chosen as the field demonstration site. It is located near the town of Hobbs, NM, as shown in the map in Figure 1.1, in the Delaware Basin amid myriad oil fields and the associated infrastructure for drilling and producing hydrocarbons. The field was first developed in 1984, producing about 250,000 barrels of oil, but production slowed in recent years as reservoir pressures dropped. No secondary or tertiary recovery operations have been applied in the field, although both secondary and tertiary recoveries are common in the area.

A site map, with structural contours, is shown in Figure 1.2. The field is primarily located in sections 27, 28, and 33 of T19S, R34W. The Stivason Federal #4 is the injection well, while the Stivason Federal #5 is available for monitoring and for crosswell surveys (Figure 1.2). At this time, the Stivason Federal #5 is the only producing well in the field. Wells 1 and 3 are currently used for water injection into numerous zones, and well 2 has been plugged and abandoned. General characteristics of the reservoir sandstones are given in Table 1.1. The geologic analysis section (section 2 of this report) indicates that there are heterogeneities within the sandstone facies and interbedded units of the Shattuck Sandstone Member that are not necessarily captured in the generalized table provide in Table 1.1.

The field demonstration project was comprised of three phases, including (I) pre-injection baseline characterization of reservoir characteristics, (II) CO_2 injection and soaking, and (III) post-injection reservoir characterization. Phase I consisted of the development of a geologic model for the depleted reservoir, assembly of historical well-production behavior, calculation of the expected behavior of the CO_2 plume for typical injection conditions, well preparation, acquisition of legal permits, collection of reservoir fluids and core samples, and acquisition and processing of baseline geophysical surveys.

Phase II consisted of the design of a field injection test, preparation of the surface facilities, refinement of the computer simulation models, injection of 209 tons of CO_2 over a nearly two month period, and geophysical surveys of the plume.

Phase III of the project included wellhead venting of the injected CO_2 sampling of reservoir fluids, final geophysical surveys, and modeling and assessment of the reservoir behavior in response to injection of CO_2.

In summary, for fifty days (December 20, 2002, to February 11, 2003), 2090 tons of CO_2 were injected into the Shattuck Sandstone Member of the Queen Formation at the West Pearl Queen site. The injection rate was 40 tons per day, significantly lower than the 100 tons/day expected from pre-injection characterization. Early during injection, the surface injection pressure reached 1400 psi and thus the calculated bottom-hole constraint of 2900 psi. This pressure was kept constant for the remainder of the experiment. At the end of the injection phase, the injection well was shut in, and the CO_2 soaked for six months. Before venting, a post injection 3-D seismic survey was acquired. The injection well was then connected to a separator and allowed to vent. The well flowed freely for nine days, after which it stopped flowing and a pump was installed. After three months, only 17% of the total injected CO_2 was recovered, and 43% was recovered after two years. Pre- and post-injection production of oil and water proved to be very similar. It was nearly three years before CO_2 was produced in the nearest production well (Pawar et al., 2006, included as Appendix A). Appendix A is a copy of a journal article (Pawar, et al., 2006) highlighting the summary achievements and potential areas for future study. Appendices B and C are additional papers published during this project.

Table 1.1. Characteristics of West Pearl Queen Reservoir

Depth	4508 – 4531 ft
Thickness	23 ft
Permeability	5–30 md
Porosity	18%
Oil Gravity	30° API @ 150° F
Rock Composition	65% Quartz
	25% Feldspar
	5% Clay
	5% Carbonate Cement
Total Production	250,000 bbls oil

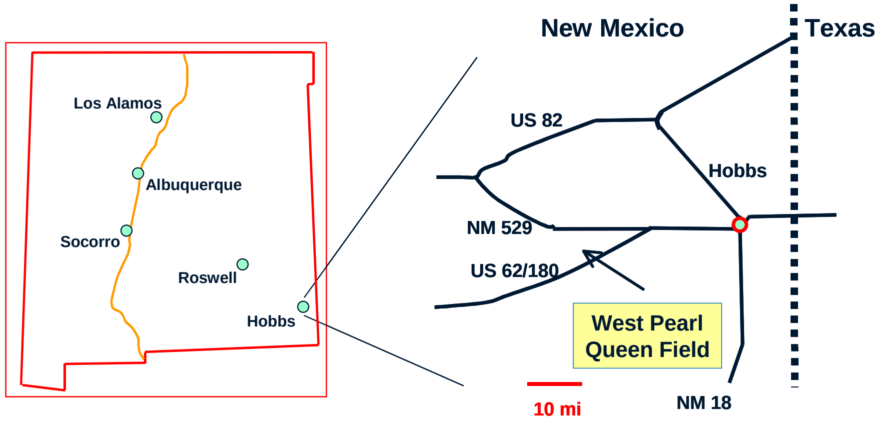

Figure 1.1. Location of Sequestration Project near Hobbs, NM.

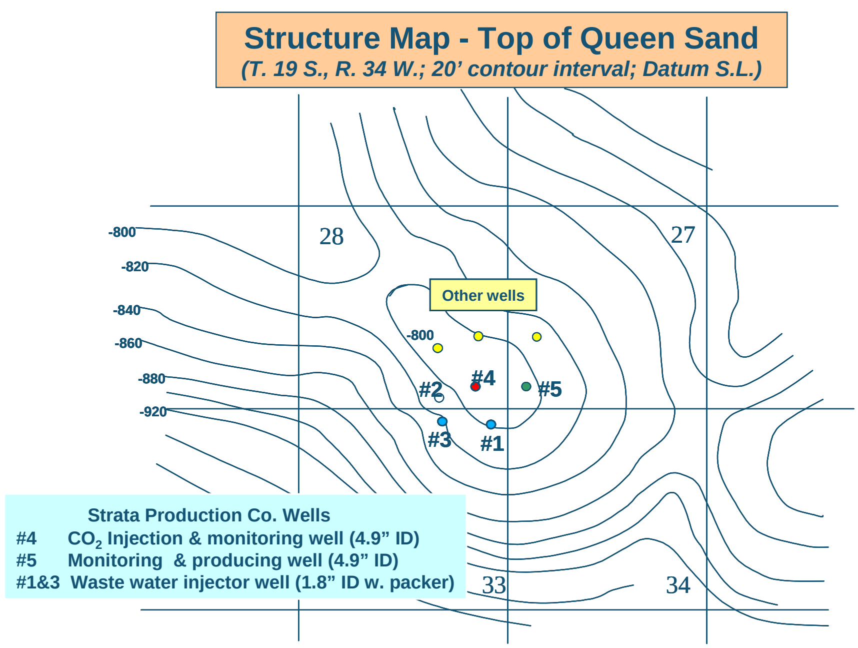

Figure 1.2. Location of Strata West Pearl Queen Wells Relative to Sections and Structural Contours.

2.0 GEOLOGIC ANALYSES

During the early phases of this project, data were available from two physical sources (core and outcrop) for an initial reservoir characterization. This section details these data and interpretations.

2.1 CORE STUDIES

The core consisted of approximately 30 ft of predominately unslabbed, discontinuous, four-inch-diameter core from the Queen Formation in the Stivason Federal #1 Well (Figure 2.1) and 24 ft of slabbed core from the Sulimar Queen Field. This core had been used as a teaching sample at Marietta College and was located and recovered for the project by Reid Grigg. Both cores were examined at the Petroleum Research and Recovery Center (PRRC) at the New Mexico Institute of Mining and Technology in Socorro, New Mexico on October 19 and 20, 2003.

The surface of the core was thoroughly cleaned and logged in detail. The core was in relatively good shape, although numerous short (1/2 in. to 2 in.) pieces had apparently been removed for testing by the operating company during the original core program. The porosities and permeabilities reported in the associated Core Labs report came from the short missing intervals. Two coring-induced petal fractures were observed at 4510.7 ft and 4512 ft. No natural fractures are present in this core, although this absence in the small sampling represented by the core does not preclude fracturing in the reservoir.

A B

Figure 2.1. The entire core available for study from the Stivason Federal #1 Well. A) Core boxes 1 to 5 (boxes are 3 ft long for scale). B) Core boxes 11, 17, and 18. Green arrows on core indicate uphole direction. Therefore, the numbering system (explained further in Figure 2.4) is “upside down” to maintain a convention in which the direction “uphole” is to the top of the page.

2.1.1 Previous Work

Mazzullo et al. (1991) described cores from the Central Corbin Queen Field, located approximately 10 miles to the northwest of the West Pearl Queen Field and the South Caprock Queen Field, which is approximately 20 miles to the northwest of the West Pearl Queen Field.

Mazzullo et al. (1991: pp. 943 and 944) describe the Shattuck Sandstone Member (used as the injection horizon for this experiment) as follows:

> …largely composed of fine to very fine sandstone, silty sandstone, and siltstone, but it also contains some silty mudstone, medium to coarse sandstone, detrital clay, and anhydrite. The fine and very fine quartz sand grains are angular to subangular, but the medium and coarse sand grains are well-rounded. The sandstones and siltstones are arkosic to subarkosic in their detrital composition, and they are cemented by anhydrite and dolomite, and traces of hematite, secondary quartz, feldspar, halite, and corrensite (mixed-layer smectite-chlorite clay). The silty mudstone is largely composed of quartz, feldspar, and smectite-illite clay, but it also contains traces of either hematite or carbonaceous debris. The detrital clay is primarily composed of poorly crystallized mixed-layer smectite-illite, but it is stained reddish-brown by trace amounts of hematite and other iron oxides.

In general, Shattuck sandstones consist of a heterogeneous mix of oxidized detrital sands, with detrital and authigenic cements (Mazzullo et al., 1991). The cementing materials in the Shattuck consist of interstitial dolomite, gypsum, anhydrite, and halite. The dolomite cement is typically porous and permeable, but the other mineral phases, more common on the flanks of most reservoirs, occlude porosity and permeability. Nonreservoir strata contain more pore-lining illite and chlorite, as well as illite/smectite and anhydrite cements.

Mineralogical changes caused by CO_2 injection into these heterogeneous strata were probable to occur in the cementing mineral phases, most likely in the carbonates and sulfates. The heterogeneity of the cements suggested that a thorough base-line characterization prior to injection was necessary to fully understand and document any changes caused by injection. The typically arkosic to sub-arkosic Shattuck sand composition indicates the Shattuck Sandstone Member sands may consist of 15 to 25% feldspar. Although this effect is minimal in logs from the West Pearl Queen, a high content of potassium-bearing feldspar sand grains in the Shattuck locally caused higher than normal gamma-ray counts and thus deflection of gamma-ray log profiles to the right relative to the interbedded carbonates and evaporites. Figure 2.2 compares gamma ray logs for the core and a digital version of the wireline log for the Stivason Federal #1 Well. There is an apparent depth shift of approximately 5 ft between the logs; this is attributed to depth measurement differences between the wireline run and the coring run.

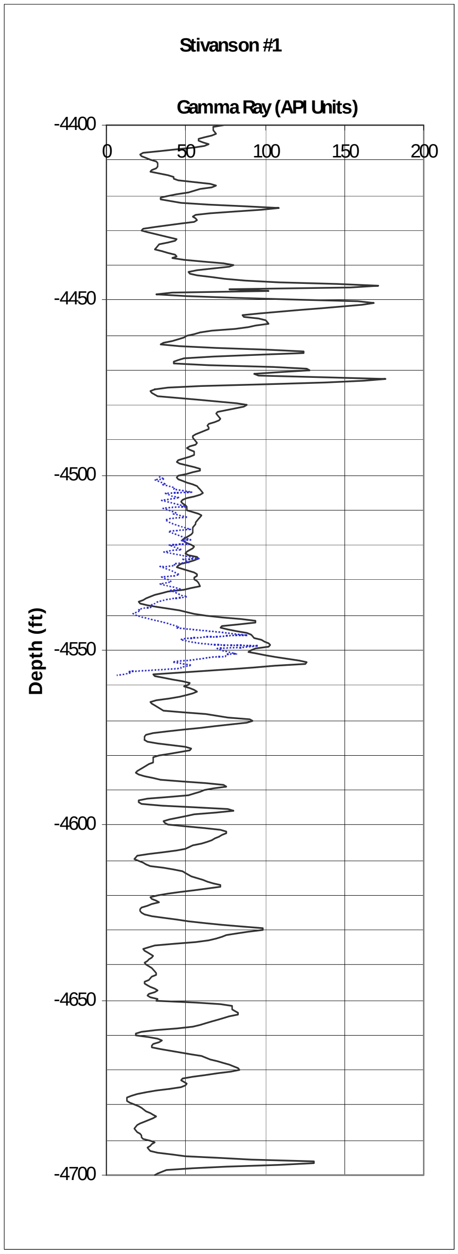

Figure 2.2. Digital wire-line gamma ray log (black line) of the Stivason Federal #1 Well and gamma ray log from the core (blue line).

Main reservoir facies: The Shattuck Sandstone Member interval is a generally laterally continuous and tabular interval of relatively constant thickness across a reservoir, having sharp upper and lower contacts with the over and underlying strata. Strata within the Shattuck Sandstone Member were described by Mazzullo et al. (1991) as consisting of three dominant facies.

Facies 1 consists of deposits related to deposition of a fluvial sandflat. This facies can be subdivided in subfacies recognized as sheetfloods (1A), channel deposits (1B), or river mouth deposits (1C). Subfacies 1A is composed of ripple cross-bedded fine to very fine-grained sandstones, wavy and planar laminated siltstone, silty mudstone, and detrital clay. Subfacies 1B is composed of cross-bedded medium to very fine-grained sandstone, and planar laminated fine to very fine-grained sandstone. Subfacies 1C is composed of planar and wavy laminated siltstone with silty mudstone drapes.

Facies 2 is made up of eolian sandsheet deposits. This facies is composed of cross-bedded to planar laminated fine to very fine-grained sandstone and thin course to medium grained sandstone laminae.

Facies 3 consists of clastic dominated sabkha deposits. This facies contains deformed wavy and planar laminated sandstones and siltstones with silty mudstone drapes and detrital clay. Microfolds and fluid escape structures are also observed within this subfacies, as are evaporite nodules. Although the relative percentages of these three facies vary from location to location, the basic Shattuck Sandstone interval consists of irregularly bedded sandstones, siltstones, and sandy siltstones, containing irregular anhydrite beds and nodules. Gasses injected into such a formation were likely gather preferentially in the cleaner (and therefore higher porosity) Facies 2. It should also be noted that the limited volumes available in this facies could fill quickly during flooding.

<u>Reservoir-bounding strata</u>: The Shattuck sandstones are underlain and overlain by heterogeneous, shallow-marine strata of the Queen Formation and the Seven Rivers Formation respectively (Figure 2.3). Mazzullo et al. (1991) indicate that there are two additional facies within these bounding beds.

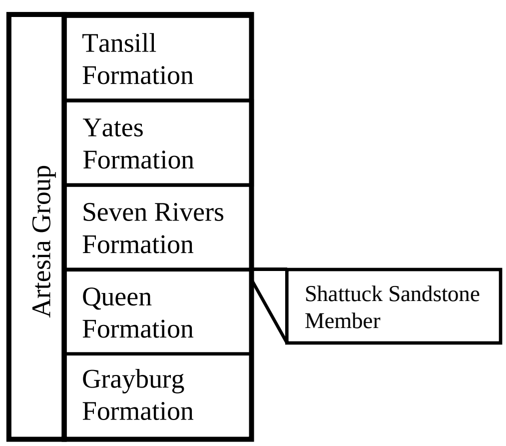

Figure 2.3. Stratigraphic positions of the formations within the Permian (Guadalupian) age Artesia Group. The Shattuck Sandstone Member of the Queen Formation is highlighted.

Facies 4 consists of intertidal and subtidal deposits of a shelf-interior lagoon. This facies is composed of interbedded dolomicrites, dolomitic siltstones, anhydrites, and arkosic silty mudstones.

Facies 5 consists of deposits of a coastal sabka along the edge of a shelf-interior lagoon. This facies is composed of anhydrite beds, deformed silty sandstones, and very fine-grained sandstones with detrital clay coatings.

The bounding units (Queen Formation and Seven Rivers Formation) of the Shattuck Sandstone consist of dolomicrites, bedded to nodular anhydrites, carbonates, arkosic sandstones, and siltstones. Clean, ductile, clay-rich shales have not been reported. Obtaining absolute containment of CO_2 injections within such strata, even if injected at pressures below the fracture gradient, could be difficult.

Underlying the Queen Formation is the Grayburg Fm. The Grayburg Fm is primarily composed of dolomite, anhydrite, and sandstone and is 360 feet thick within Federal Bogle Well No. 1 (Sec. 30 T16S R30E; Tait et al., 1962). The contact between the two formations is somewhat arbitrary with Queen Fm generally considered to contain more sandstones relative to the Grayburg Fm (Hayes and Koogle, 1958). Within the same well the overlying Queen Fm is 420 feet thick.

Any CO_2 escaping from the Queen Fm would tend to migrate upward through the overlying formations. These formations are the Seven River Rivers, Yates, and Tansill. The contact between the Queen Fm and the Seven Rivers Fm is conformable and is traced at the top of the Shattuck Sandstone. The Seven Rivers Fm is composed essentially of anhydrite and dolomite with thin interbeds of shale, siltstone, and sandstone and is 565 feet thick.

The Yates Fm conformably overlies the Seven Rivers Fm. The Yates Fm consists of interbedded siltstone, sandstone, dolomite, and limestone and is 261 feet thick. The Yates Fm contains more sandstones and siltstones than the underlying Seven Rivers Fm and the overlying Tansill Fm.

Conformably overlying the Yates Fm is the Tansill Fm. Tait et al. (1962) describe this unit as composed primarily of anhydrite and split by a thin siltstone member. Thickness of the Tansill as measured within the Federal Bogle Well No. 1 by Tait et al. (1962) is 105 ft. Hayes and Koogle (1958) describe the Tansill as a fine-grained to pisolitic (at specific locations) dolomite, with rare sandstone and siltstone beds.

2.1.2 Stivason Federal #1 Core Description

The core is comprised of three basic lithologies. These grade into one another and are mixed together locally, but can be generalized into the distribution shown in Figure 2.4. Two coring induced petal fractures were observed within the core. One petal fracture at 4510.7 ft depth, the second at 4511.9 ft.

Lithology A (Mazzullo et al. facies 1) consists of thinly bedded to laminated alternations of gray siltstone and light-gray, very fine-grained sandstone (Figures 2.5, 2.6). It is generally well cemented, probably with dolomitic cement, and is poorly to moderately sorted. This facies has very poor reservoir potential, with relatively low porosities and permeabilities, and probably acts as both an impedance to vertical permeability between the better reservoir lithologies and as a confining layer at the top of the reservoir. Silty mudstones to siltstones within this facies may be significant permeability barriers (Figure 2.7).

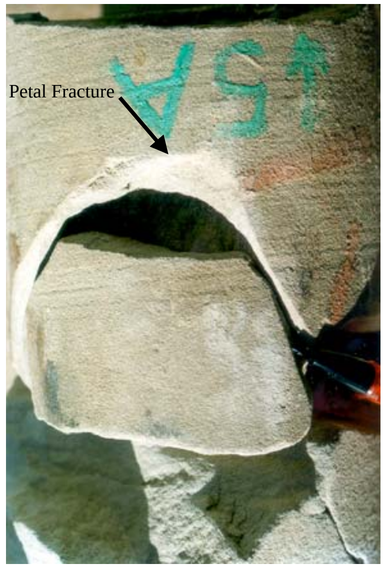

Figure 2.4. Coring induced petal fracture within lithology C at a depth of 4512 ft. Blue/Green arrow points uphole; Blue/Green label indicates box number (5) and relative position of that piece of core in that box (A – first section of core). All the boxes of core were labeled using this convention prior to examination. For photographs in this report, up is toward the top of each page/photograph.

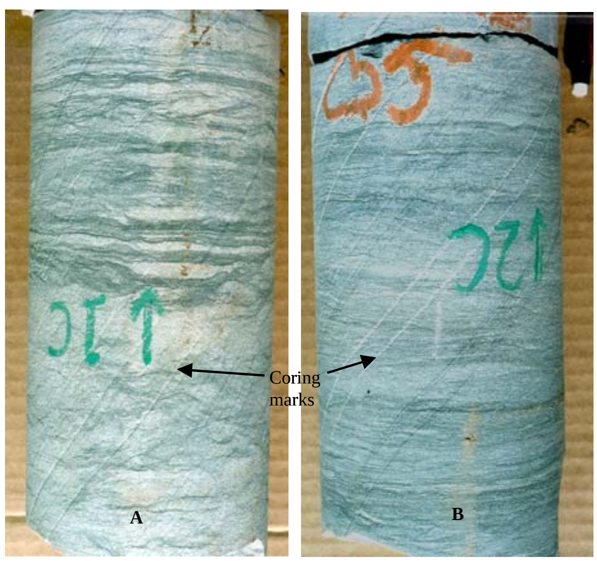

Figure 2.5. Photographs illustrating the thinly bedded nature of Lithology A. A) Note the change in bedding at the center of section 1C near the tip of the green arrow; this illustrates the sometimes abrupt transition between lithology A (upper half) and lithology B (lower half). B) Illustrates a change in gray siltstone laminae from the "wispy" bedding in A to a more planar style of bedding. Spiral coring induced marks or grooves are observed on both sections of core.

Figure 2.6. Poorly sorted and fine grained sandstones of lithology A near the top of the reservoir (4500.5 ft depth) – ½ mm wide pencil point for scale.

Figure 2.7. Layer of silty mudstone surrounded by sandstones of lithology A that is probably a large-scale permeability barrier (core section 17A, 4549 ft depth).

Lithology B (Mazzullo et al. facies 1) consists of laminated to massive very fine-grained, light-gray sandstones (Figure 2.8). They are well sorted and well cemented. This does not appear to be a reservoir facies but should have a generally intermediate range of porosities and permeabilities.

Much of the missing core (indicated by blanks on the accompanying core description figures (i.e. Figures 2.27 - 2.32), especially that interval with reported low measured permeabilities and porosities between the two main pay zones, probably consists of lithologies A and B.

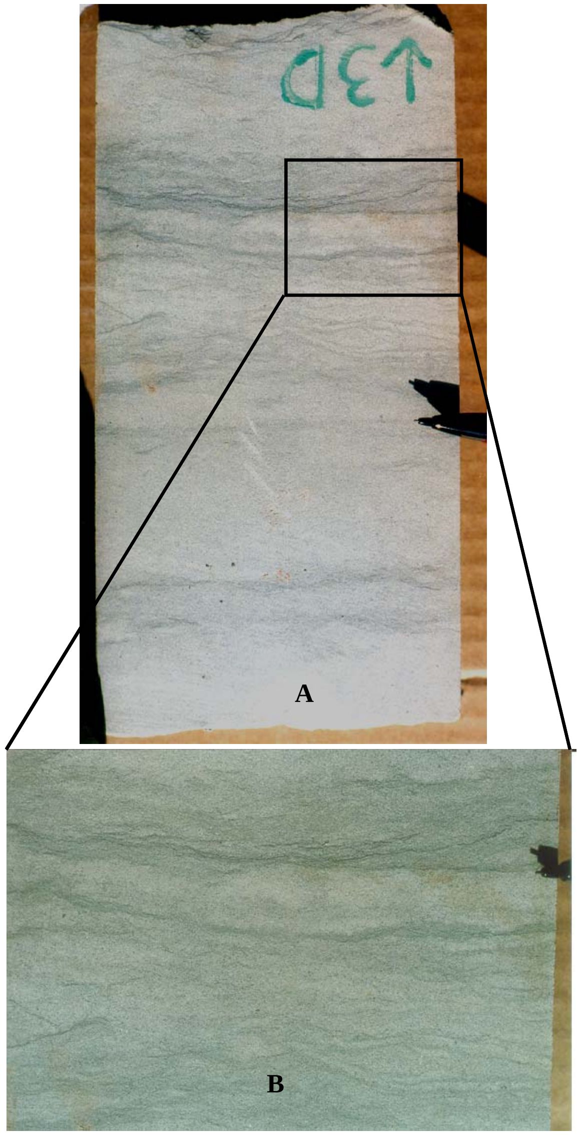

Figure 2.8. The laminated to massive bedding character of lithology B (at a depth of 4507.1 ft – 4507.8 ft). A) Changes from wispy laminae (top of core section 3D) to more massive sandstone near the base. B) Enlarged view of laminae within the boxed area of A.

Lithology C (Mazzullo et al. facies 2) is the main reservoir facies, and 9 feet of the available core consist of this facies. It is a crossbedded to apparently massive moderately to well sorted, fine to very fine grained, oil-stained sandstone (Figure 2.9). The oil staining varies from light to very dark brown, apparently as a function of the changes in cementation and related porosity, and much of this facies is relatively friable because of poor cementation (Figure 2.10).

However, a 1-ft-thick zone with heavy dark brown oil staining, which occurs at about 4513 ft (Figures 2.11, 2.12) and is noted as a short rightward extension on the lithology column (Figure 2.13), is within a nonfriable interval of sandstone. Invasive testing may have altered another heavily stained section of core at about 4511.5 ft (Figure 2.14), as suggested by holding the core upside down and looking directly at the base. In this orientation, a color change (light to dark) is observed from the center of the core to the rim, indicating either surficial invasion around the circumference of the core, or, more likely, flushing of the central regions of the core by a whole-core vertical permeability test. A plug taken from this core or slabbing of the core would help to indicate whether invasion or flushing have in fact occurred.

Lithology C typically has relatively high porosities, between 15% and 20%, but it has inconsistent permeabilities. Oil staining suggests high porosities, and as a result, zones consisting of this lithology will be the primary hosts for injected CO_2 as long as fracture break-down pressure is not exceeded during injection. Abrupt changes in oil stain are primarily observed at small-scale bed boundaries (Figures 2.15, 2.16). The variability in oil staining and measured permeability shown by this lithology suggests that some of the residual oil may be difficult to displace during CO_2 injection.

Figure 2.9. The massive and irregularly oil-stained nature of lithology C (core sections 4C, 4D, 4E, 4F, 4G, 4510.5 ft depth).

Figure 2.10. Portions of lithology C that are poorly cemented and friable—the rock disintegrates under minimum pressure.

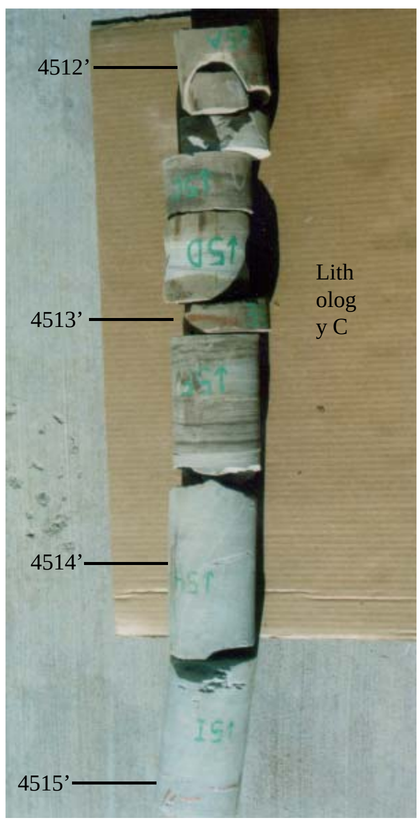

Figure 2.11. Core interval with numerous areas of oil stain. The sandstones are well cemented near the base of this core section. Core near the 4513 ft mark is also well cemented yet highly oil stained.

This is not typically the case regarding oil staining within lithology C (i.e., most oil stain occurs in friable zones).

Figure 2.12. A heavily oil stained zone within lithology C near the 4513 ft mark. Enlarged photograph illustrates the bedding-parallel nature of the heaviest oil stain. This area is on the “backside” of core section 5F.

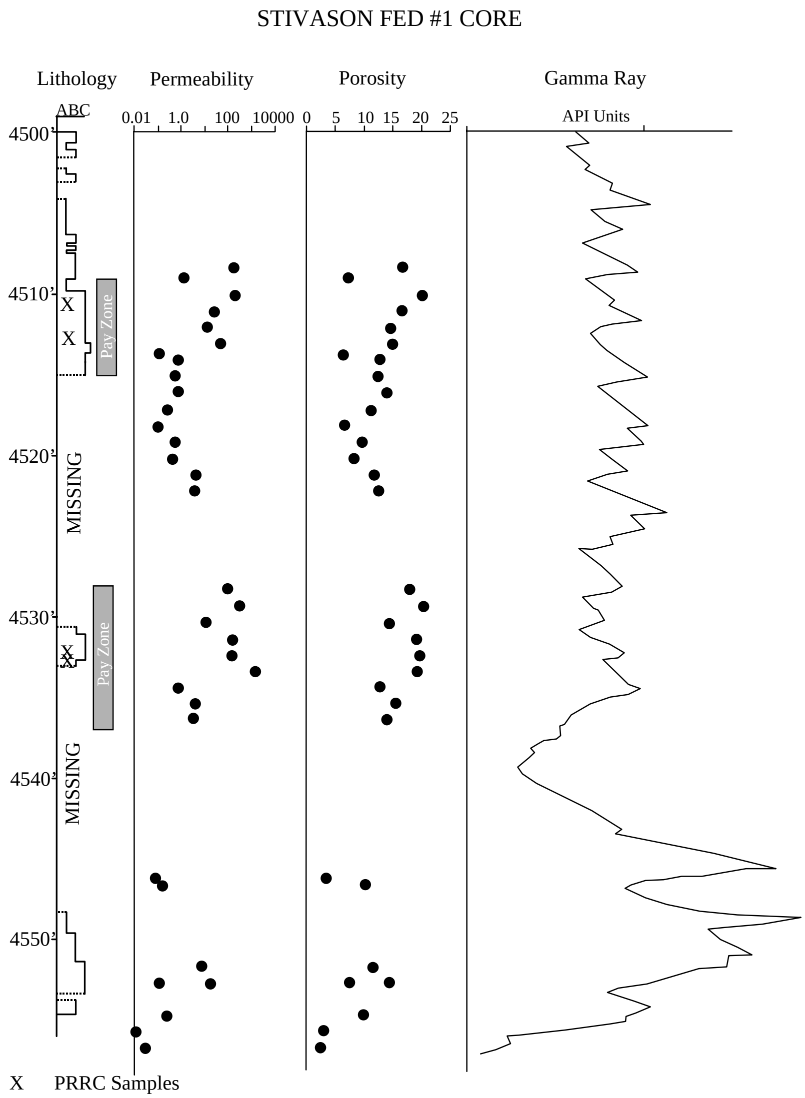

Figure 2.13. Chart showing the three generalized lithologies present in the Stivason Federal #1 well core with depth, and correlated to permeability and porosity data provided by Core Labs and to the core gamma ray log.

A B

Figure 2.14. An abrupt color change between core section 4J (lower right hand corner of photo A) and the adjacent sections suggests invasive testing may have altered this section. B) Enlargement of core section 4J.

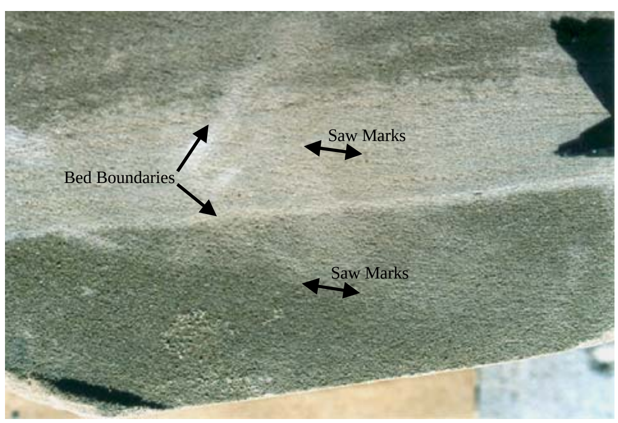

Figure 2.15. Abrupt changes in oil staining are observed at bed boundaries. Diagonal lines (from upper left to lower right) are saw marks.

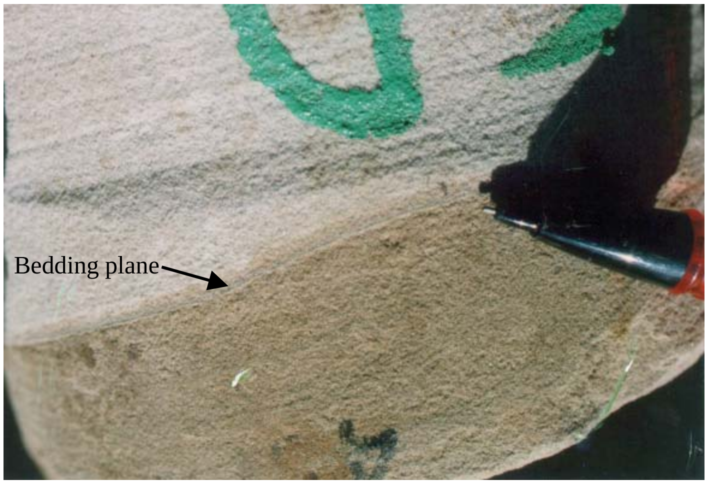

Figure 2.16. Oil stain is confined to the area below a small bedding plane even though the grain size across this plane is essentially unchanged (core section 5D, 4512.8 ft depth).

2.1.3 Comparison with the Sulimar Queen #116 Slabbed Core

Twenty-four feet of core slabs from the Sulimar Queen #116 were also examined in Socorro. This core comes from a field several tens of miles west of our field and would not appear to be a good analog for the West Pearl Queen lithologies. Based on this core, strata in the Sulimar Queen have a much higher percentage of laminated carbonate lithologies, some of which contain short but pervasive, vertical natural fractures (Figure 2.17). Many vertical extension fractures terminate at carbonate beds that contain significant vugs and associated vuggy porosity (Figure 2.18). Similar limited, laminated carbonates may occur within the missing core intervals of Stivason Federal #1, as suggested by the Core Labs report that lists dolomite as the dominant lithology for some of the missing intervals, specifically from 4545.6 to 4547 ft and 4555 to 4557 ft. Lithologies similar to B and C described above are present in the rest of the Sulimar core.

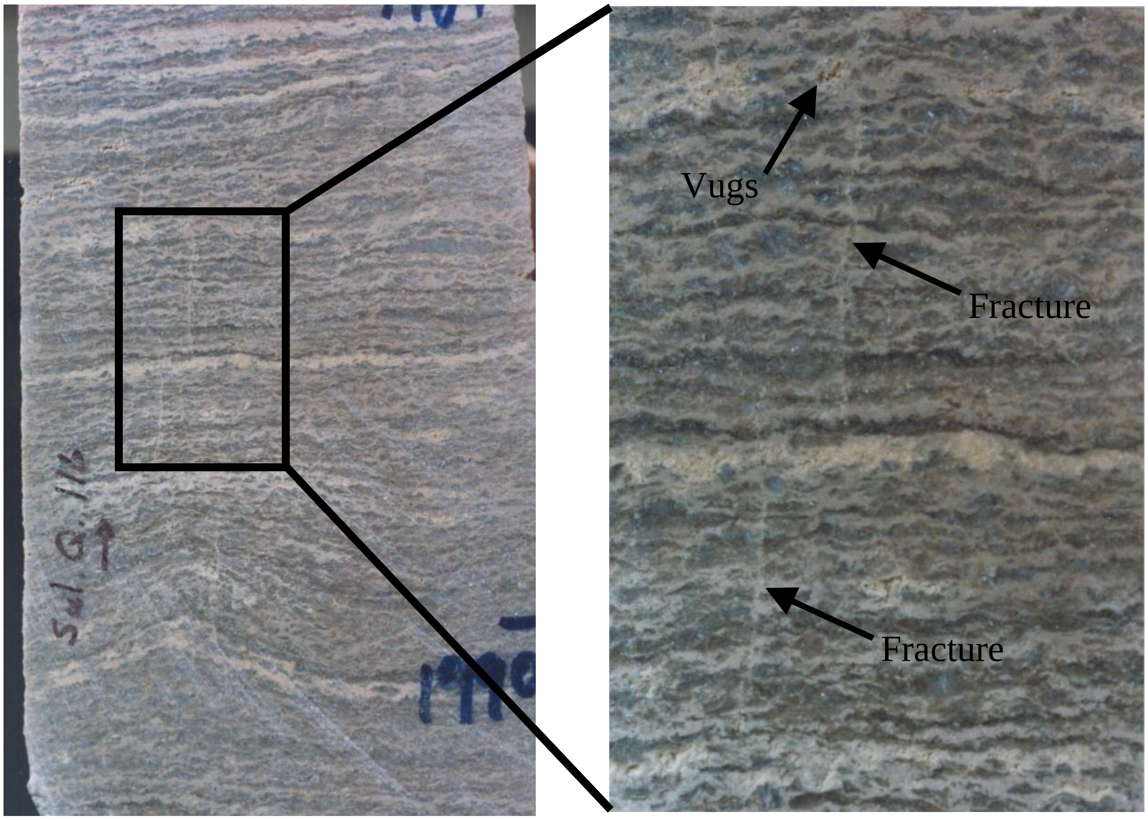

Figure 2.17. Laminated carbonate lithologies within the Sulimar Queen #116 core. Note the numerous short, vertical natural fractures and the vugs associated with bedding planes.

Figure 2.18. White circles denote areas where fractures within the Sulimar Queen core terminate at bedding intervals that contain vugs (i.e., intervals with vuggy porosity).

2.1.4 Conclusions from Core Analysis

Three generalized lithologies are present in core from the Stivason Federal #1 Well. The main reservoir lithology (lithology C) is a poorly cemented, oil-stained sandstone exhibiting between 15 and 20% porosity and irregular permeabilities (up to 200 millidarcies; Figure 2.13). The percentage of the reservoir represented by this lithology is unknown because of missing core, although about a third of the core available consists of this facies. The upper parts of the core (predominantly consisting of lithology A) represent the confining strata rather than the reservoir rock: lithology C represents about 80% of the core available from the designated main reservoir intervals (Figure 2.13).

2.1.5 Detailed Core Information

Figures 2.19 to 2.26 are photographs highlighting each box of available core. Depth and numbered core sections are shown on the side of each photograph. Depth intervals are not uniform along some sections of core because of missing pieces of core. The blue/green arrow drawn directly on the core indicates up-hole direction. The blue/green label on individual sections of core indicates box number (1) and relative position of that piece of core in that box (A = first/upper section of core). The numbering system appears upside down on the core photographs to maintain a convention in which the up-hole direction on the core is at the top of the page. All the boxes of core use this labeling system, and each core section is labeled to the right of the photograph. In only a couple of instances (as the core was put back together) did the numbering system not correctly correlate. This mix up of core sections is to be expected for core that has been used as a teaching aid for several years. Permeability and porosity provided by Core Labs are correlated to areas where pieces of core were taken for sampling. Some pieces of the remaining core had the Core Labs sample numbers written on them, indicating the above and/or below missing piece of core was taken for sampling. It is apparent that in some 1-ft intervals two pieces of core were taken for sampling. At these locations, the Core Labs data are shown twice. Figures 2.27 to 2.32 provide a lithologic description of the core. The porosity and permeability data provided from Core Labs are also shown on the lithologic log.

2.1.6 Acoustic Velocity Anisotropy of the Stivason #1 core

Two tested pieces of sandstone from the Stivason #1 core show a consistent horizontal acoustic velocity anisotropy, indicating that there is probably a significant horizontal stress anisotropy and possibly a related horizontal permeability anisotropy to consider during CO_2 injection in the West Pearl Queen Field.

The two sample sandstone cores were taken from a high-porosity interval at 4531.7 ft and a denser interval at 4508.7 ft. Anisotropies of 3.5% and 1.5%, respectively, were observed between the maximum and minimum travel times (acoustic velocities) in orthogonal horizontal directions in these cores. In the absence of natural fractures and sedimentary fabric, such acoustic anisotropy is most likely related to a preferentially oriented population of microcracks formed when the core was cut free and released from an anisotropic confining stress at depth.

The measured anisotropies in the Stivason core are of a similar order of magnitude to measurements made in other sandstone reservoirs in the Rocky Mountain area where the causative differential horizontal stresses have been more fully documented. In such reservoirs, stress anisotropy controls the orientation of hydraulic fractures created when fluids are injected into the formation at pressures greater than the fracture gradient. The measured maximum compressive stress is also most commonly aligned with the strike of any natural fractures in a reservoir, since the stress anisotropy typically caused the natural fracturing. Thus, the long axis of any fracture-related permeability-anisotropy ellipse in a reservoir is parallel to the natural fractures, to the maximum horizontal compressive stress, and to the direction of the maximum acoustic velocity. This affects preferential flow directions in a reservoir at pressures well below the hydraulic fracture gradient (Lorenz et al., 1996).

The presence of a velocity/stress anisotropy in the West Pearl Queen Field does not mandate an anisotropic permeability ellipse. However, it does suggest that elliptical permeability (affecting both drainage and injection) is possible or even probable, even if the CO_2 is not injected at pressures exceeding the fracture gradient.

NE-SW is the most likely orientation for the long axis of that ellipse given the existing information, although as indicated earlier this is not yet well constrained at our site. (It may be possible to orient the two tested samples magnetically and thus predict more accurately the axes of any ellipse.) However, without more subsurface data, it is impossible to predict the ratio of the maximum to minimum horizontal axes of an ellipse might be. Ratios of 10:1 are not uncommon elsewhere, and ratios of up to 100:1 have been measured (Elkins and Skov, 1960; Lorenz and Finely, 1989; Lorenz et al., 1996; Nelson, 1985).

2.2 SHATTUCK OUTCROP STUDIES

Natural fractures have the potential to control the direction and facility of fluid flow within a reservoir. The Shattuck Sandstone Member of the Queen Fm, the host reservoir for CO_2 sequestration pilot project in the West Pearl Queen Field, was examined where it crops out in Rocky Arroyo and the Guadalupe Mountains west of Carlsbad, NM, during a brief field trip in early February, 2001. These outcrops are 100 to 130 km (50 to 80 mi) west of the West Pearl Queen Field; but they are the closest outcrops available, and many of them are fractured.

These outcrops were examined to see whether natural fractures capable of significantly affecting CO_2 injection and distribution might be present in the formation. The outcrops are, in fact, fractured to highly fractured, but *if* the West Pearl Queen subsurface reservoir is fractured, outcrop fractures may not be the equivalent set(s). Nevertheless, the fact that fractures are present in outcrop indicates that the formation has been susceptible to fracturing, and the presence of subsurface fractures cannot be ruled out. The probability of intersecting potential fractures with a wellbore or core is low if the subsurface fracture spacings are similar to those observed in outcrop. Although it may not be possible to extrapolate the fracture sets observed in outcrop directly into the subsurface, the presence or absence of fractures in outcrop indicates whether the reservoir strata have the potential to be fractured.

2.2.1 Fracture Descriptions

2.2.1.1 Fracture Distributions and Mineralization

Two systematic sets of bed-normal extension fractures, striking approximately northeast/ southwest (NE-SW) and north-northwest/south-southeast (NNW-SSE), are present in outcrops of both the Queen and Seven Rivers formations (Figures 2.33 - 2.40). The Shattuck Sandstone is the upper member of the Queen Fm and is definitively fractured in outcrop. Many fractures in the Shattuck sandstones extend vertically for meters to tens of meters, cutting across thinner (half-meter thick) bedding discontinuities within the sandstones.

Apertures of the NNW-SSE-striking fracture set may be up to 4 millimeters, but they have been partially to completely filled with crystalline calcite. The fractures of this set commonly consist of meter-scale, right-stepping, en echelon segments. Fractures of the other NE-SW striking set are more planar and are typically unfilled but stained with iron oxide. No surface ornamentations such as plumose structure or slickensides are observed on any of the fracture faces.

Calcite mineralization of the NNW-SSE set but not the NE-SW set indicates that the two fracture sets formed at different times, but the relative ages of the two sets, important to making extrapolations to the subsurface, are obscure. Exposures of abutting relationships allowing relative age determinations are rare and present contradictory evidence. The parallelism between the NE-SW fracture set and an inferred horizontal compressive stress of Laramide age (40 to 80 million years ago) suggests that these fractures were created during northeast-directed thrusting in southwestern New Mexico and northern Mexico. Similarly, the NNW-SSE striking fracture set is oriented parallel to the numerous local faults formed during Miocene to Recent (25 to 0 million years ago) rifting. If parallelism indicates a genetic relationship, as is likely, the NNW-SSE set, related to formation of the Rio Grande graben system that abruptly truncates the Guadalupe Mountains on the west, would be younger than the NE-SW striking set related to the older, Laramide tectonics.

2.2.1.2 Fracture Orientations

Fractures of the NNW-SSE set are present in all outcrops of the Shattuck Sandstone (Figures 2.33 to 2.35). Although the other NE-SW striking fracture set is ubiquitous in strata adjacent to the Shattuck Sandstone, it is entirely absent from many of the Shattuck and related sandstone outcrops studied (Figures 2.36 and 2.39). A present-day NE-SW trending maximum horizontal compressive stress in the West Pearl Queen reservoir was postulated in an earlier memo and has been documented in other parts of the Delaware Basin. In fact, the NE-SW fracture set is well developed in the thin-bedded carbonate units associated with the Shattuck Sandstone outcrops (Figure 2.39). However, the relative rarity of the NE-SW fracture set in Shattuck outcrops suggests that the sandy strata were not highly susceptible to fracture when the stresses were configured to form such fractures. Thus, this fracture set is probably also rare or absent from the subsurface Shattuck sandstones of the West Pearl Queen Field, even if the present-day, in situ stress has a NE-SW trend as postulated.

If the NNW-SSE striking fracture set was created by rifting along the Rio Grand trend as suggested, it seems improbable that the extensional effects of rifting would have been felt, creating fractures, in strata as far east as the West Pearl Queen reservoirs. No related NNW-SSE striking faults have been mapped in the reservoir area. Although fractures of the latter set would be compatible with the trend of fluid breakthrough observed in the nearby Vacuum Field, both the NE-SW and the NNW-SSE fracture sets may be absent in Shattuck sandstones of the West Pearl Queen Field.

2.2.1.3 Fracture Spacings

Although neither of the fracture sets found in outcrop were observed in the core, fractures may still be present in the subsurface. This seemingly inconsistent evaluation is based a basic sampling problem related to core. In this case the observed fracture spacings in outcrop are large relative to the horizontal distances interrogated with a wellbore or with a 4-inch diameter core, and thus the probability of intersecting fractures with a wellbore or core is low (Lorenz et al., 1996).

Fracture spacings in outcrop are in part related to bed thickness (i.e., spacings tend to be closer in thinner than in thicker Shattuck beds). However, bed thickness is only one of several controls, as shown by the difference in spacing between NE-SW and NNW-SSE fractures (average of 0.6 meter and 1.9 meters respectively) in the same 1.2-meter thick bed (Figure 2.35).

Fractures in outcrops of the thicker, underlying unit of Shattuck Sandstone (Figures 2.36, 2.40), which is at least 4.5 meters thick, have an average spacing of 2.1 meters if each fracture is measured. However, the fractures in this unit, probably more analogous to the subsurface reservoir than the thinner bed, occur as groups of up to three fractures within 5 to 25 centimeters of each other, and the average spacing of the fracture groups is 4.8 meters. Other, more isolated patches of this unit display intervals up to 10 meters across without apparent fracturing.

2.2.2 Fracturing in the Overlying, Reservoir-Seal Formation and Associated Strata

The overlying strata of the Seven Rivers Fm that provide a seal for the Shattuck reservoirs are also exposed in outcrop. The Seven Rivers Fm consists of interbedded carbonates, evaporites, and shales. The carbonate beds, centimeters to a few meters in thickness, are extensively fractured in both the NE-SW and NNW-SSE directions (Figure 2.41). It appears that the unfractured, interbedded, more ductile evaporites and shales provide the seal integrity necessary to maintain the fluid in the reservoir. However, it would not be hard to break through these sealing units with the localized pressures of an injection.

Fractures in the older Cherry Canyon (sandstone) Fm at Sitting Bull Falls strike consistently NNW-SSE (Figure 2.38). Exposures at this location show that fractures of this set may have great vertical extent despite prominent horizontal discontinuities provided by bedding (Figure 2.42). It is possible that many of the fractures in the Shattuck outcrops have similar vertical extent, although the Shattuck outcrops are of insufficient dimension to prove this.

2.2.3 Conclusions from Outcrop Studies

Outcrops of the Shattuck sandstones contain two fracture sets, having strikes of NE-SW and NNW-SSE. The former are typically stained with iron oxide, and the latter are typically mineralized with crystalline calcite. Although both fracture sets are equally well developed in associated carbonate strata, NNW-SSE fractures dominate the Shattuck and related sandy intervals. Fractures of this set have average spacings from tens of centimeters to a few tens of meters. Geologic arguments suggest that neither fracture set may be present in the subsurface reservoirs of the West Pearl Queen Field, but the presence of fracturing in outcrop indicates that the formation has been susceptible to fracturing and that the possibility of subsurface fracturing should not be ignored.

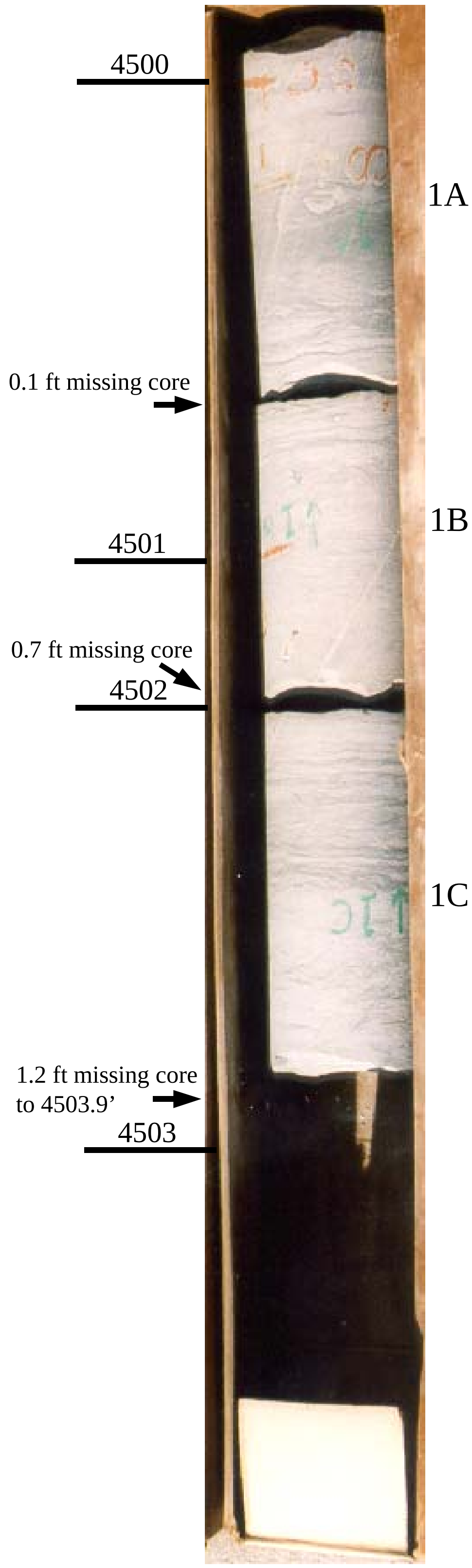

Figure 2.19. Core box #1.

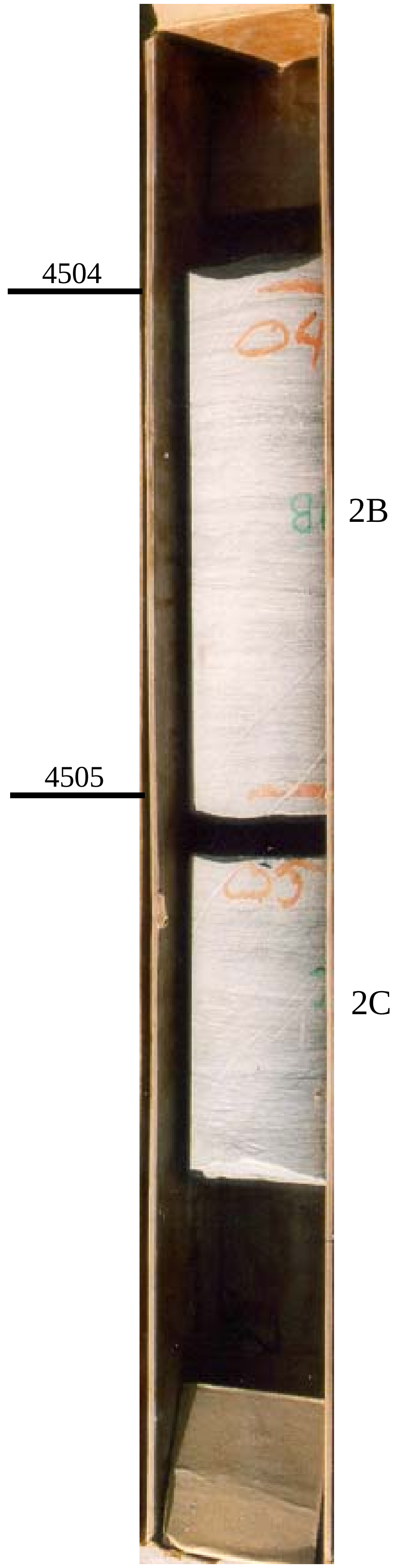

Figure 2.20. Core box #2.

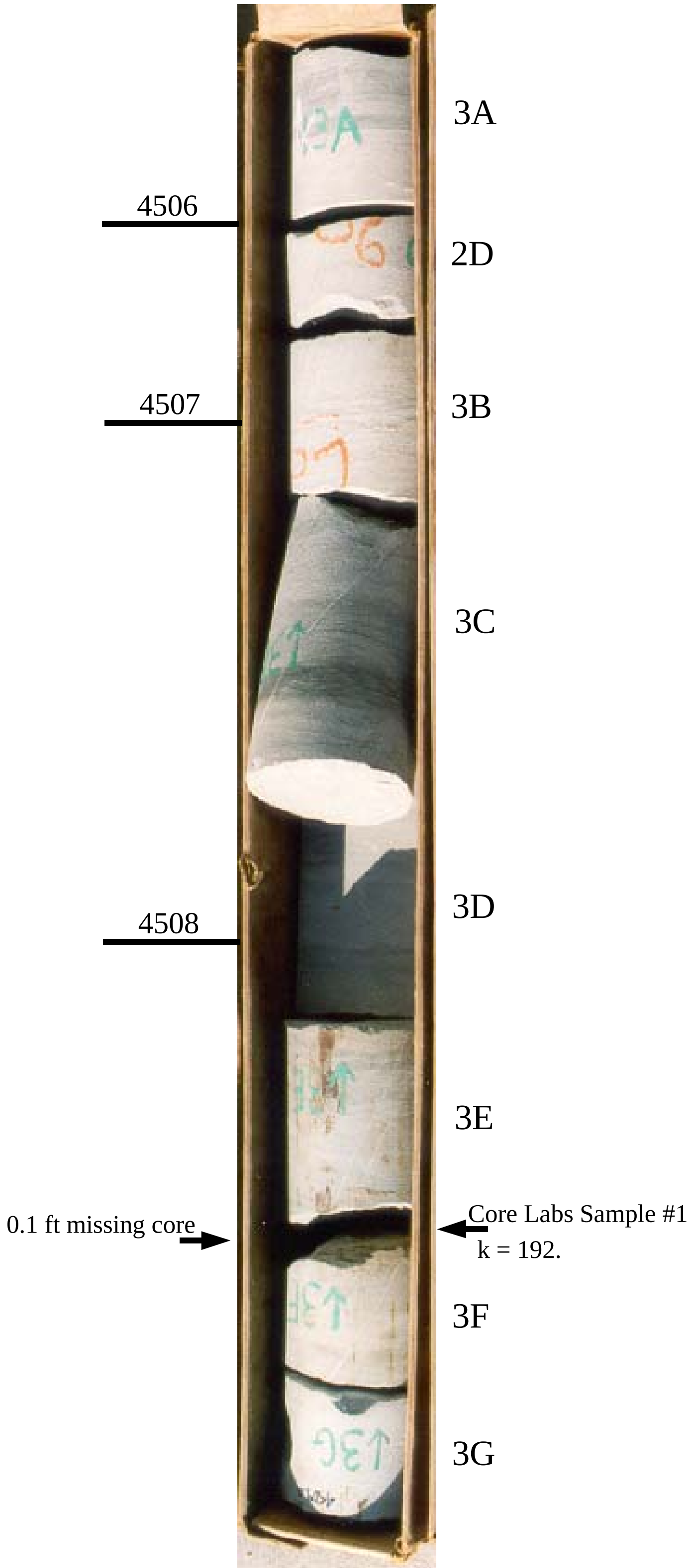

Figure 2.21. Core box #3.

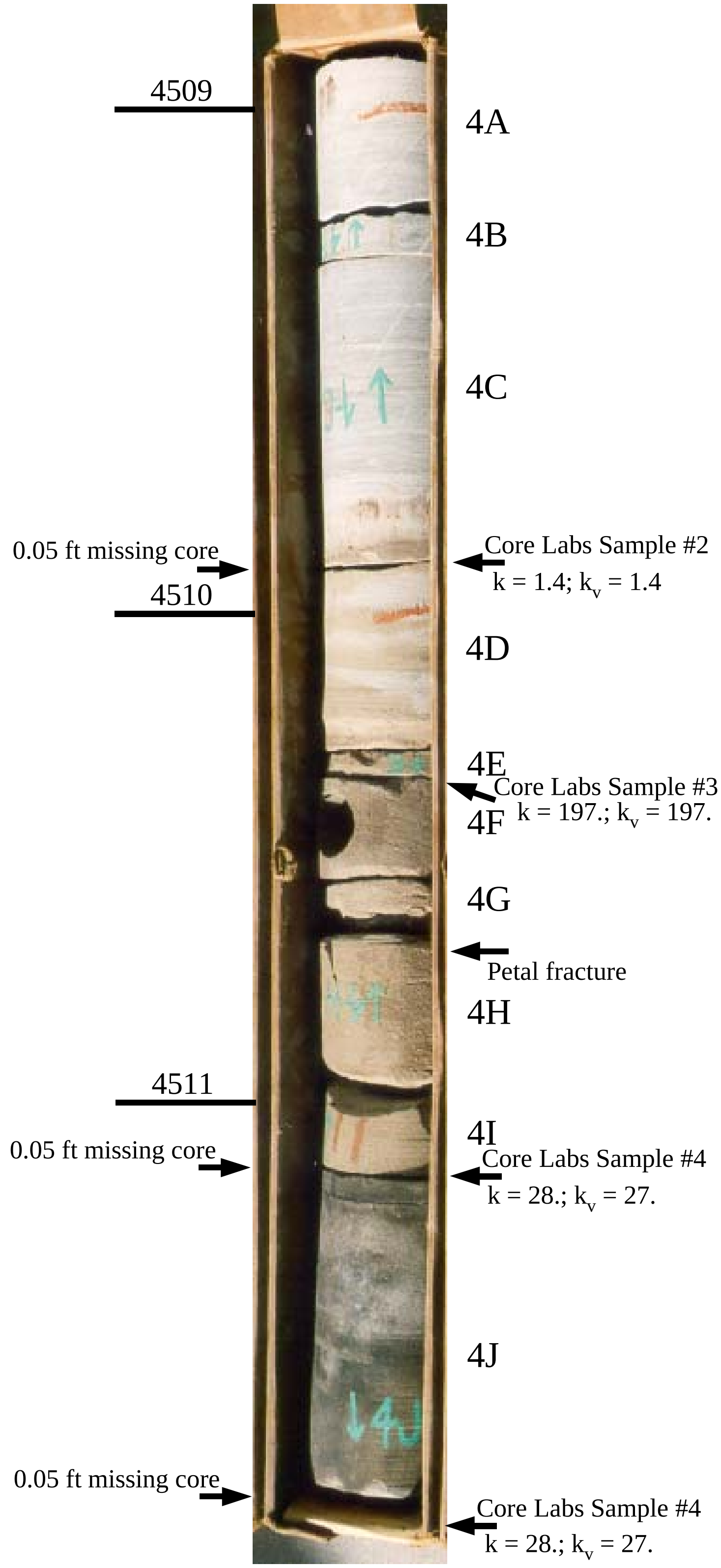

Figure 2.22. Core box #4.

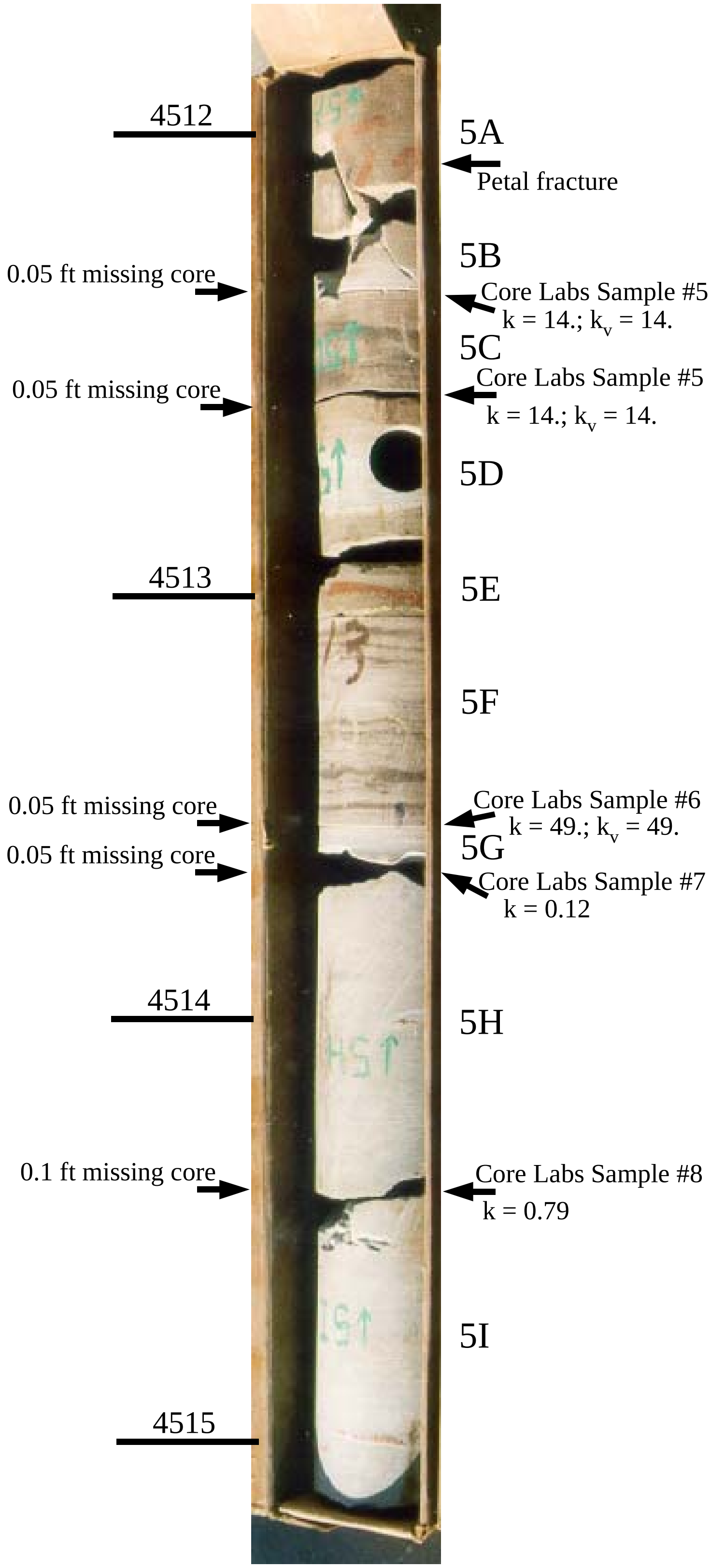

Figure 2.23. Core box #5.

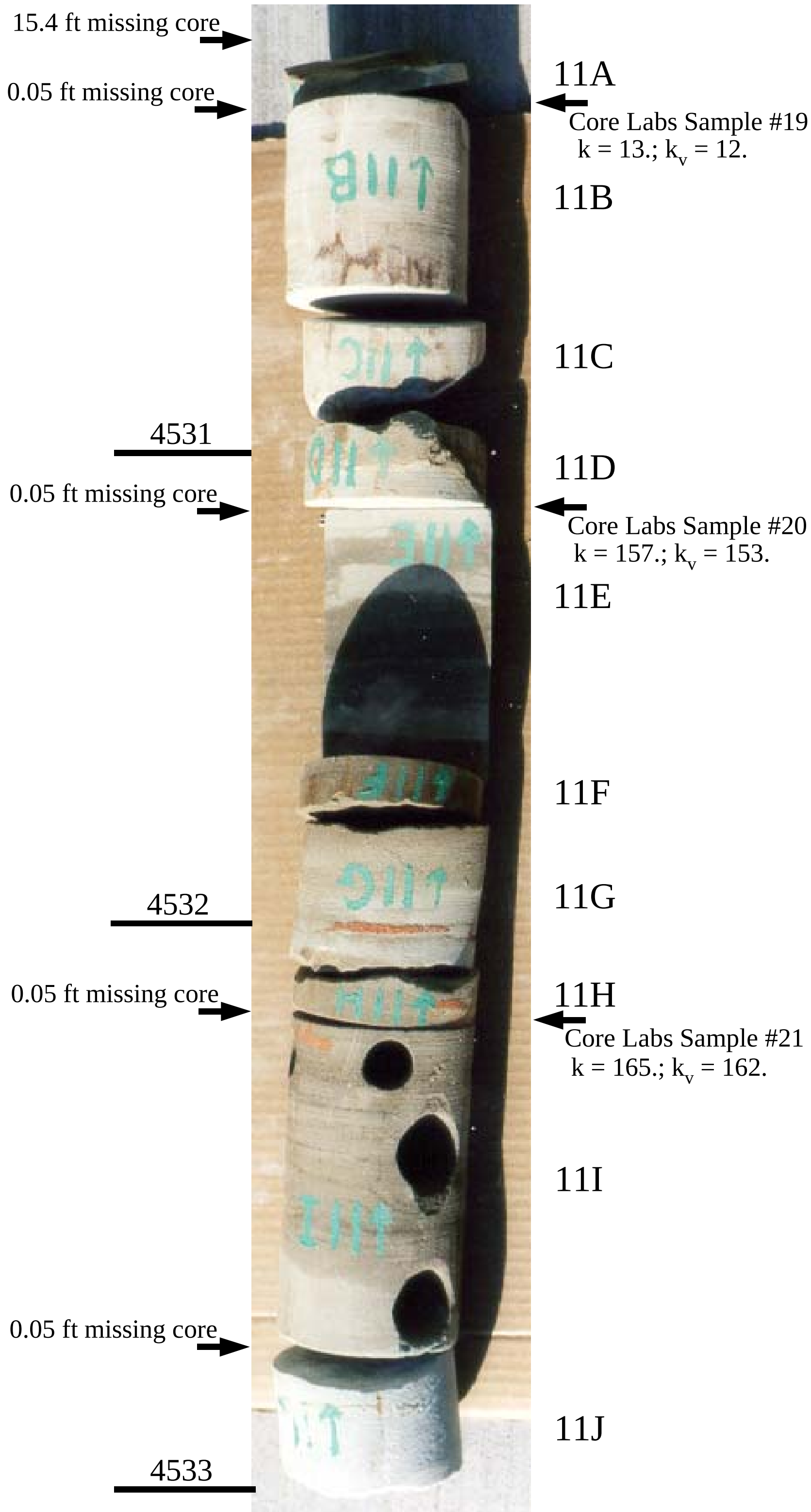

Figure 2.24. Core box #6.

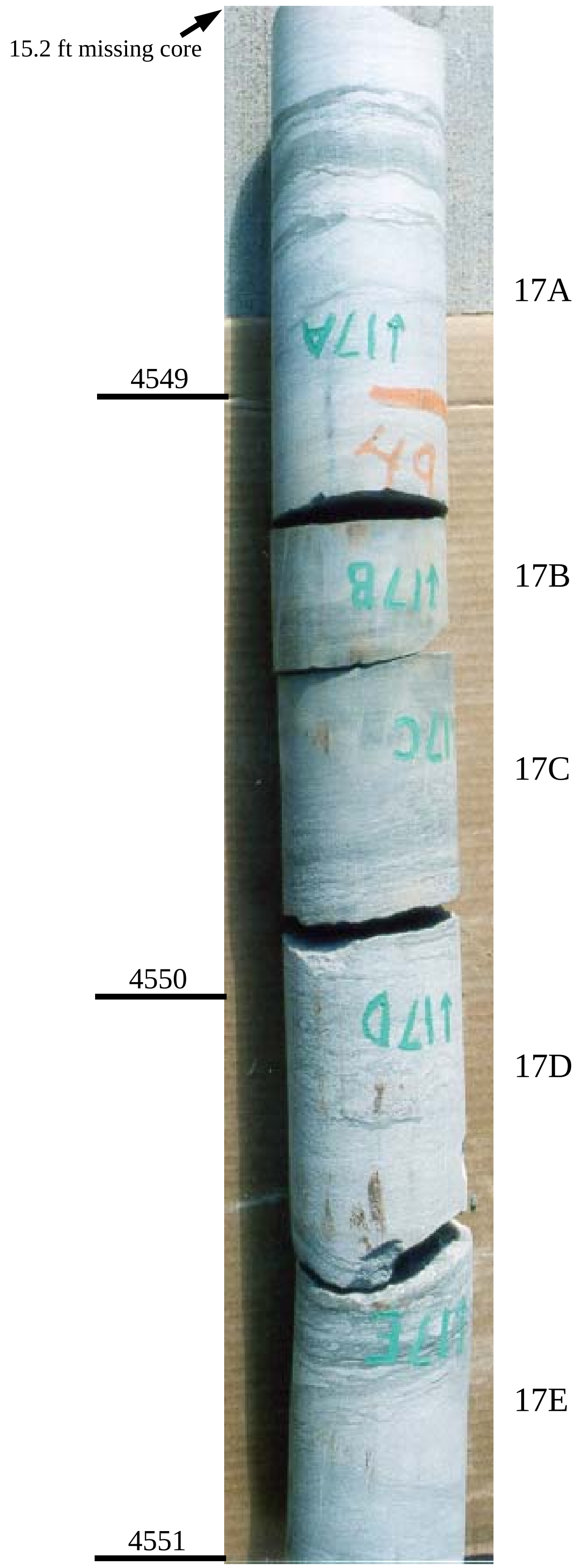

Figure 2.25. Core box #7.

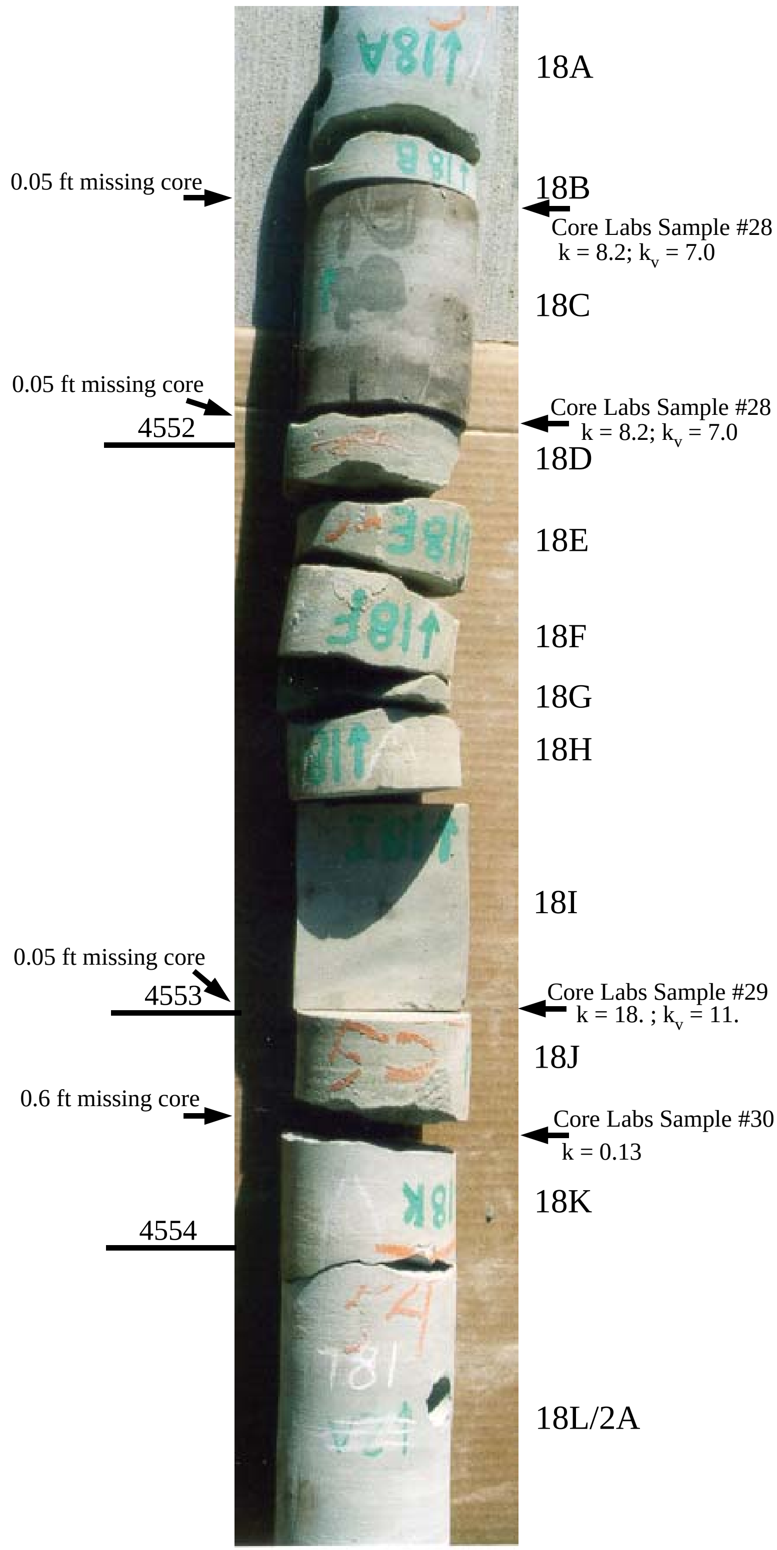

Figure 2.26. Core box #8.

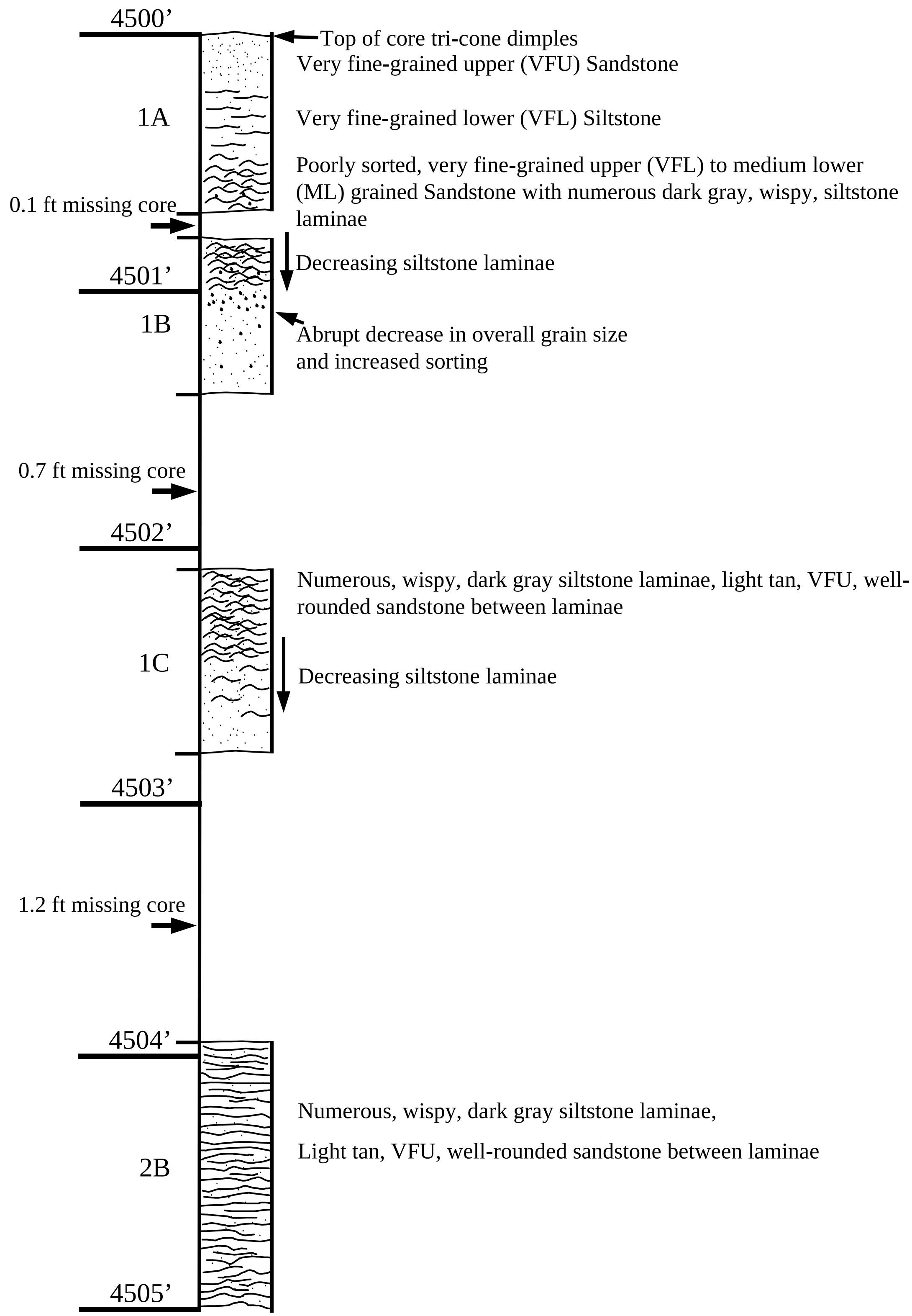

Figure 2.27. Lithologic description of core.

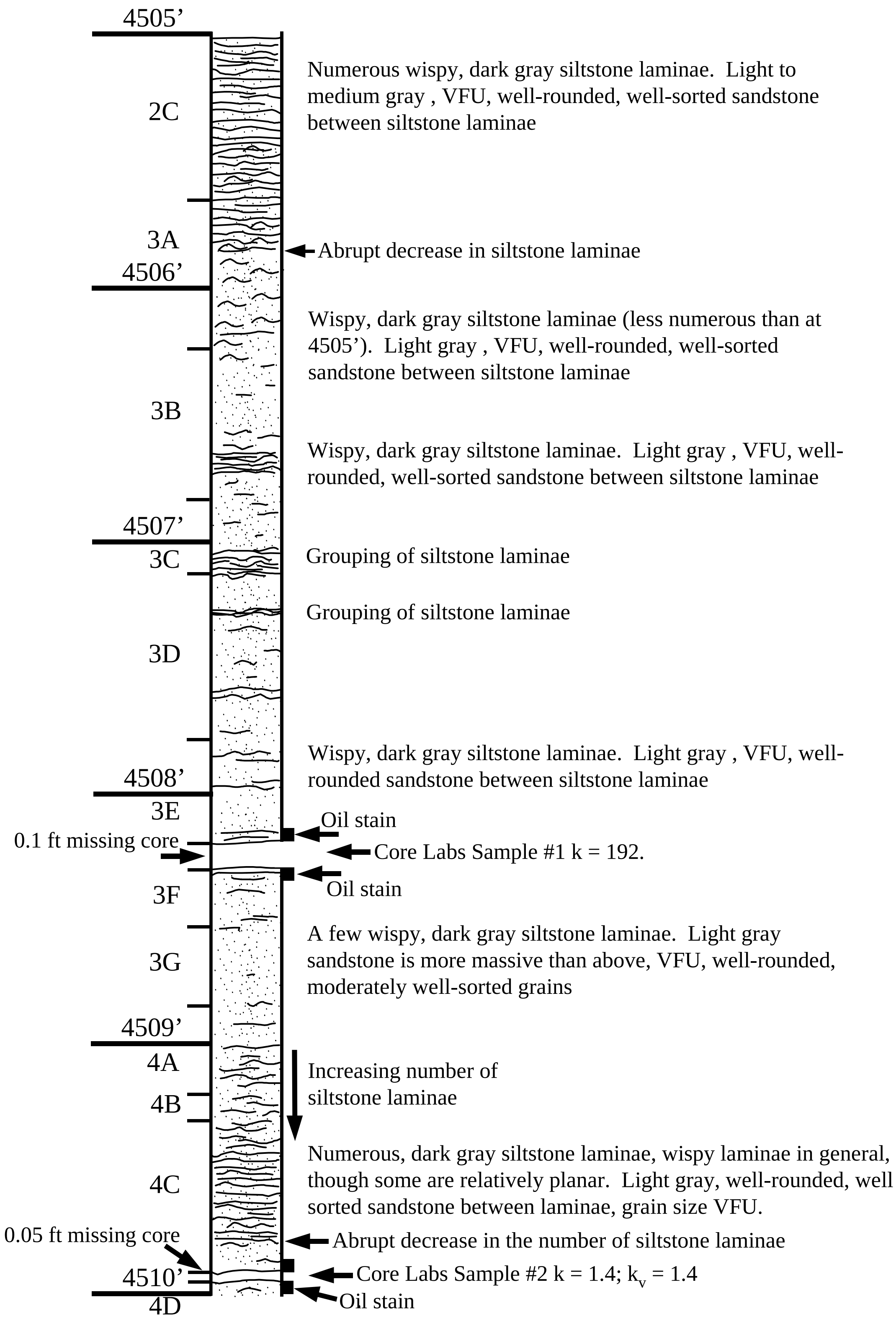

Figure 2.28. Lithologic description of core.

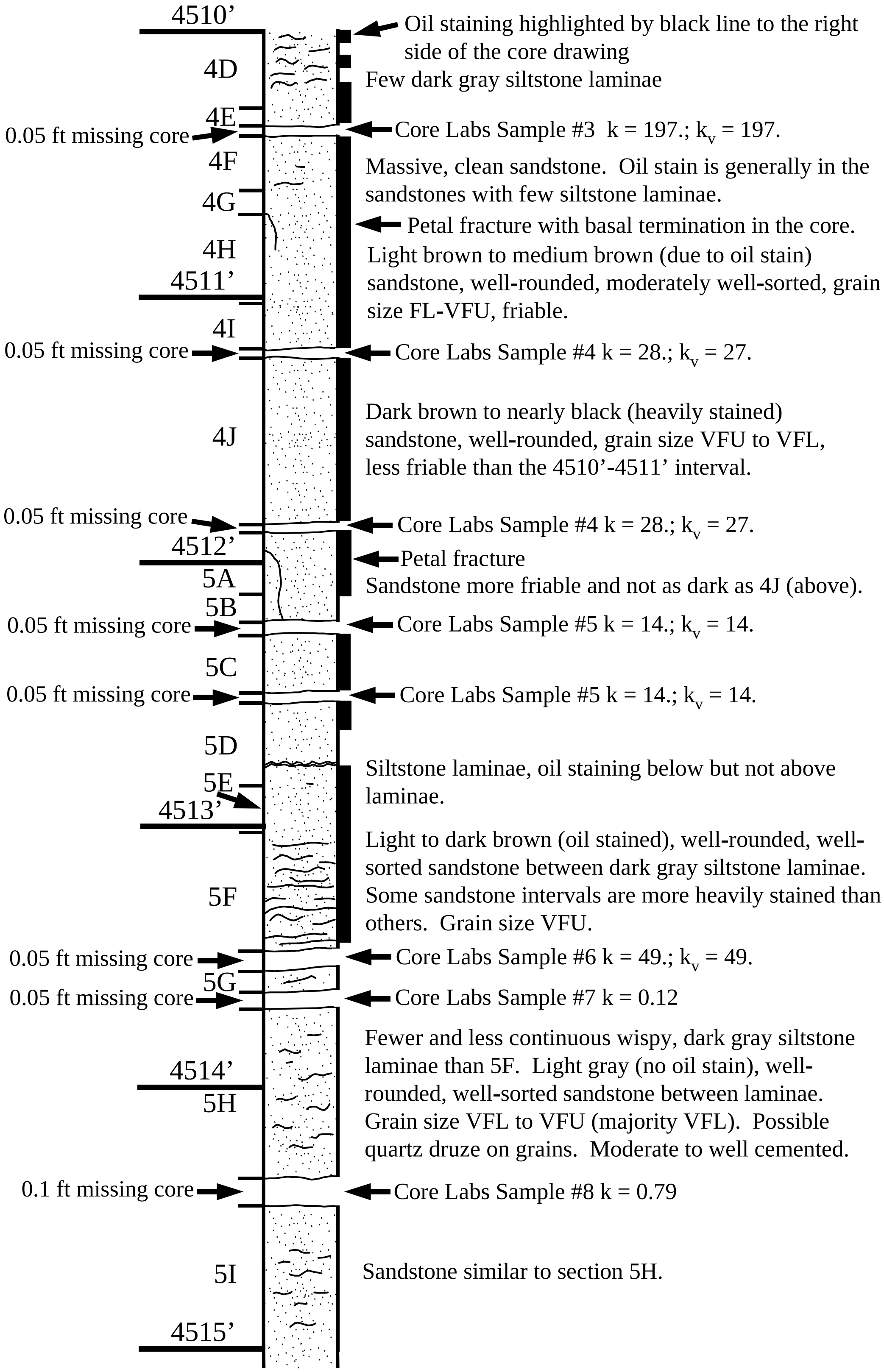

Figure 2.29. Lithologic description of core.

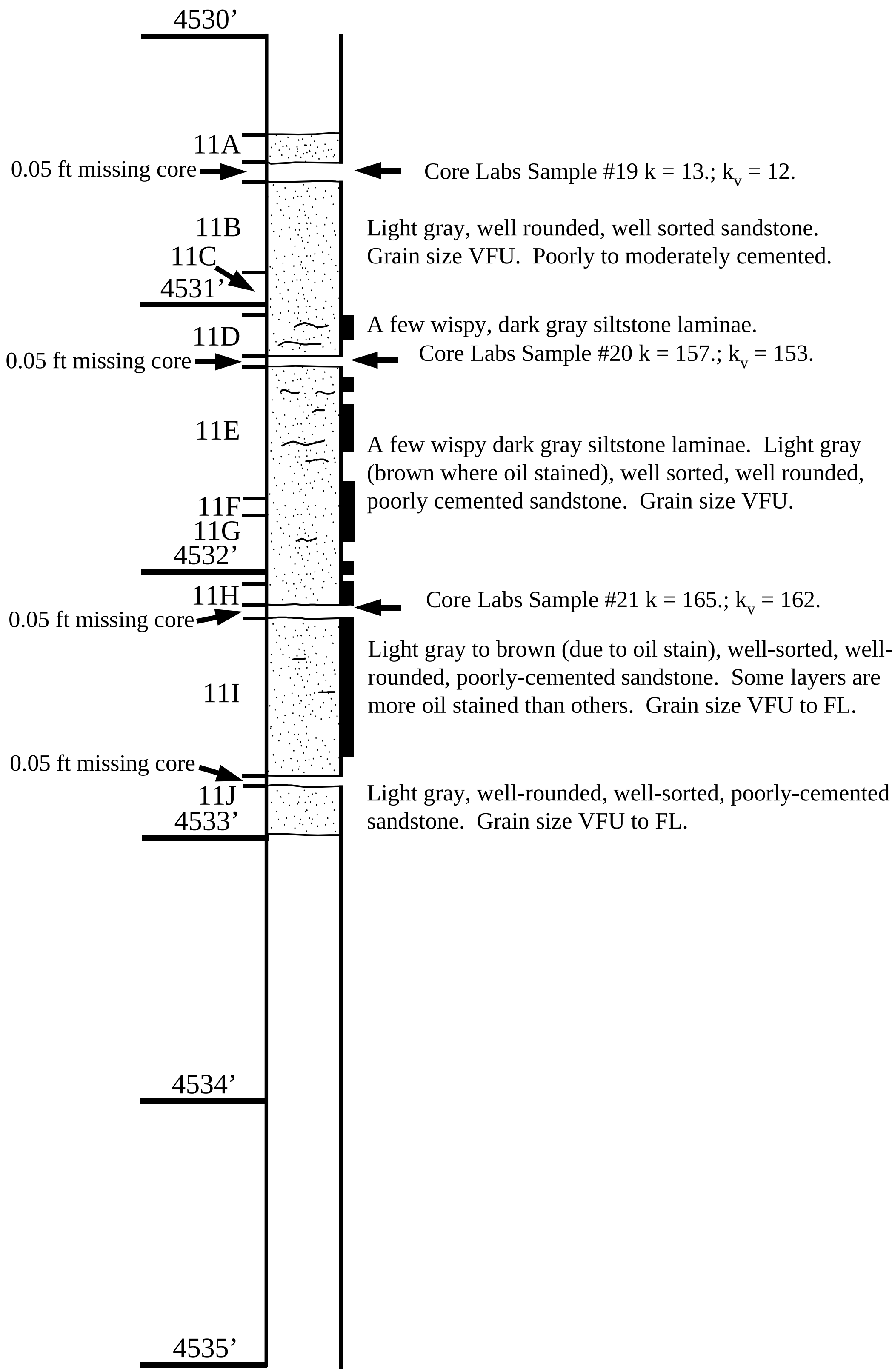

Figure 2.30. Lithologic description of core.

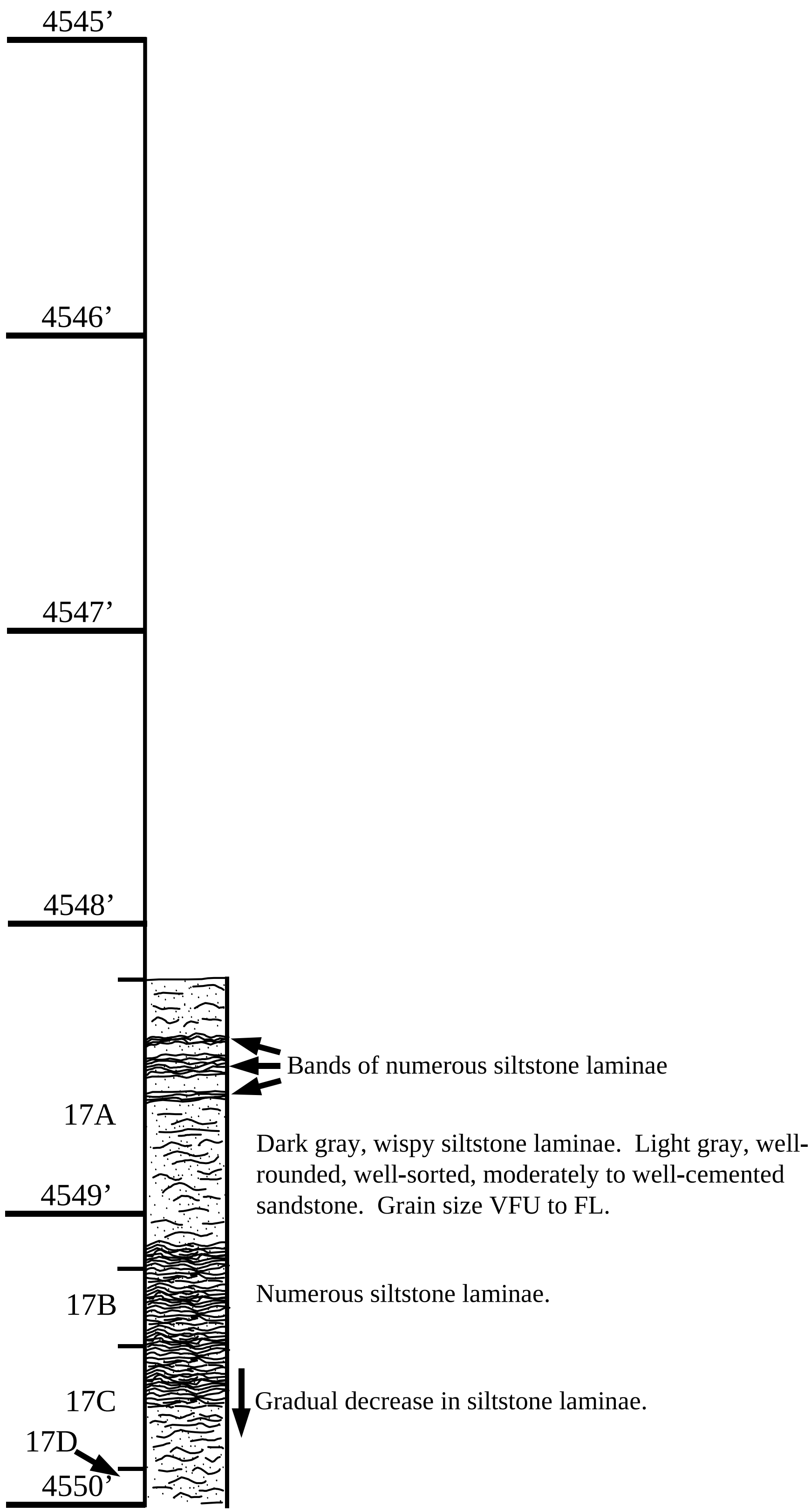

Figure 2.31. Lithologic description of core.

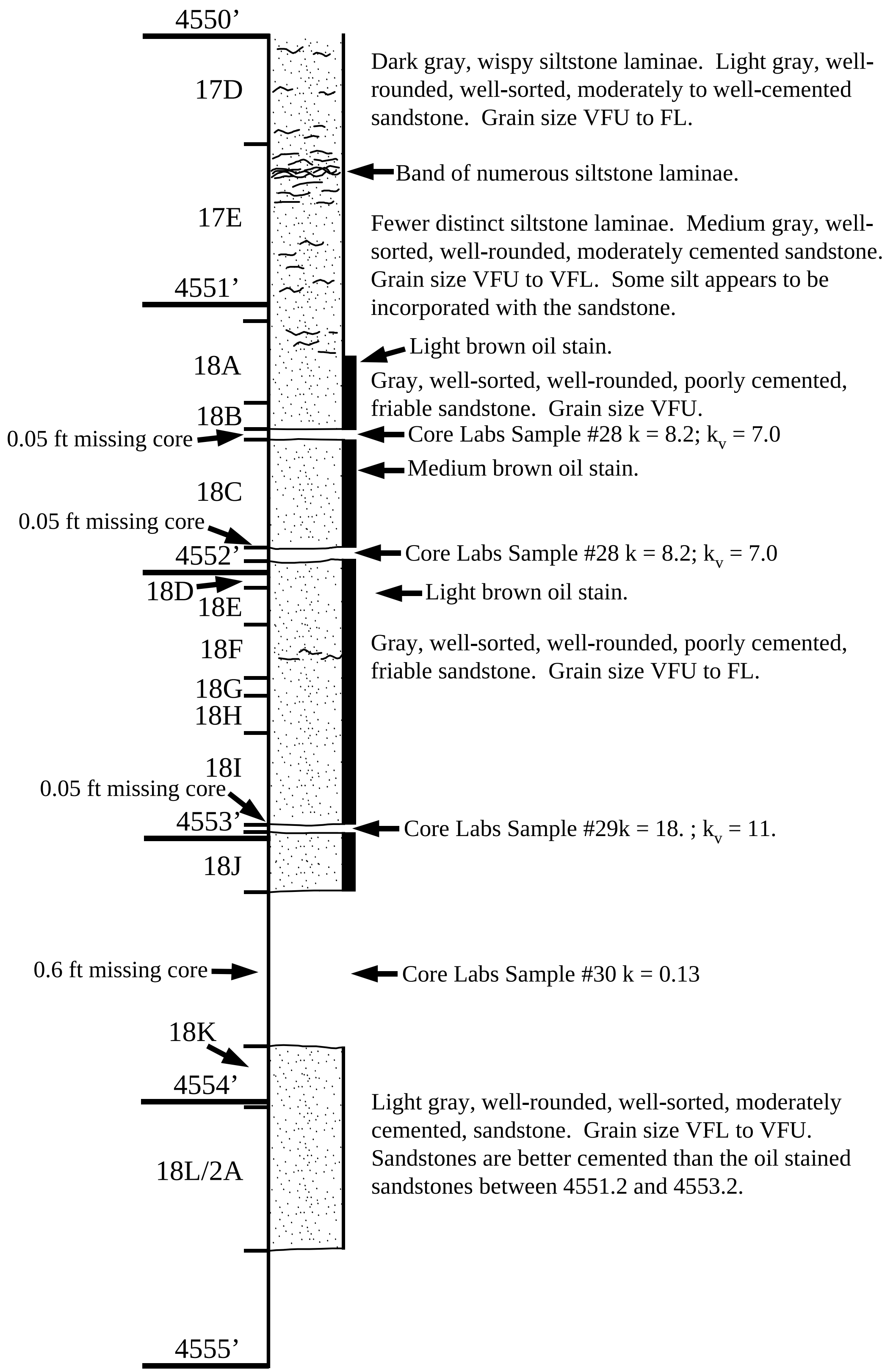

Figure 2.32. Lithologic description of core.

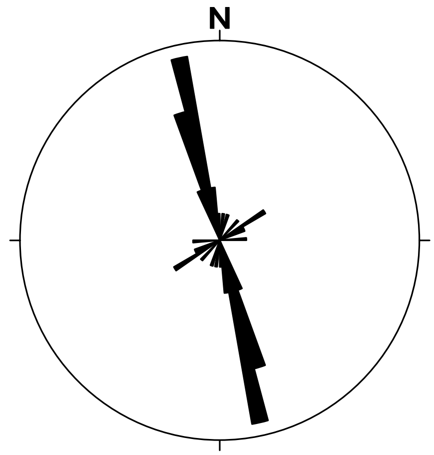

Figure 2.33. Fracture strikes in the upper Shattuck sandstone along County Route 540: n = 25, ring = 15%.

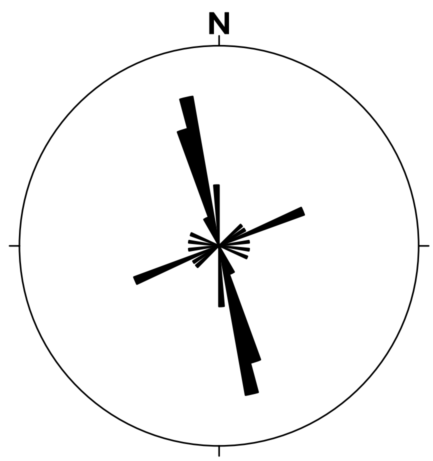

Figure 2.34. Fracture strikes in outcrops of the lower Shattuck Sandstone along County Route 540: n = 22, ring = 15%

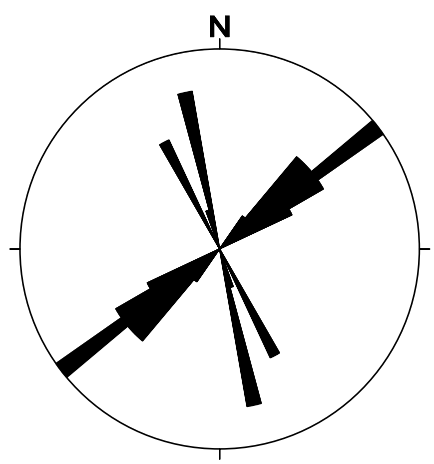

Figure 2.35. Fracture strikes within the Shattuck Sandstone, Rocky Arroyo roadcut: n =25, ring = 10%. Bed thickness 1.2 m.

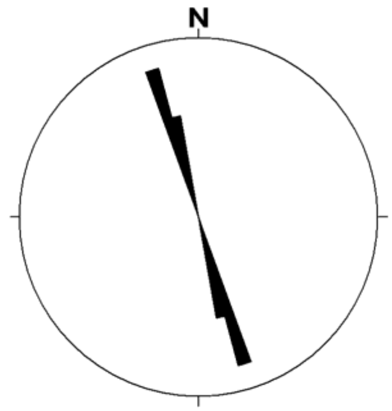

Figure 2.36. Fracture strikes in the Shattuck Sandstone, Rocky Arroyo riverbed: n = 10, ring = 25%.

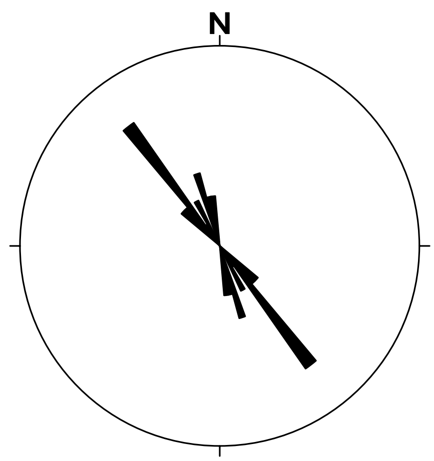

Figure 2.37. Fracture strikes in the unnamed sandstone below the Queen Dolomite, Rocky Arroyo: n = 20, ring = 15%.

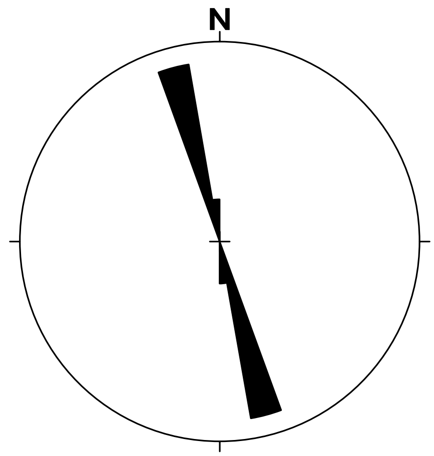

Figure 2.38. High angle, bed-normal fractures near Sitting Bull Falls, sandstone tongue of the Cherry Canyon Fm: n = 21, ring = 45%. These fractures extend for several tens of meters vertically, crossing numerous bedding planes.

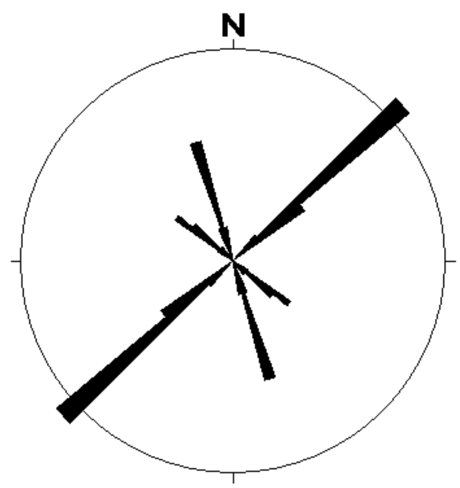

Figure 2.39. Fracture strikes in the Queen Dolomite (immediately underlying the Shattuck Sandstone Member), Rocky Arroyo: n = 22, Ring = 15%.

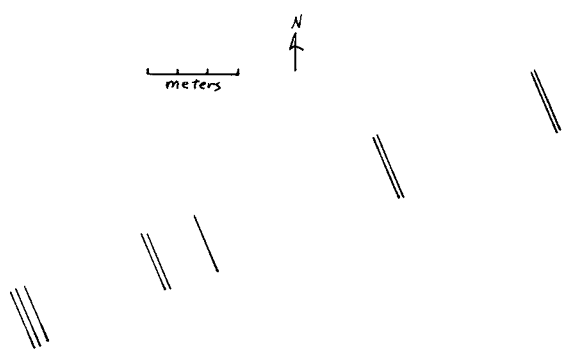

Figure 2.40. Map-view presentation of natural fracture spacings in the Shattuck Sandstone at the bottom of Rocky Arroyo (same outcrop as Figure 4).

Figure 2.41. Fractured carbonate beds of the Seven Rivers Fm, overlying the Shattuck Sandstone Member of the Queen Fm. Two fracture sets are present: parallel and perpendicular to the plane of the page.

Figure 2.42. Natural fractures near Sitting Bull Falls have vertical extents in the tens of meters range within sandstones of the Cherry Canyon Fm (scale is approximate).

3.0 GEOCHEMICAL STUDIES

Part of the uncertainty in geologic sequestration stems from the complex geochemical interactions of subsurface processes. For example, the pH falls and bicarbonate concentrations increase when high-pressure CO_2 comes in contact with formation waters. These changes, in turn, can initiate rock-brine interactions with the potential for altering the transport properties of the rock. A related issue is the extent to which such interactions transform the CO_2 to carbonate, thus fixing it in a nongaseous form as dissolved bicarbonate or carbonate minerals.

The objective of the geochemical studies was to determine how changes in CO_2 pressure and pH would affect the rock of the Shattuck Member sandstones within the Queen Formation. The experimental dataset provides a standard, against which it is possible to calibrate the predictions of "reaction path" models. With the appropriate adjustments, the models reflected both the long- and short-term changes observed experimentally.

Over the longer term, the models indicate that, if the pressure of CO_2 is maintained, the complete feldspar inventory of rock would be converted to clays, and that part of the carbonates that were initially removed would reappear. However, in spite of its pervasive impact on the rock, these processes only roughly double the dissolved bicarbonate level in the brine. Even with this, the amount of bicarbonate in the brine is small compared with amount CO_2 that remains as dissolved gas. Sensitivity studies also revealed similarly stringent limits on the amounts of CO_2 that could be scavenged by the dissolution of calcite and dolomite. Thus, in the case of the Shattuck, reactions with the formation minerals do not provide a sink that will permanently fix in place a large percentage of the injected CO_2. However, if pervasive growth of clays occurs it would significantly impede any long-term leakage from the formation.

3.1 EXPERIMENTAL STUDIES

One approach to understanding the chemical changes that result when CO_2 is injected into the Shattuck Member of the Queen Fm is to experimentally simulate the situation in the laboratory. This was done by placing sandstone chips (1 to 2 grams) in small stainless steel autoclaves with about 2.5 grams of formation brine under 700 psi (~48 atm) CO_2 pressure at 40^o C (the ambient formation temperature at the injection depth). One autoclave was disassembled after 6.5 months, and the other after 19 months. Fluids were analyzed by ion chromatography for anions. Cation analyses were obtained by either direct current emission spectroscopy (early samples) or inductively coupled plasma mass spectrometry (later samples). As with the original core, post-test samples were characterized using scanning electron microscopy (SEM) and energy dispersive spectrometer (EDS) and by X-ray diffraction.

Several significant changes took place during these tests. Figure 3.1a illustrates typical pre-treatment material, with rounded sand grains overgrown by angular K-feldspars and rounded carbonate (both Mg-rich and nearly pure calcium carbonate) overgrowths. Clays, and indeed all sheet silicates including the micas, are absent from the pre-test core. After 6.5 months of treatment, shown in Figure 3.1b, almost all of the carbonate mineral grains are gone, but, occasionally, a Mg-rich carbonate grain can be found (Figure 3.2a). It is also possible to find rare instances where clay overgrowths are displayed along the edges of the grains (also in Figure 3.2a). After 19 months, the clay overgrowths are much more common and well developed, as shown in Figure 3.2b. It is also evident that the plagioclase feldspars have become etched (e.g., Figure 3.3a), which provides the silica and aluminum needed for clay growth. At this point, even the Mg-rich carbonate grains have dissolved.

By virtue of the very high magnifications employed, SEM examinations can only evaluate changes in a very small percentage of a sample. In contrast, changes in fluid chemistry characterize the bulk interactions between solid and fluid. Fortunately, in this case the fluid chemistry confirms the trends identified using the SEM. Aluminum, initially in very short supply, has risen as feldspars dissolved, and silica has fallen to reflect the subsequent precipitation of clays. The largest changes are the increases in Ca and Mg, which are consistent with the dissolution from the carbonate cements. In spite of the increase in calcium, the sulfate did not decrease. This is consistent with the absence of either gypsum or anhydrite from the SEM observations. Neither sodium nor chloride concentrations changed appreciably. This confirms the absence of new minerals containing large amounts of Na or Cl, as well as precludes widespread formation of new hydrated minerals (other than clays) that would have withdrawn water from the solution.

3.2 GEOCHEMICAL MODELING

The preceding section illustrated that exposure to high-pressure CO_2 could initiate mineralogic changes with the potential for altering the porosity and, presumably, the permeability of a potential host formation. Unfortunately, it is not practical to initiate long-term laboratory studies, or expensive field tests, for every reservoir setting that might be considered as a CO_2 sequestration site. A way around this is to develop "reaction path" computer models (which can run many times at minimal cost) to evaluate the impact of changing formation mineralogy and indigenous brine chemistry. These models computing the equilibrium state of an assemblage of components. Inherent in this approach is the inability to evaluate formation of metastable phases unless the most stable phase(s) are manually "suppressed" before starting the computation. This approach can also be used to simulate reaction kinetics if outside information exists (as shown above) indicating whether reactions progress quickly or take a long time. Most of what follows is based on results from a commercially available reaction path-modeling package called REACT (Bethke, 1998) that employs extended Debye-Huckel activity coefficients. However, the discussion concludes with a comparison between these results and a parallel computation using the EQ3/6 (public domain) program and recently developed Pitzer coefficients for CO_2 in high ionic strength brines.

Since phase suppression is done manually, it is best to start by calibrating the model on a simple system. In this case, we asked what was needed to produce a model of the brine chemistry that predicted compatibility with the minerals actually observed in the core samples at the nearly neutral pH that was measured for the brine. Simply "plugging in" the brine chemistry (Table 3.1) suggested numerous minerals, some plausible and others that clearly are absent from the formation, notably well-crystallized micas (muscovite, phlogopite, paragonite), magnesium silicates of dominantly metamorphic origin (antigorite, chrysotile, tremolite, talc clinochlore), and two carbonates (magnesite, well-ordered dolomite). This, then, was the initial list of suppressed phases. Once these minerals were removed, the model predicted minerals that were in reasonable agreement with the actual formation mineralogy at pH values near neutrality, as shown in Figure 3.4.

The predicted occurrence of Na-saponite above pH 6.5 represents a special problem. This is a magnesium-rich smectite clay and a legitimate sedimentary mineral, though in fact it is absent from the pre-test core. The principal effect of suppressing Na-saponite in Figure 3.4 would be to extend the upper limit of potassium feldspar ("maximum microcline") to a pH of 7.8, rather than having it drop out at around a pH of 6.6. Another problem is that calcite only appears above a pH of 8.8, where brucite formation extracts magnesium from the mixed carbonate phase. However, in this particular system (but not those evaluated later), there is just a trifling difference between the saturation state of calcite and disordered dolomite. Thus, here a better interpretation would be that above pH 7 both phases coexist. It is also noteworthy that although albite does not actually appear, it almost reaches saturation between pH 5.8 and 6.7. Overall, the pH range that comes closest to providing a mineral assemblage that mimics the actual formation lies between pH 6.5 and pH 7.0. This agrees with the nearly neutral pH measured on the brine.

The above calculation only assumes the presence of components in the brine, which, in fact, contains only minuscule amounts of silicon and aluminum. The next step is to equilibrate the brine with an excess of the minerals present in the formation (per liter: 0.26 mole of albite, 0.67 mole of quartz, 0.01 mole of dolomite, 0.03 mole of calcite, 0.03 mole of potassium feldspar). When this is done, a mineral assemblage of quartz, kaolinite, saponite, albite, calcite, and potassium feldspar is predicted. The effect of suppressing saponite is to add disordered dolomite to the final phase assemblage and greatly decrease the amount of kaolinite predicted to be present.

Finally, increasing the CO_2 partial pressure (Figure 3.5) to that of the experiment drops the pH, quickly eliminating calcite, saponite, and albite. Potassium feldspar persists until the pH has fallen to 5.6, which corresponds to a CO_2 pressure of about 65 psi or about 10% of the experimental CO_2 pressure. At about 70% of the final CO_2 pressure, calcite reappears because the bicarbonate increases so that saturation is again achieved.

The utility of such models lies not in their ability to mimic a particular experiment or natural setting, but in what they can tell about the behavior of related systems. In this study, one concern is comparing the short- and long-term responses of the formation. Figure 3.5 illustrates the expected long-term response when clays form, while Figure 3.6 illustrates the contrasting short-term behavior when all clays are suppressed. In the absence of clays, a lower pH is attained, and carbonate removal is complete once a few atmospheres of CO_2 pressure are present in the system. Complete carbonate removal is consistent with the experimental observations.

Contrasting Figure 3.6 with Figure 3.5 provides considerable insight into how this particular host formation would evolve over time. Once clays form to a significant degree, the pH rises (from pH 4.6 to pH 5.1 once argillization is completed), and the mineralogy alters dramatically. Ultimately, large-scale argillization is predicted to consume the entire feldspar inventory in the rock, assuming the CO_2 pressure can be maintained above 65 psi. At the highest CO_2 pressures, one might also anticipate the reappearance of carbonate minerals. Unfortunately, these chemical changes only about double the level of dissolved bicarbonate in the brine. At this concentration, the dissolved bicarbonate is still a factor of six less than that of aqueous (e.g., dissolved) CO_2. Thus, argillization is not a significant CO_2 fixation mechanism.

With Permian sediments (such as are the focus of the present study) another key variable is the availability of sulfate, and whether calcium liberated by carbonate dissolution will initiate precipitation of anhydrite or gypsum. The models used in generating Figure 3.5 and Figure 3.6 were run iteratively while varying the level of sulfate. These results suggest that when all clays are suppressed, about 12 g/l sulfate would be needed to initiate calcium sulfate precipitation. If clays are allowed to form, about 23 g/l sulfate are needed to accomplish this result. One might also consider a system that starts out with enough anhydrite to maintain calcium sulfate saturation throughout the ramp-up in CO_2 pressure. In this case, essentially none of the carbonates present initially dissolve if clays are allowed to form, but they have all disappeared by the end of the pressure build-up if clay formation is completely suppressed. An immediate application of these results would be to rule out the possibility that injecting high-pressure CO_2 into the Queen Sandstone is likely to clog the pores by forcing the precipitation of calcium sulfate. However, at a site with slightly more sulfate in the groundwater, this could occur quickly and seriously impede the injection process.

One can also use such models to investigate the effects of changing the proportions of the major rock-forming minerals in the rock. For example, the same two models were run again except, this time, the amounts of both disordered dolomite and calcite were increased by a factor of five. Even in the absence of clay formation, the calcite persists along with the disordered dolomite to the lowest pH attained (a little above 4.8 in this case, as compared with about 4.6 with less carbonate). When clays are allowed to form, essentially none of the original carbonates dissolve. It was shown previously that argillization was not a significant CO_2 fixation mechanism. In this example, only small amounts of calcite and dolomite were needed to maintain carbonate mineral saturation across the board. Thus, stringent limits also apparently exist on the amount of CO_2 that can be fixed by interactions with limestone, dolomite, and carbonate cements.

The preceding discussion illustrates how the utility of reaction path modeling can be significantly enhanced through the judicious use of the mineral suppression option. A second refinement of the technique would be to switch from the use of extended Debye Huckel activity coefficients (used by REACT) to those computed using a Pitzer formalism. Activity coefficients are the correction factors needed to transform bulk dissolved concentrations into thermodynamic activities needed for computing the equilibrium configuration for the system (e.g., they essentially allow one to derive effective concentrations for components that account for all the interferences from the other components dissolved in the same solution). It is generally recognized that when solutions with ionic strengths in excess of 0.5 molar are involved, the use of Pitzer activity coefficients will improve the reliability of a model. However, a much larger supporting database is needed to develop Pitzer coefficients for evaporite systems (Greenberg, and Møller, 1989; He and Morse, 1993; Pabalan and Pitzer, 1987; Pitzer, 1991); one that is only now being slowly assembled by the geochemical community for CO_2-rich systems.

To assess the importance of such an improvement, the authors reran the basic model (Figure 3.5) using the EQ3/6 reaction path program with Pitzer coefficients. Activity coefficients from this run were then compared with those predicted with REACT (Table 3.2). For ions such as Na^+, K^+, $SO_4^=$, and HCO_3^- the differences are not large, and the REACT activity coefficients only slightly under-predict the effective concentrations of these components relative to their Pitzer counterparts. However, the Pitzer activity coefficients for Ca^{++} are roughly twice as great as those obtained from REACT, while for magnesium the situation is reversed. Thus, the predicted stabilities for Ca- and Mg-containing minerals would differ somewhat depending on which model is used.

In practical terms, dolomite solubility (e.g., the dissolved concentrations of the constituent components in equilibrium with the mineral) calculated with EQ3/6 would be about half that calculated with REACT, while for anhydrite the number is closer to a third. In an example presented above, REACT predicted anhydrite precipitation would occur in brines with 12 g/l (clay free) and 23 g/l (with clays: kaolinite, saponite) dissolved sulfate, but the Pitzer coefficient approach suggests that these values might be reduced by a half to two-thirds. However, neither model suggests that the indigenous sulfate concentrations in the Pearl Queen brine would lead to calcium sulfate precipitation (or a subsequent decrease in formation permeability) as CO_2 is being injected during the current field test.

3.3 DISCUSSION OF RESULTS

For CO_2 sequestration in geologic formations, the two most important questions are (1) Can we get it into the ground? and (2) Will it stay there? Both issues are complex, and geochemical studies can only give a part of the answer. Studies of this nature can provide information on changes in the bulk porosity of a potential host formation, identify minerals that are likely to appear (or disappear) as injected CO_2 interacts with the host formation (and indigenous groundwater), and ultimately identify (or disprove) the presence of long-term sinks for sequestered CO_2.

Relating these studies to this specific field project suggests that the first impact of injecting the CO_2 will be dissolution of the carbonate cement. In the field, it was noted that over the six-week injection period, the flow into the formation (at a fixed injection pressure) remained essentially constant. This contrasts sharply with the short-term increased resistance to flow noted when CO_2-brine mixtures were forced through cores (Westrich et al., 2002; Krumhansl et al., 2002) during which, apparently, no dissolution of the carbonate cement occurred (compare Figure 3.3b with Figure 3.1a vs. 3.1b). The underlying cause for the short-term resistance is still subject to discussion, but the lodging of fine carbonate particles where the flow channels narrow is certainly a plausible explanation. In the field, the subsequent dissolution of these particles may provide an explanation for why it was possible to maintain a steady flow into the formation, rather than having the flow fall off as would be predicted based on the laboratory flow tests.

If one were to ask whether a steady input flow might be maintained for many years (e.g., as would be necessary at an "industrial scale" sequestration site) the answer would probably be "no." The incipient clay growth was observed experimentally after less than two years, and our models indicate that (eventually) argillization will become a pervasive theme in the mineralogic evolution of the formation. The new clays will certainly block the pore throats and should greatly impede the flow of fluids into the rock. However, this development has a positive side in that the clays will also greatly impede CO_2 leakage out of the formation, thus improving the long-term performance of the site. This is particularly important, since the models also suggest that CO_2-rock-pore fluid interactions are unlikely to transform a large percentage of CO_2 into a nongaseous form that could be permanently fixed in the rock.

Finally, with regard to other potential sites, one concern would be the onset of calcium sulfate precipitation. This could, in short order, significantly decrease the permeability of a potential host rock and create problems in getting the gas into the ground. Our models suggest that this problem is unlikely at our field test site. However, one might plausibly encounter enough sulfate elsewhere for this to be a problem. Another general observation is that only very limited amounts of carbonate minerals dissolve, even at high injection pressures. In addition to further limiting the ability of a formation to permanently "fix" the CO_2, this also implies that the development of an increased volume of new pore space would not be anticipated, even though a potential host rock might contain a high proportion of carbonate minerals.

Table 3.1. Pre- and post-test brine chemistry.

	Al (ppm)	Si (ppm)	Na (ppt)	K (ppt)	Mg (ppt)	Ca (ppt)	Cl (ppt)	SO4 (ppt)	HCO3 (ppt)
Pre-Test	0.05	12.3	52.4	1.6	3.1	3.1	109	1.8	0.12
Post-Test	0.33	3.6	53.5	1.6	4.2	3.8	104	1.8	-----

19 Months at 40º C, CO_2 pressure of 47.6 atm, starting fluid, "Pre-Test", from Stivason Federal wells #4,#5

Table 3.2. Comparison of activity coefficients from REACT and EQ3/6 using a Pitzer database: EQ3/6 (top) and REACT (bottom)

Cl^- Gamma	Na^+ Gamma	$CO_2(aq)$ Gamma	Mg^{++} Gamma	Ca^{++} Gamma	K^+ Gamma	SO_4^{--} Gamma	HCO_3^- Gamma	
0.937346	0.702425	1.715537	0.444017	0.093972	0.537898	0.087801	0.651178	EQ3/6
0.625893	0.712689	1	0.30662	0.210426	0.625749	0.111199	0.748859	**REACT**

Gamma EQ3/6 divided by Gamma REACT

Cl^- Gamma	Na^+ Gamma	$CO_2(aq)$ Gamma	Mg^{++} Gamma	Ca^{++} Gamma	K^+ Gamma	SO_4^{--} Gamma	HCO_3^- Gamma
1.497614	0.985598	1.715537	1.448105	0.446581	0.859607	0.789587	0.869561

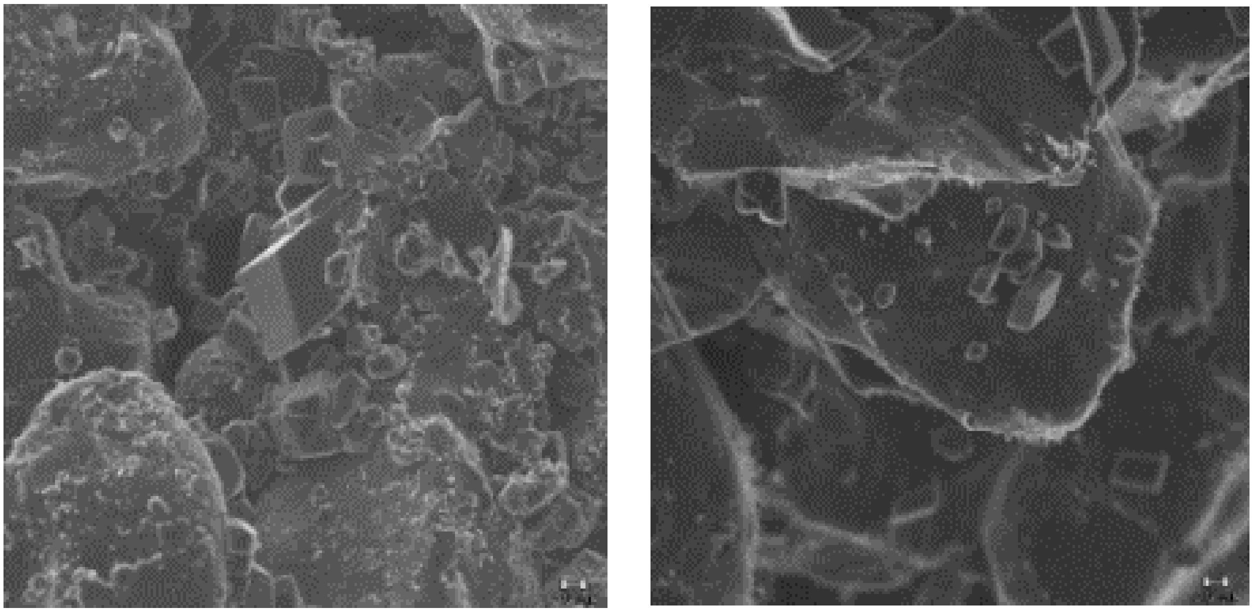

Figure 3.1. Left (a) – Pre-test sample not exposed to CO_2. Right (b) – Appearance after being exposed to 700 psi CO_2 for 6.5 months.

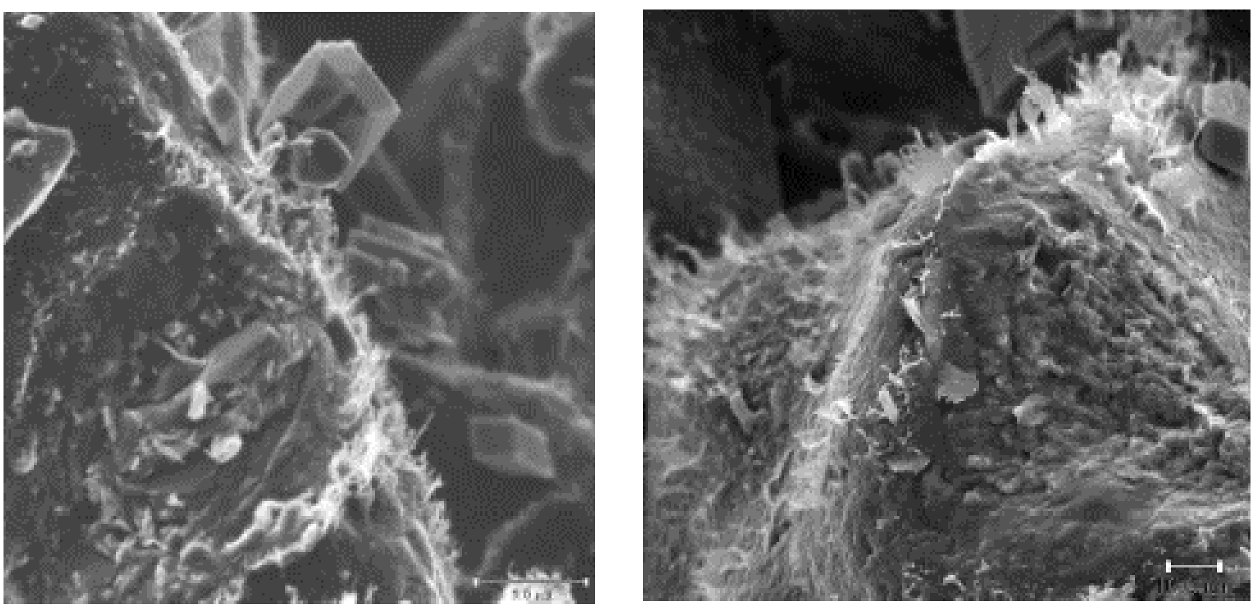

Figure 3.2. Left (a) – 6.5 months CO_2 exposure, Note high-Mg carbonate crystal at top of the picture and incipient clay growth on the edge of the grain. Right (b) – Well developed clays formed after 19 months exposure to 700 psi CO_2.

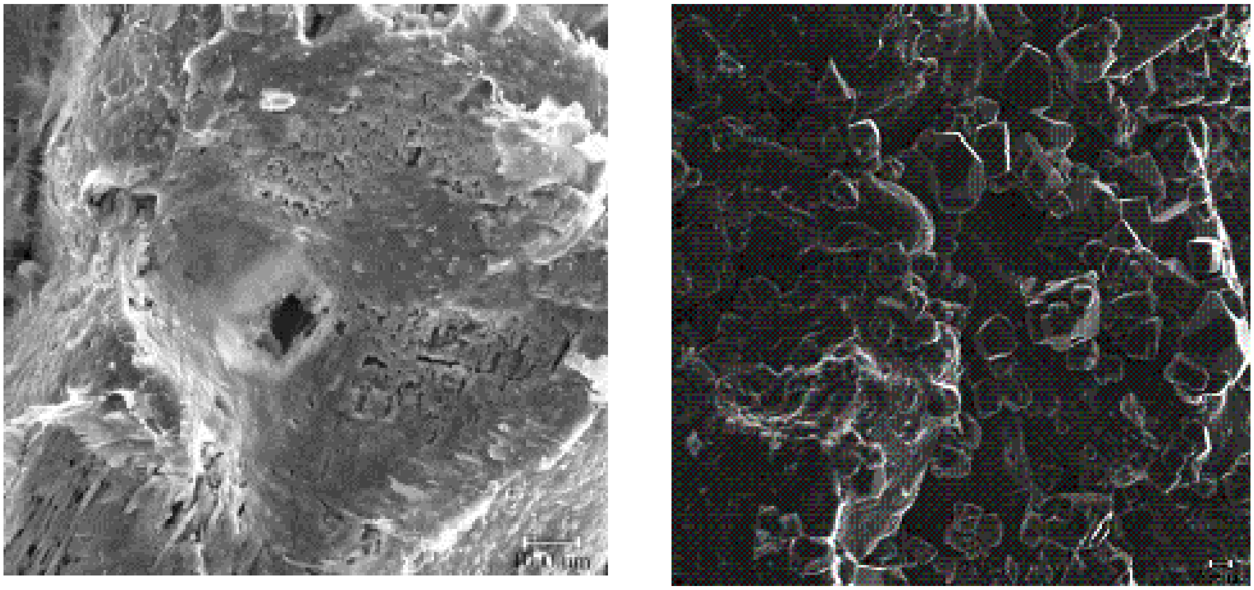

Figure 3.3. Left (a) – Etched plagioclase grain formed after 19 months exposure to 700 psi CO_2. Right (b) – Post-test sample from flow-through experiment. Note: short-term exposure removes little carbonate (Krumhansl et al., 2002).

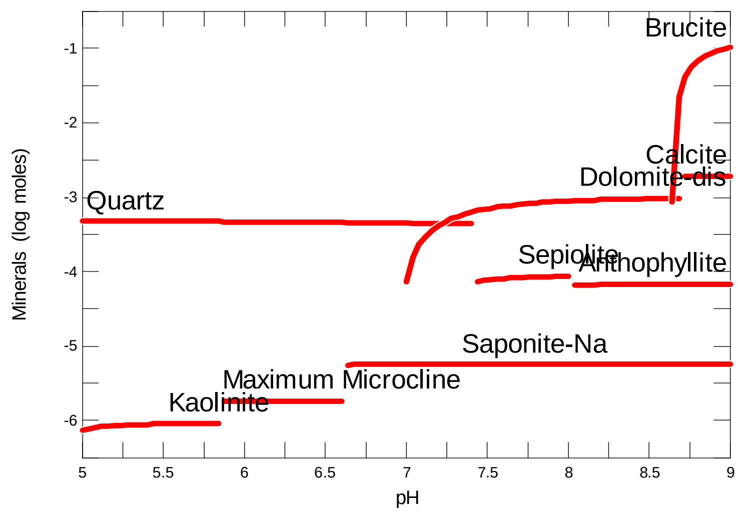

Figure 3.4. Minerals predicted to be compatible with Pearl Queen brine as a function of pH. (Suppressed minerals include antigorite, muscovite, phengite, phlogopite, chrysotile, dolomite-ord, tremolite, magnesite, saponite-Ca, saponite-Mg, saponite-H, saponite-K, talc, paragonite, clinochlore-14A, diopside, dawsonite, clinochlore-7A, amesite-14A.)

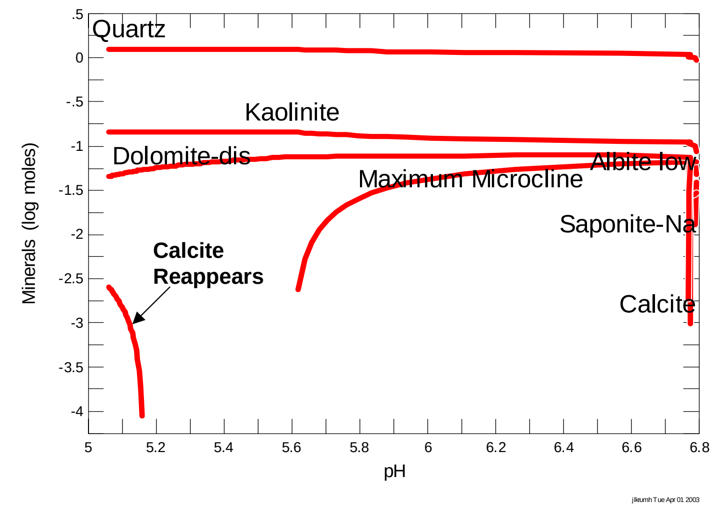

Figure 3.5. Impact of reacting CO_2 with Pearl Queen brine plus minerals. Prior to adding CO_2 (right side of figure) the pH was about 6.8. When the CO_2 partial pressure reaches 700 psi (far left of figure) the pH is about 5.1. Curve in lower left of figure marks reappearance of calcite. (Suppressed species: antigorite, muscovite, phengite, phlogopite, chrysotile, dolomite, dolomite-ord, tremolite, magnesite, saponite-Ca, saponite-Mg, saponite-H, saponite-K, talc, paragonite, clinochl-14A, diopside, dawsonite, clinochlore-7A, amesite-14A, gibbsite, and alunite.)

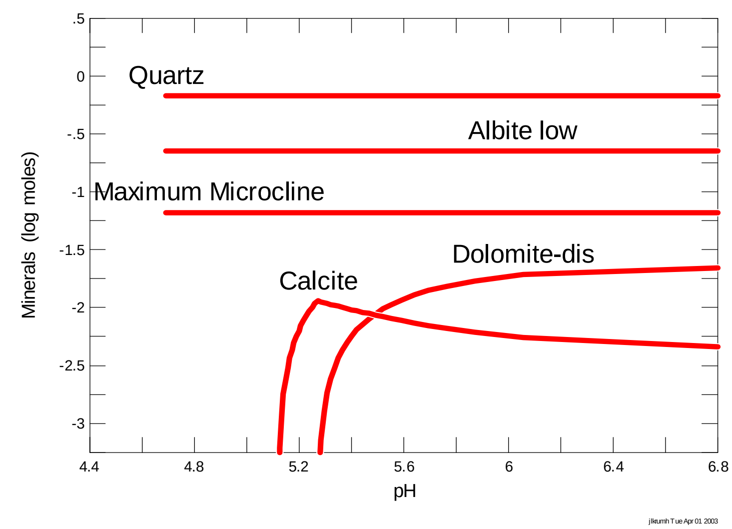

Figure 3.6. Effect of reacting CO_2 with Pearl Queen brine plus minerals while suppressing the appearance of all clays. The model was the same as that which produced Figure 5 except that kaolinite and Na-saponite were also suppressed. Prior to adding CO_2 (right side of figure) the pH was about 6.8. When the CO_2 partial pressure reaches 700 psi (left side of the figure), the pH is about 4.6.

4.0 PRE-INJECTION BOREHOLE GEOPHYSICS

Geophysical site characterization studies consisted of running deviation surveys in wells 4 and 5, running dipole sonic logs in wells 4 and 5, and performing a crosswell survey between wells 4 and 5. Most of this work was performed in 2002.

4.1 DEVIATION SURVEYS

Figure 4.1 shows relative deviation plot of wells 4 and 5, and Figure 4.2 shows the difference in separation distance between the wells. Figures 4.3 and 4.4 show the individual deviations of the two wells. Both wells are very straight, and the little deviation that there is occurs in the same directions. Distance between the two wells varies only marginally with depth and is about 1310 ft at the depth of the reservoir. Table 4.1 gives values of the deviation as a function of depth.

4.2 DIPOLE SONIC LOGS

Compressional (P) and shear velocities (S) for wells 4 and 5, as obtained from cased-well dipole-sonic logs, are shown in Figures 4.5 and 4.6. There is considerable variation in the noncarbonate p-wave velocities between the two wells and, in particular, for the Queen Sandstone at about 4500 to 4530 ft. This discrepancy could be partially because of difficulty in measuring the velocity through casing, but the crosswell tomogram verified these results (to the extent possible, given that the log velocities are used as mild constraints on the tomogram). The carbonates are fairly consistent with P-wave velocities at about 22,000 ft/sec in both wells and S-wave velocities at just under 12,000 ft/sec in both wells. Shaley rocks have P-wave velocities around 12,000 ft/sec and S-wave velocities around 7000 ft/sec, while sandstones have P waves in the 14,000 to 15,000 ft/sec velocity range and S waves in the 8000 to 9000 ft/sec velocity range.

4.3 CROSSWELL SURVEY

The pre-injection crosswell survey was performed by Geospace Engineering Resources, Inc., and analyzed by Wellseismic Computing Services. The survey was run in April of 2002. The airgun source was located in well 4, and shots were taken between depths of 3523 and 4935 ft at separations of 9.84 ft at depths less than 4015 ft and separations of 4.92 ft at greater depths. The receivers were situated in well 5, and they were spaced at 4.92 ft and positioned at depths from 4023 to 4929 ft. A 24-level array of triaxial geophones (SMC 1850–15 Hz) sampling at 0.5 msec was used for acquisition. The geometry of the survey relative to the P-wave velocities is shown in Figure 4.7.

4.4 PROCESSING

The data quality was only fair, but both P-wave and S-wave velocity tomograms were able to be computed. The time picks on the P-wave arrivals were more reliable than those for the S waves, since the S waves were contaminated by tube wave noise. Figure 4.8 shows an example of a raw common receiver gather (4697 ft) that is typical of the observed data. Some points noted during processing include the following:

- Tube waves are very strong. They are generated in the source well and couple into the formation at perforations or other irregularities inside the well. There appear to be many such coupling locations, and the tube waves are converted to both P and S waves.

- The H1 component is dominated by reverberations of some sort. This is very common on at least one, and often times both, of the horizontal components.
- The direct P-wave can be seen on the H2 and vertical components intersecting the right side of the sections at about 80 msecs.
- The direct S-wave is seen on the vertical component intersecting the left side of the section at about 200 msec.
- Numerous S-wave reflections can be seen on the vertical component emerging from the direct S wave and dipping downward to the right. P-wave reflections, however, are not visible.

Figure 4.9 shows the same 4697-ft common receiver gather after using a 15 msec AEC and 20–40/150–300 Hz band-pass filter. The 32 msec airgun time delay was also removed from the data. In this case, the P-wave direct arrival can be seen fairly well on both the vertical and the H2 components, and the S-wave direct arrival is strong on the verticals. The shear reflections are very clear, but it is still difficult to identify any P-wave reflections.

An enlarged view of the vertical component of this common receiver gather is shown in Figure 4.10. The P-wave reflections can be seen in this plot, although they are not as clear as the shear reflections. Source-well tube waves can be seen to originate from many different depths. Most interesting is the inconsistency of the waveforms associated with direct arrivals, with direct arrivals disappearing over some depth intervals and shear-wave reflections looking more stable than the direct shear waves.

The processing steps taken on the data are as follows:

1. Pick airgun time delays for each shot and subtract them from the traces.
2. AEC with a time gate of 15 msec to equalize trace amplitudes and attenuate noise bursts.
3. Band-pass filter; full pass between the frequencies of 40 and 150 Hz with a fairly gentle attenuation outside the pass band.
4. Pick the arrival times for both the P and S direct arrivals.
5. Sort all data by common receivers and apply FK filter to remove tube wave noise. Filter parameters were specified to attenuate coherent energy with apparent velocities between +7000 and –7000 ft/sec.
6. Re-sort FK-filtered traces into common shot gathers. Separate up-going and down-going reflections by FK filters designed to attenuate coherent energy dipping in a direction opposite to that of the reflections.
7. Apply fxdecon, a trace-to-trace coherency enhancement filter, to improve the signal to noise ratio.
8. Apply a modified prestack Kirchhoff depth migration to each of four datasets (up and down going P and S-wave reflections on common-shot gathers). Merge the up and down going P-wave reflections and the up and down going S-wave reflections.

The primary objective was to attenuate tube waves and other noise, equalize the waveforms, and separate the up and down going reflections. About 10% of the P-wave travel-time picks were questionable and were sometimes made with the help of theoretical computed times using the sonic log. However, picking the arrival times on both common-shot and common-receiver gathers helped assure consistency. About 20% of the S-wave travel-time picks were questionable, and many of those could not be resolved when shot and receiver gathers were correlated. These uncertainties make the S-wave velocity tomogram less reliable than the P-wave velocity tomogram.

Figures 4.11 and 4.12 show the up and down going P-wave reflections, respectively, and Figures 4.13 and 14 show the up-going and down-going S-wave reflections, respectively, for the vertical component. Some additional points noted in processing are the following:

- The modification to the Kirchhoff migration makes it similar to a VSP-CDP transform. The migration operator weights are zero unless the migrated data point is a specular reflection from an assumed horizontal reflector.
- Since both wells were deviated as much as 40 feet from the wellhead position, the migration operator had to be computed in three dimensions. The image section, however, is in two dimensions; it is a vertical slice connecting the two wells at an offset 20 feet south of the wellheads. This is approximately the crossline deviation of the wells at the survey depths.
- The migration velocities were determined by linearly interpolating the sonic and S-wave velocity logs between the two wells and assuming the velocities were invariant in crossline direction. The velocity models (P and S) were defined on a 10-foot grid, which represents the averaging length on the log velocities.
- The pre-migrated reflections shown in Figures 4.11 to 4.14 are the vertical component; the data quality was just not good enough to see reflections on the horizontal components.
- The down-going reflections are of better quality than the up-going, since they occupy a region that is less affected by tube wave noise. The S-wave reflections are also of better quality than the P waves. This may be because the reflections are hitting the receivers at a fairly high vertical angle of incidence so more of the S-wave energy appears on the vertical components. Also, some P-wave reflections may have been over-ridden, and consequently muted out by the direct S waves.
- There is a lot of “wormy” coherence, particularly on the P-wave sections, which is from the FK filter response on the high-amplitude noise. Some of this coherence gets attenuated by the considerable amount of trace mixing that takes place in migration; however, some of this filter noise will remain to have a deleterious effect on the process.

4.5 TOMOGRAPHIC INVERSION

The tomography inversion program used by Wellseismic Computing Services is the classical one that determines the velocities on a uniform gridded model by minimizing the r.m.s. difference between the observed travel times and the theoretical travel times through the model. The theoretical times are computed by a finite difference solution to the Eikonal equation, and rays are backprojected through the model along the path of steepest travel time descent. Each observation creates an equation stating that the travel time of the ray through the model is equal to the observed time. As in migration, the model is in three dimensions to accommodate the deviated wells. Also as in migration, the model was constrained to be invariant in the Y dimension. The model cells are 10 feet on a side with 142 of them in the X direction and 144 in the Z direction. However, tomogram velocities were computed only for depths between 4000 and 4900 feet, the interval covered by both shots and receivers. The number of unknown velocities was therefore 90*142 = 12780. For both P and S waves, there are about 34,000 travel time equations and 12780 unknown velocities. With more equations than unknowns, the solution is obtainable using some form of least-squares technique, which in this case is a modified form of conjugate gradients.

The following constraints were used to regularize the solution from the inversion. These constraints are necessary because these types of inversions are typically unstable.

1. Augment the travel time equations with equations stating that the unknown velocities are equal to those of the starting model. Weights were applied to these constraint equations, which were about 10 percent of the maximum strength of the travel time observations. Thus, zones in the model that were densely sampled by crisscrossing raypaths were not influenced by the constraints nearly as much as the sparsely sampled areas.
2. Augment the travel time equations with equations stating that the velocities are smoothly varying; this constraint is sometimes referred to as Tikhonov regularization.
3. Enlarge the horizontal grid interval from 10 to 200 feet within the solution equations. For raytracing, however, the velocities were interpolated from the coarse grid back to the fine grid. The final tomograms are expressed on the fine grid.

Velocity tomograms derived from the inversion are shown in Figures 4.15 and 4.16 for P waves and S waves, respectively. In addition to the tomograms, derived velocity logs (magenta) are also shown for the two wells, and these are plotted with the measured velocities using a dipole sonic log (black). Note that the dipole-sonic data have been averaged to the same resolution as the crosswell data to facilitate identification of differences and similarities. The West Pearl Queen reservoir is the low velocity zone between 4500 and 4600 ft depth. Some additional features noted during processing include the following:

- The trace plots on either side of the computed tomogram are the 10-ft-averaged log velocities (in black) and the tomogram velocities at the well locations (in magenta). They agree reasonably well above about 4600 feet, but there are discrepancies below that depth, particularly for the P waves in the Stivason 5 well. This may be because of the 200 foot horizontal averaging of the tomogram velocities, suggesting that the velocities may vary quite a bit in the lateral direction.
- The r.m.s. time difference between the observed and computed times is about 0.8 msec for P waves and 1.6 msec for Shear waves. The largest errors appear on the near-zero, vertical-offset traces at the top and bottom of the survey where the picks were most questionable. There does not appear to be any systematic pattern in the error distribution that would indicate an anisotropy effect—such as all positive errors on the far offset traces and negative errors on the near offset traces.
- The tomogram velocities within the reservoir remain very close to those in the starting model. The thickness of the reservoir is probably right at the edge of the vertical resolving power of the method, so details of the velocity distribution within the reservoir will not be detected. However other equally thin layers within the starting model have been significantly altered in the tomography inversion, suggesting that major changes within the reservoir from CO_2 sequestration may be detected in a future survey.
- The sharp boundaries and thin layering in the starting model carry over into the solution because such layering is below the resolving power of the data. Tomography inversion is changing only the low-frequency components of the velocity distribution. The high-frequency components are retained in the inversion by the constraint equations, so as mentioned earlier, the reliability of these results depends on the credibility of the constraints.
- The P and S wave velocities show a general consistency except for the high-velocity lens between about 4700 and 4800 feet. The two lenses are offset from one another by about 400 feet, and their shapes are somewhat different. While the small differences in the two shapes may be explained by the limited resolution, the offset is definitely an outcome of the inversion. For it to be incorrect, many hundreds of travel time picks would also have to be incorrect.

To check on the shift in layering at the bottom of the survey, two additional inversions were run to see if the results were affected by the starting model. In all cases, the offset in the high-velocity lenses were obtained regardless of starting model, suggesting that the shift is dictated by the arrivals (not the model). However, this shift is unexpected and may be from errors in the arrival-time picks or an artifact.

4.6 REFLECTION IMAGES

The P-wave and S-wave shot gathers (192 for each wave type) were migrated using a modified Kirchhoff scheme that makes it equivalent to a CDP-VSP transform. There were four migrations, one each for up-going and down-going P and S waves. The two migrations for each wave type were merged to form a complete P and S reflection image.

Figure 4.17 shows the reflection image for the P wave compared to synthetic traces computed from the logs. The negative reflection at the top of the West Pearl Queen reservoir can be clearly seen at about 4500 ft. Data quality of the P-wave reflections is good above and through the reservoir interval, but is poor near the bottom. Figure 4.18 shows the Shear-wave reflection image. The S-wave reflections are much better than the P-wave reflections in terms of both higher frequency and higher coherence. Many of the S-wave reflectors correlate well with the P-wave reflectors, and the reservoir also shows up as a strong negative reflection

Table 4.1. Differential deviation-survey data

East (ft)	North (ft)	Depth (ft)	Total (ft)
1310	0	0	1310
1309.98	0.1	200	1309.98
1309.77	1.19	400	1309.771
1309.92	2.97	600	1309.923
1310.75	5.33	800	1310.761
1310.88	6.47	1000	1310.896
1309.77	6.93	1200	1309.788
1307.64	7.34	1400	1307.661
1305.38	7.94	1600	1305.404
1303.79	8.57	1800	1303.818
1303.42	9.1	2000	1303.452
1304.14	9.69	2200	1304.176
1305.33	10.69	2400	1305.374
1307.33	11.49	2600	1307.38
1308.97	11.51	2800	1309.021
1310.93	11.62	3000	1310.981
1314.47	12.42	3200	1314.529
1317.91	13.97	3400	1317.984
1319.01	14.79	3600	1319.093
1317.93	14.79	3800	1318.013
1315.89	15.59	4000	1315.982
1313.38	16.57	4200	1313.485
1310.28	17.2	4400	1310.393
1306.66	18.02	4600	1306.784
1302.96	18.52	4800	1303.092

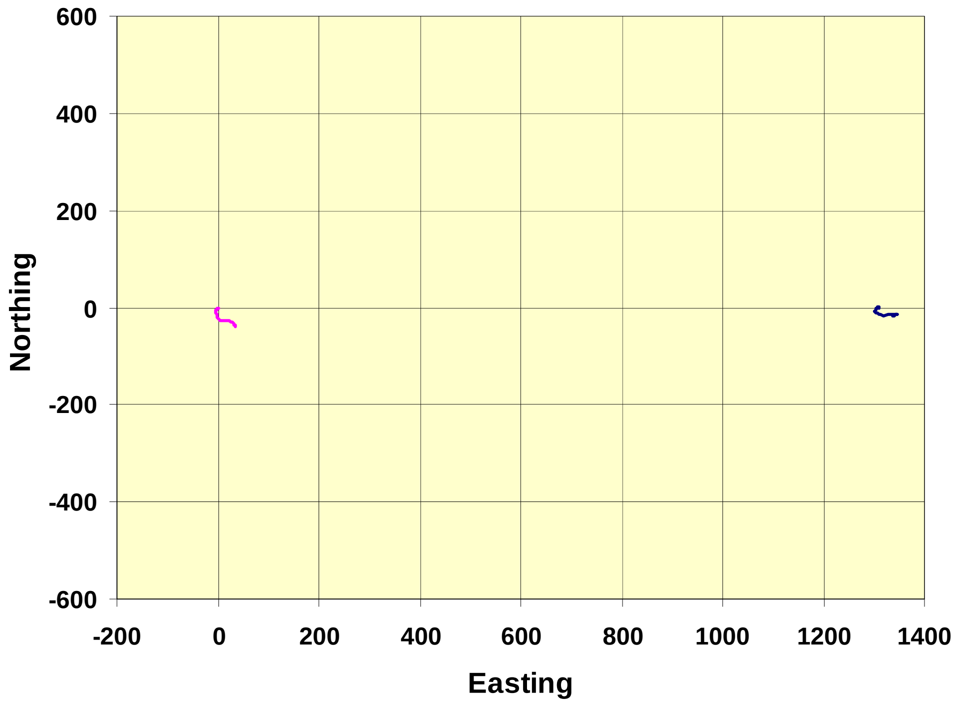

Figure 4.1. Trajectories of wells 4 and 5 from deviation survey.

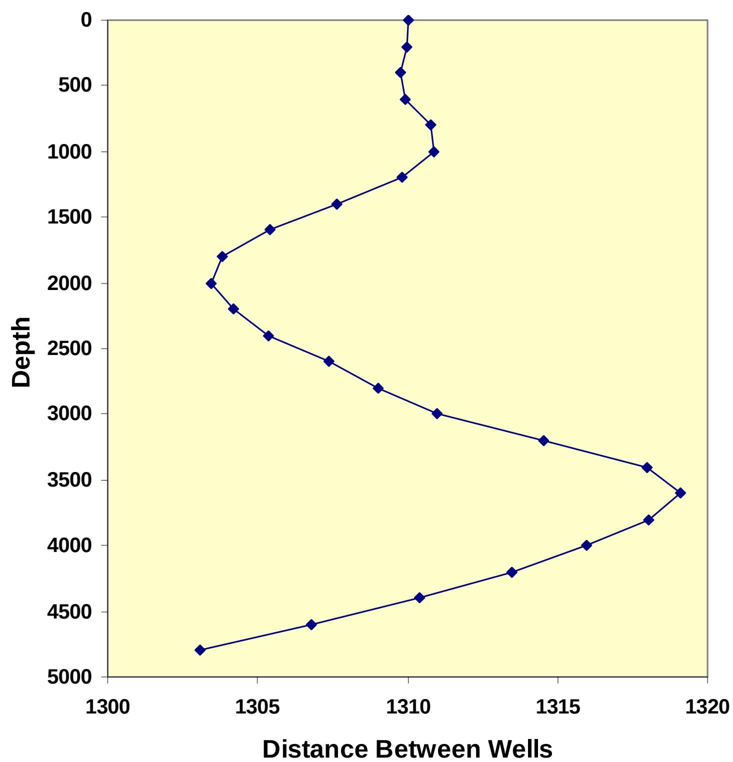

Figure 4.2. Variation of well separation with depth.

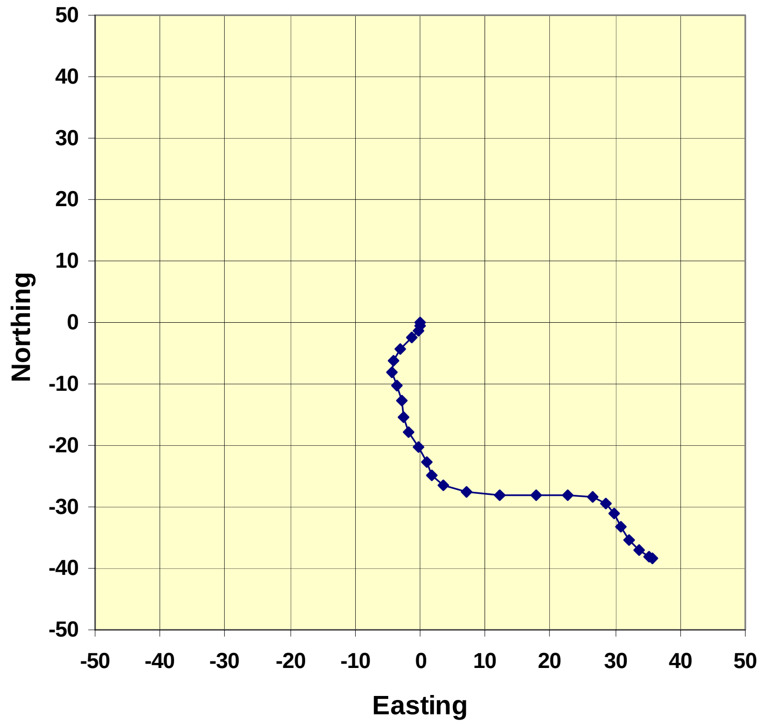

Figure 4.3. Deviation trajectory of well #4.

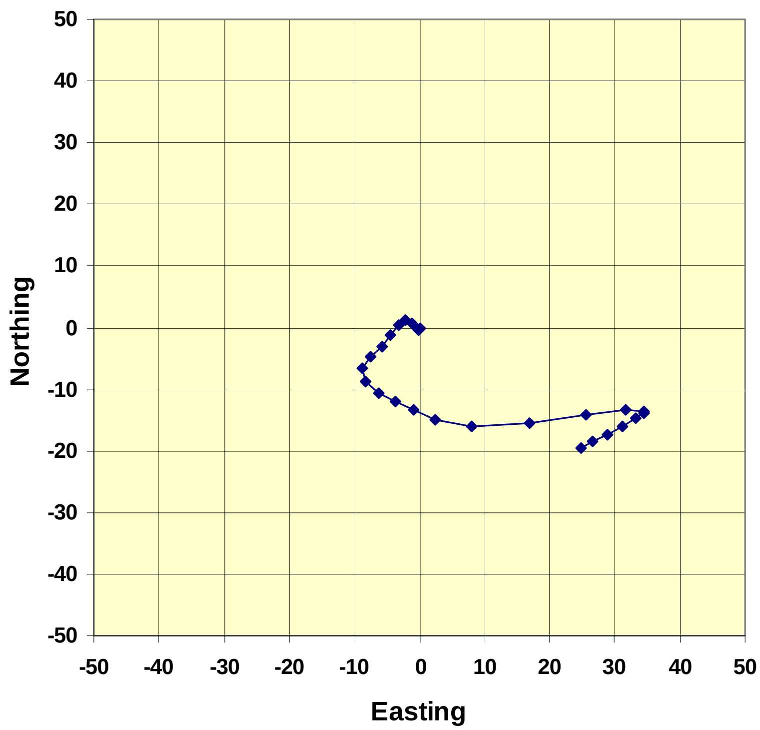

Figure 4.4. Deviation trajectory of well #5.

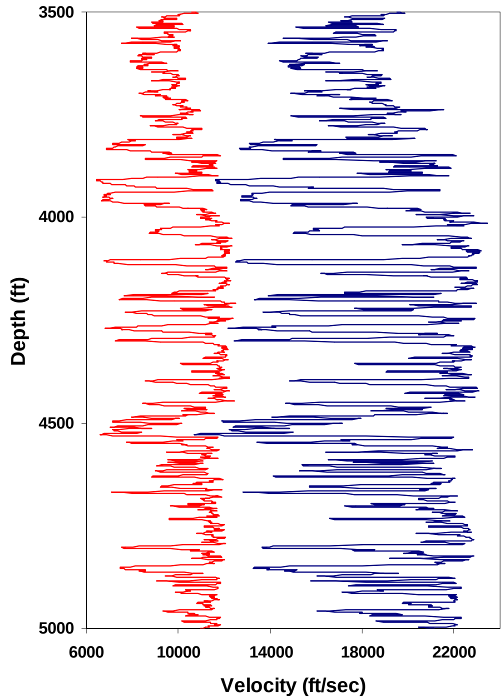

Figure 4.5. Dipole sonic log velocities for well #4.

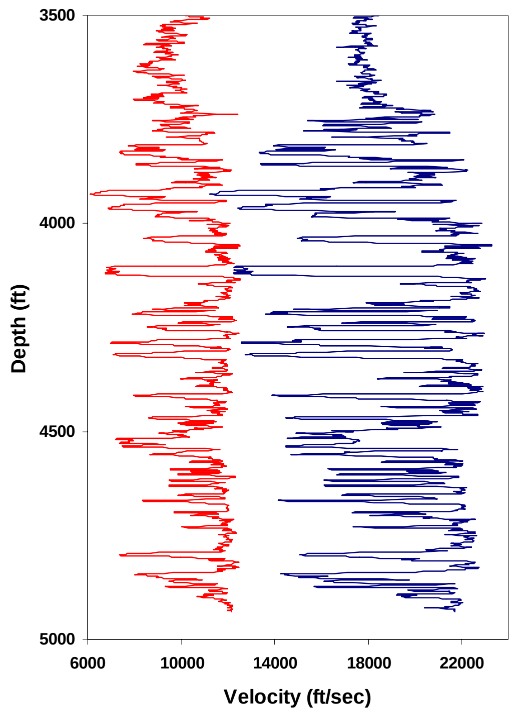

Figure 4.6. Dipole sonic log velocities for well #5.

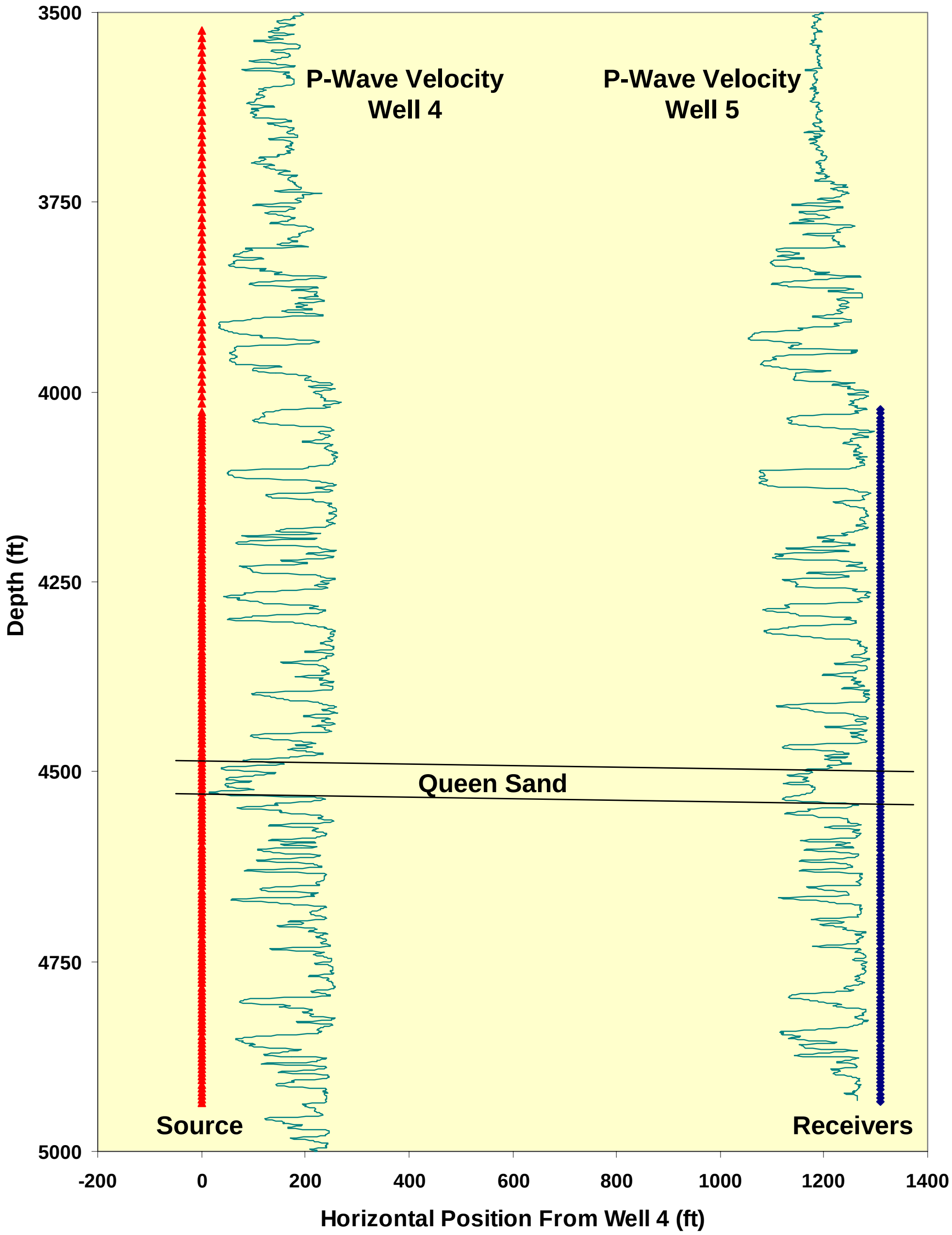

Figure 4.7. Geometry of sources and receivers for crosswell survey.

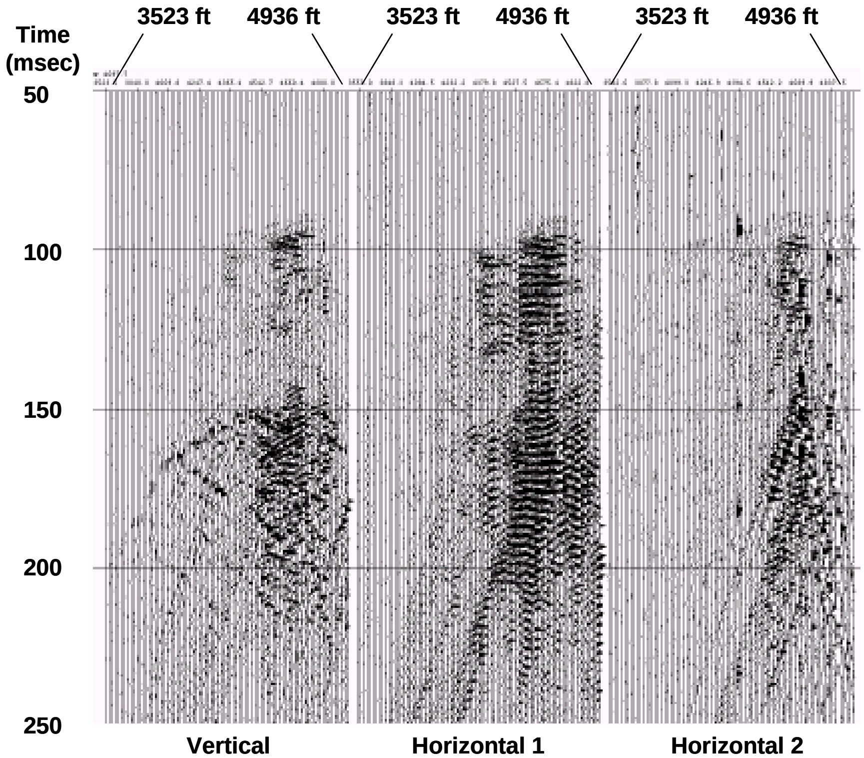

Figure 4.8. Unprocessed traces from 4697-ft common receiver gather.

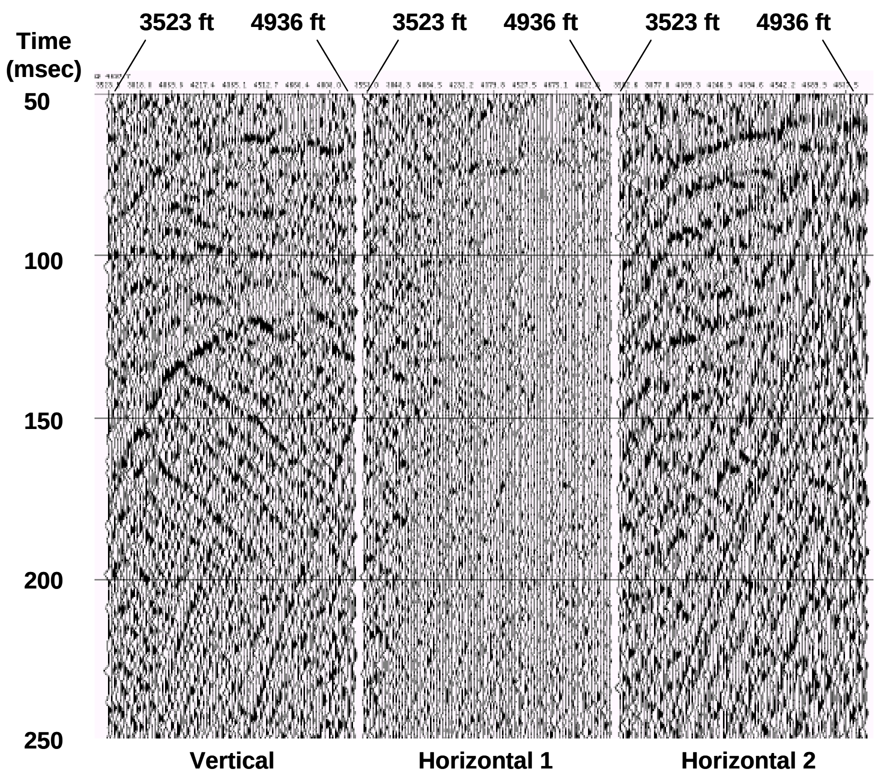

Figure 4.9. Traces from 4697-ft common receiver gather after signal processing.

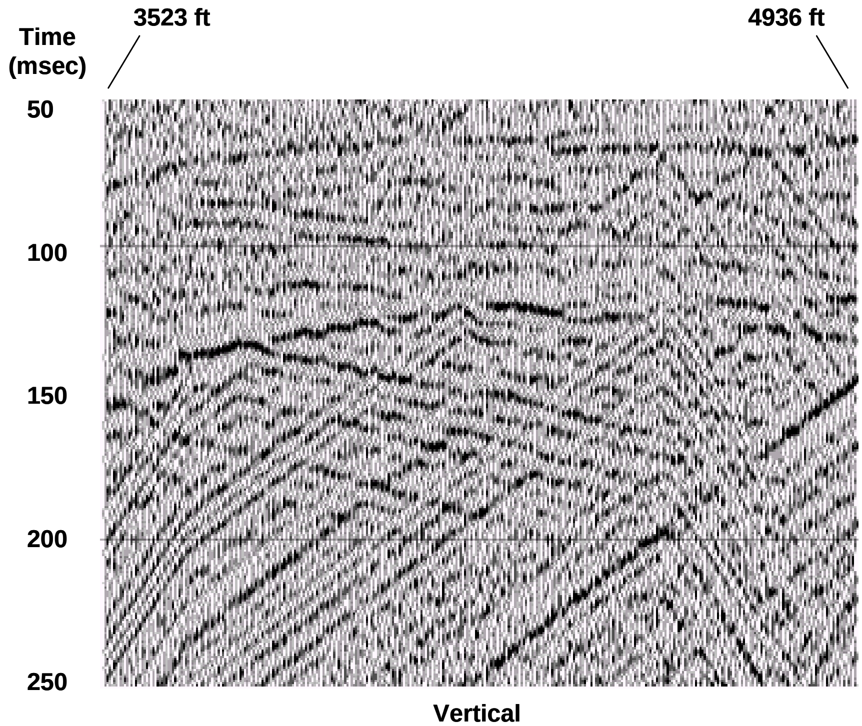

Figure 4.10. Enlarged view of the vertical component of the 4697-ft common receiver gather.

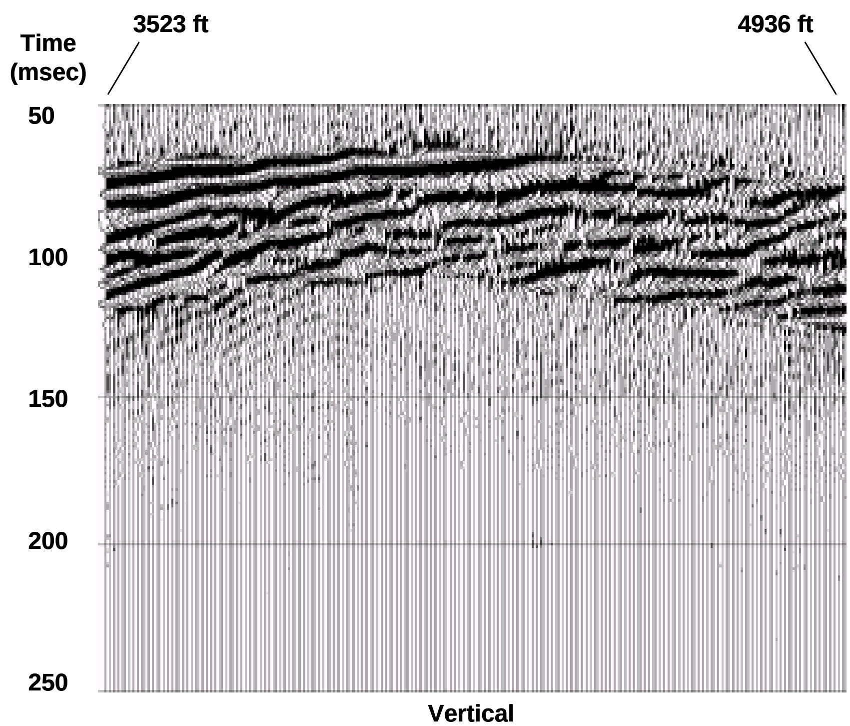

Figure 4.11. Up-going P-wave reflections from the 4415 common-shot gather.

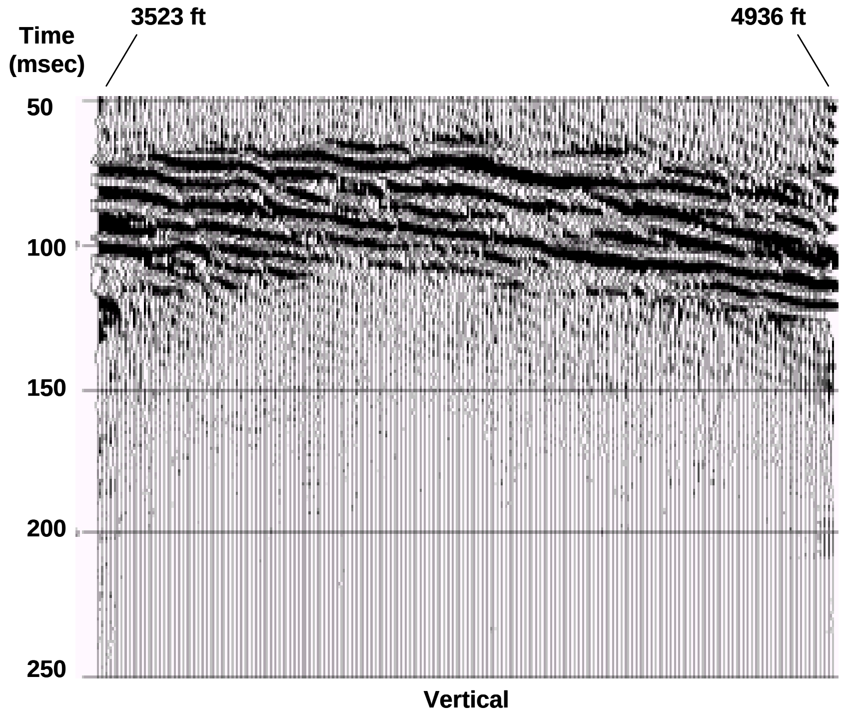

Figure 4.12. Down-going P-wave reflections from 4415 common shot gather.

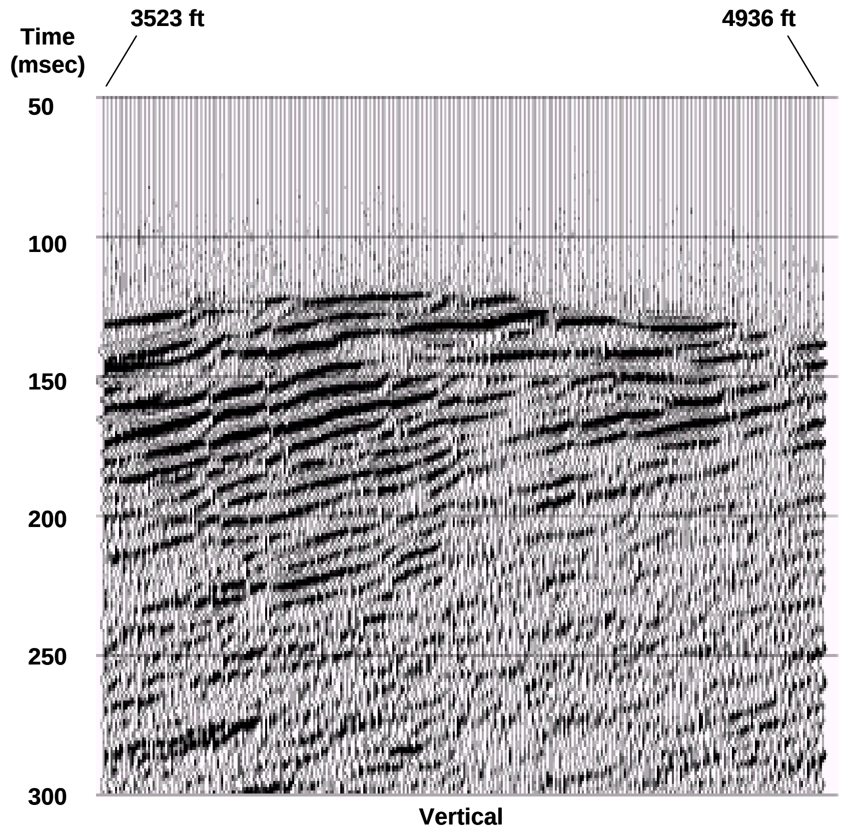

Figure 4.13. Up-going shear wave reflections from the 4415 common shot gather.

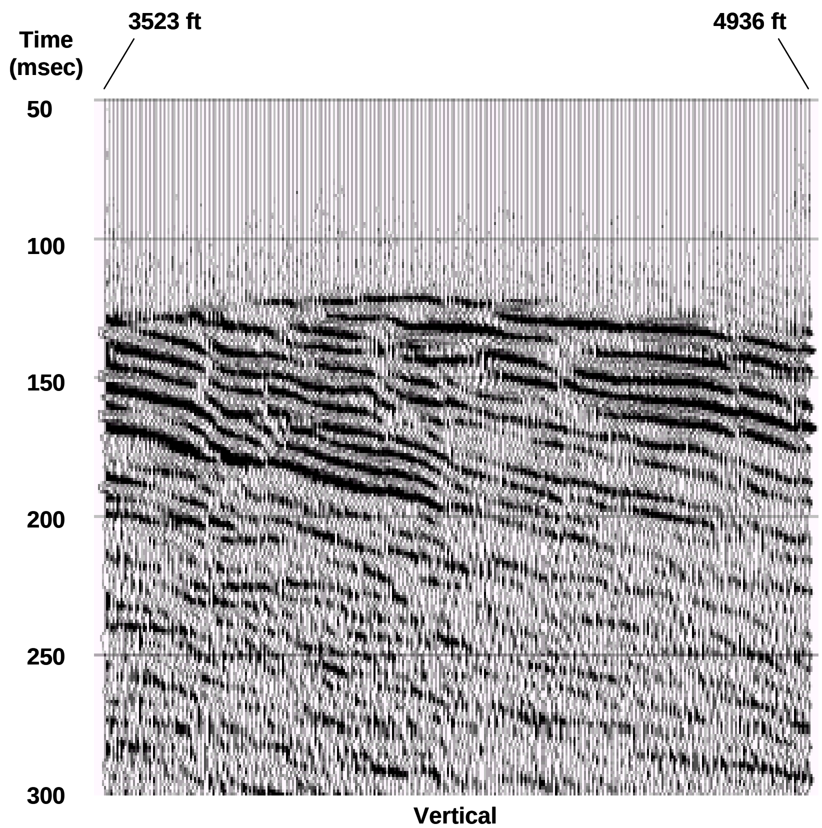

Figure 4.14. Down-going shear wave reflections from the 4415 common shot gather.

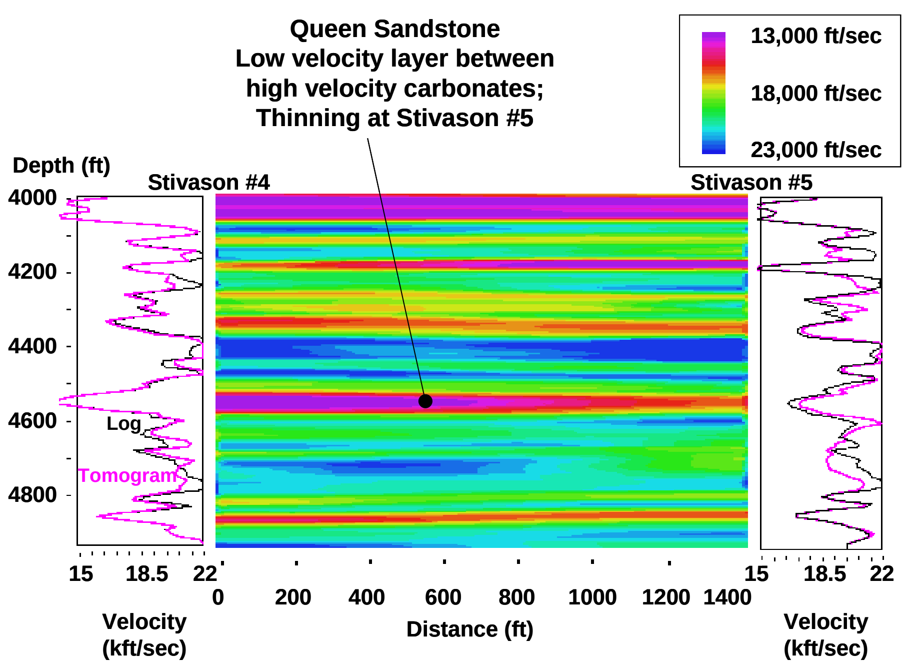

Figure 4.15. Tomogram of P wave (center) and derived and measured log velocities.

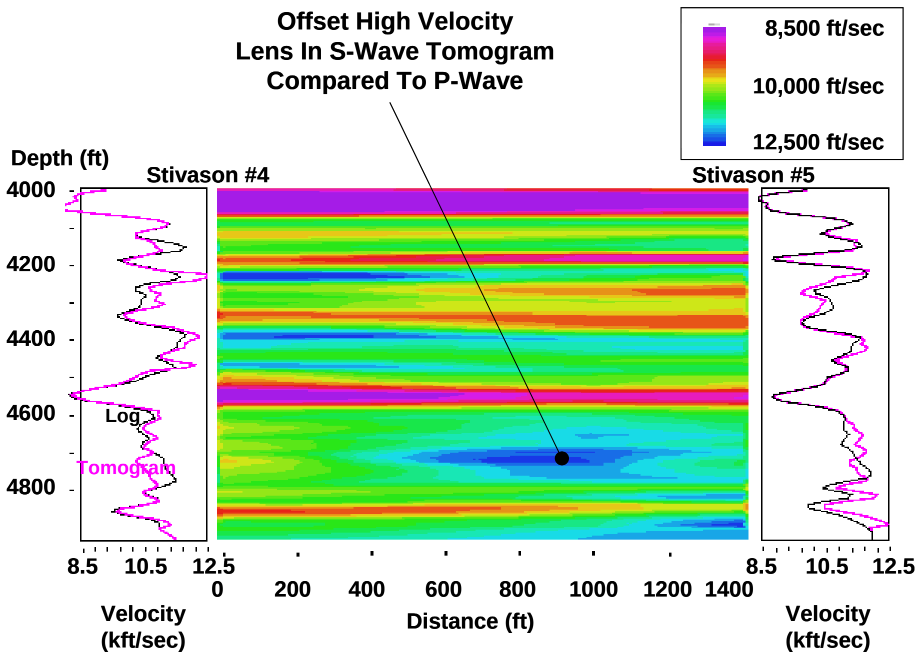

Figure 4.16. Tomogram of S wave (center) and derived and measured log velocities (sides) for pre-injection crosswell survey between wells #4 and #5.

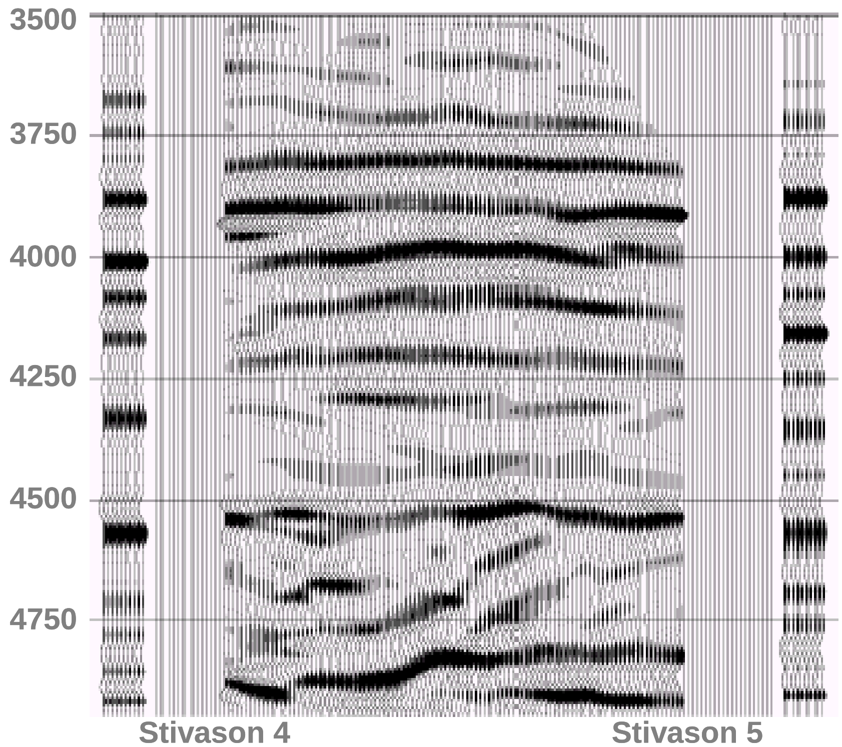

Figure 4.17. Reflection image for P waves constructed from crosswell survey data (center) and compared with synthetic reflection images at the wells (sides).

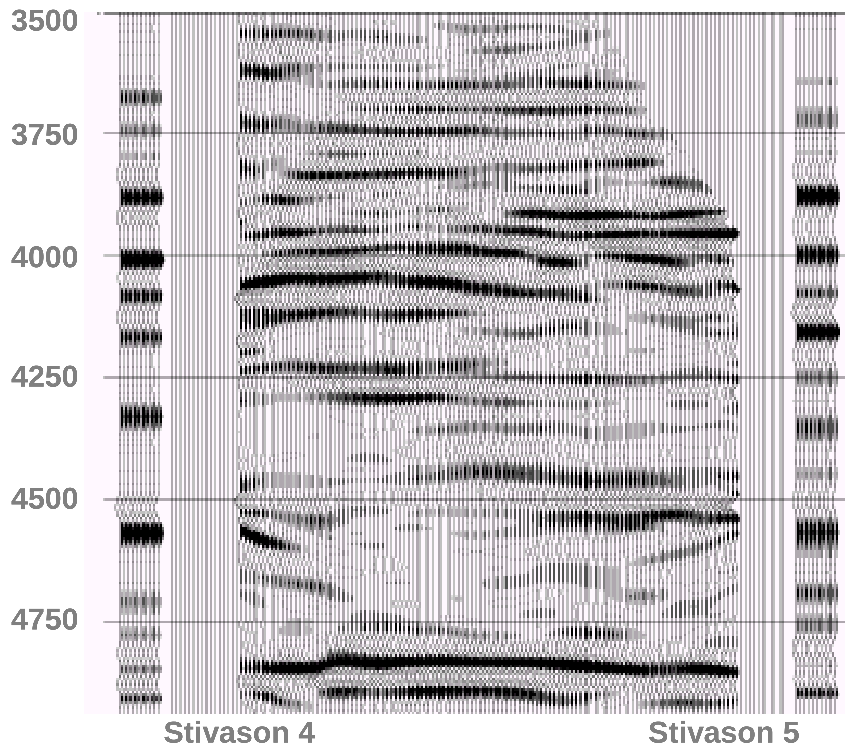

Figure 4.18. Reflection image for S waves constructed from crosswell survey data (center) and compared with synthetic reflection images at the wells (sides).

5.0 INJECTION TEST

5.1 INJECTION AND BLOWDOWN

The injection tests consisted primarily of the CO_2 injection, soak, and final blowdown, with the associated monitoring of these periods. Access to the wells was limited during much of this period, so the monitoring consists of occasional bottom-hole pressure measurements, flow rate measurements during injection and blowdown, a microseismic monitoring test during the injection, and the second 3D, 9C surface seismic survey at the end of the soak. The injection consisted of 2090 tons of CO_2 that was pumped into the well over a 42 day period at a nearly constant surface pressure of 1400 psi and constant rate of approximately 220 bpd, as shown in Figure 5.1.

Figure 5.2 shows the pressure history during the soak and the initial blowdown. Pressure data were only taken at a couple of infrequent intervals, but sufficient data are available to fully characterize the pressure decay after injection. Of primary interest here is the relatively high pressure that still existed downhole at the end of the soak. Given that the starting reservoir pressure was only a few hundred psi, these results indicate that the CO_2 did not disperse widely during the injection and soak process.

Figures 5.3 and 5.4 show the pressure and temperature at the end of the soak and during the initial blowdown of the well. Pressure drops relatively rapidly to around 400 psi, while the temperature shows a drop and recovery that are probably related to expansion of gas. The gas flow rate during the blowdown is shown in Figure 5.5. There are two extended shut-in periods during which a pump was being placed in the well and other operations were taking place. The blowdown extended for over 80 days (including shut-in periods), and at the end of this period, the gas flow rate was only a few hundred standard cubic feet per hour. About 17% of the injected gas was recovered during this period.

A Horner plot of the pressure fall-off data is shown in Figure 5.6. Two slopes are shown on the curve, one of which is a very late-time slope and the second of which is an intermediate-time slope. Analysis of the fall-off data is very complicated because of the CO_2 phase changes occurring during the soak period. A rudimentary analysis, assuming a volume factor of 1.0 and a viscosity of 0.5 cp would yield k-h values on the order of tens of millidarcy-feet, which seems quite low. However, the exact composition of the CO_2 is not considered in such an analysis (e.g., a much lower viscosity representative of a supercritical fluid would increase k-h considerably), and the actual k-h could be one or more orders of magnitude greater. Detailed modeling will be required to extract appropriate parameters.

5.2 MICROSEISMIC MONITORING

Microseismic monitoring of the injection process was attempted during the injection. Unfortunately, the rates were too low to input sufficient energy into the formation to induce large enough microseisms to be detectable at the 1350-ft interwell spacing. The microseismic array consisted of a 12-level tri-axial array covering approximately 800 ft of vertical aperture in the #5 well. Multiple surface shots using an elastic-wave-generator source at the surface were recorded to orient the geophone string. Five shot positions were occupied surrounding the monitor well, offset 450 to 800 m from the wellhead to get adequate energy on the horizontal components. While receivers were adequately oriented, all instrumentation functioned perfectly, and noise conditions were excellent, only a limited number of unanalyzable events were detected with the array.

These events were not microseisms, but rather were small events that originated at a single spot in the wellbore and then propagated up and down the wellbore as tube waves. They were not observed prior to injection, so they are probably in some way related to the stress, pressure and temperature changes that were occurring because of injection, but they could not be analyzed because there was only a clear event signature on one or two levels, and their was only one phase arrival (both suggesting that it probably happened right at the monitor wellbore). Figures 5.7 and 5.8 show two such events, one originating near the bottom of the array and one near the middle. On the possibility that these "events" were related to stress, pressure and temperature changes caused by the injection, the origination point of the events was found, and these were plotted as a function of time in Figure 5.9. At first, all of the "events" are located near the bottom of the array, but they migrate upward relatively quickly. After a few days, the activity drops off considerably, but the activity that remains is concentrated in three zones at 4400–4500 ft, 4100–4200 ft, and 3800 ft.

5.3 FINAL BUILD-UP

Early in 2005, a final build-up was performed to assess the final state of the reservoir and possibly evaluate the reservoir pressure. This build-up was conducted with an echometer to determine fluid height and deduce bottom-hole pressure, assuming that the composition of the fluids is known.

Figure 5.10 shows the pressure behavior from this test and Figure 5.11 shows the Horner plot. The build-up lasted for 77 days in the Stivason #5 well and for 52 days in the Stivason #4 well. Unfortunately, the data suggest that there is more occurring than a simple build-up in the reservoir, as the pressure would appear to extrapolate to a pressure that is much too large (unless nearby water injection is raising the pressure continuously). The slope of the build-up would suggest a k-h that appears to be an order of magnitude lower than that deduced from pressure fall-off after the injection. As with the pressure fall-off data, detailed modeling will be needed to assess the reservoir conditions.

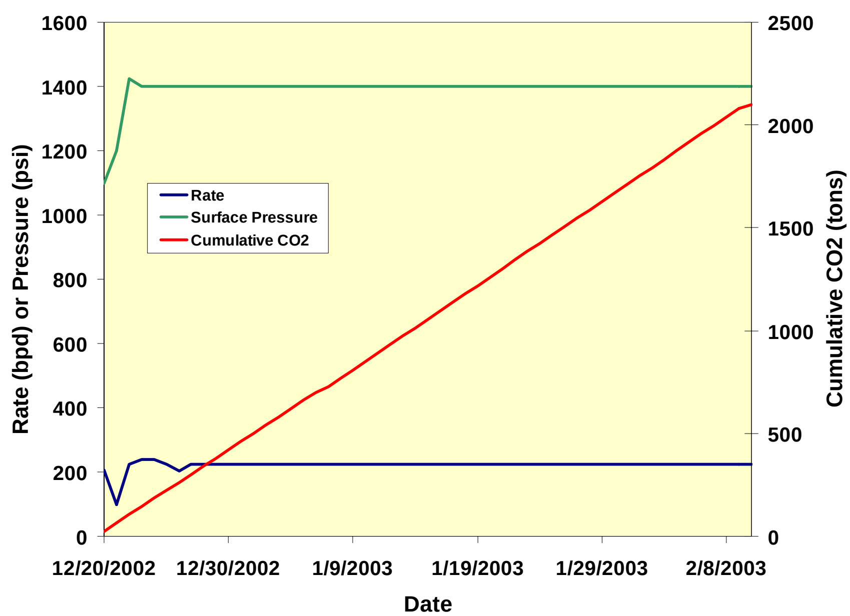

Figure 5.1. CO_2 injection history for West Pearl Queen reservoir.

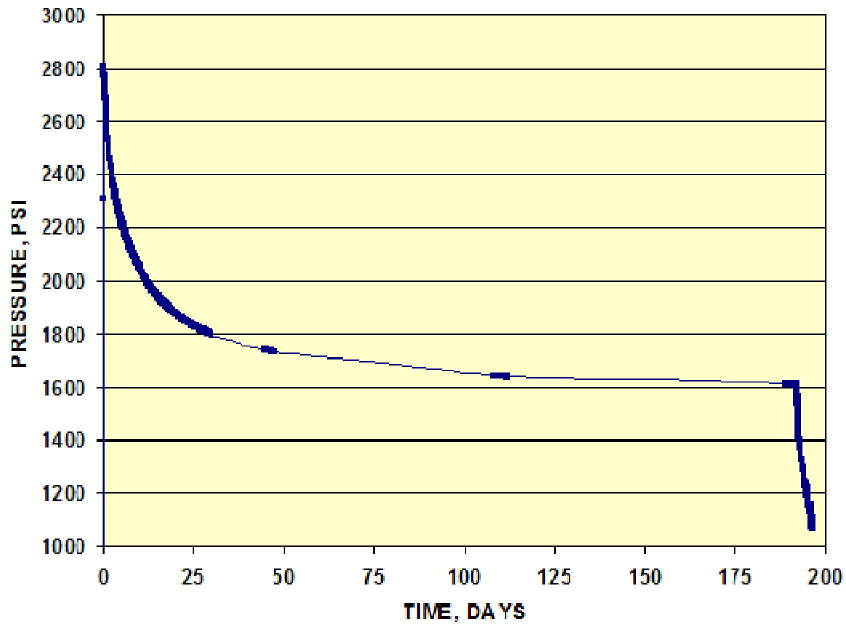

Figure 5.2. Pressure bleed off after injection in days since shut-in.

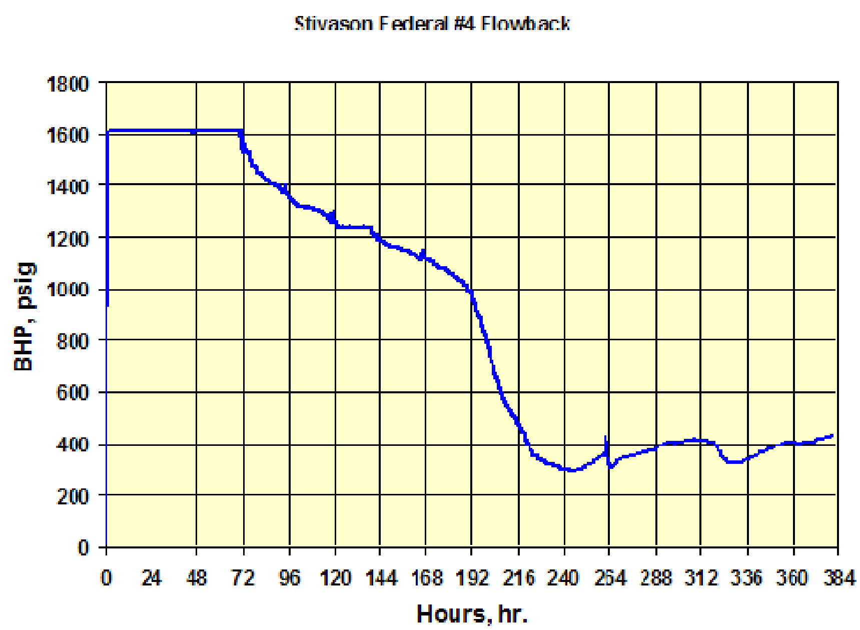

Figure 5.3. Bottom-hole pressure drop during initial part of blow down.

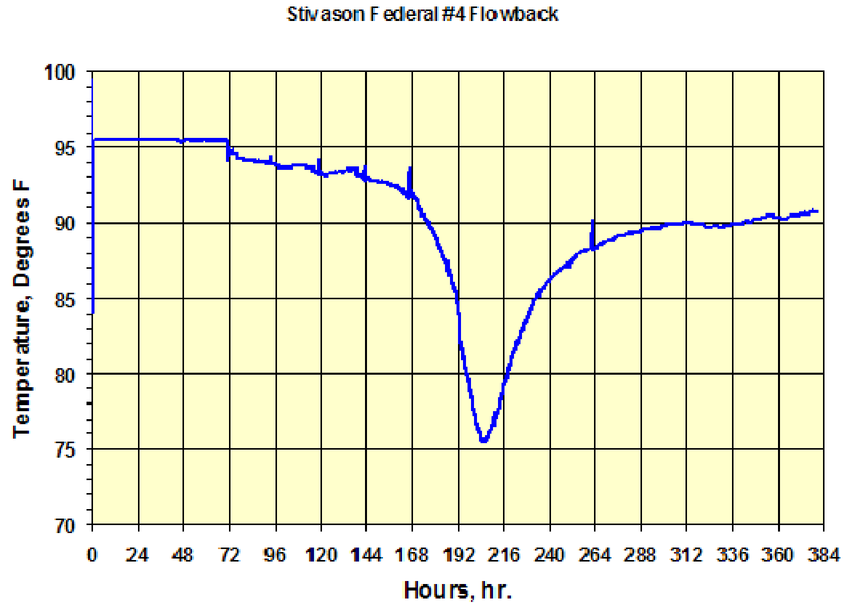

Figure 5.4. Bottom-hole temperature during initial part of blow down

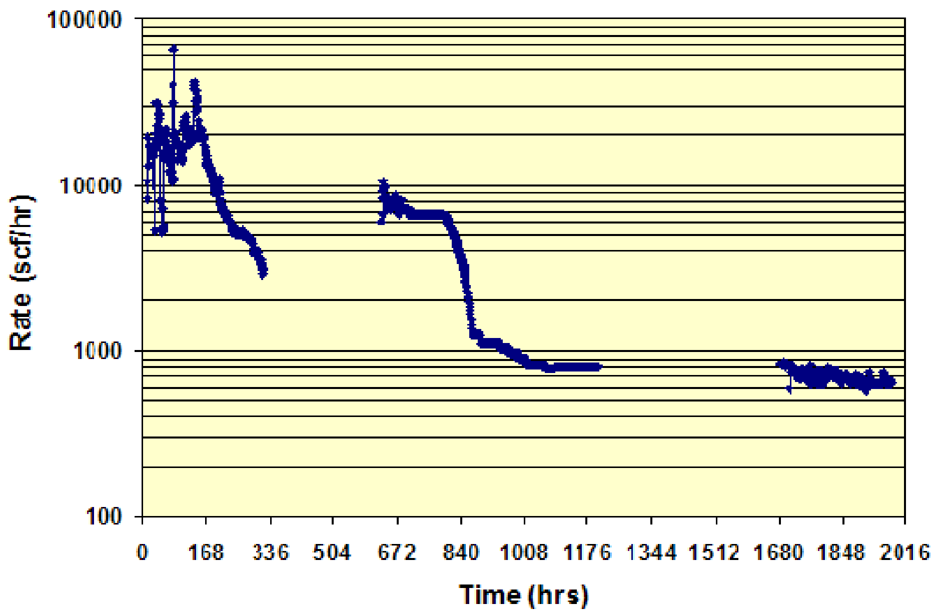

Figure 5.5. CO_2 flow rate during blow down.

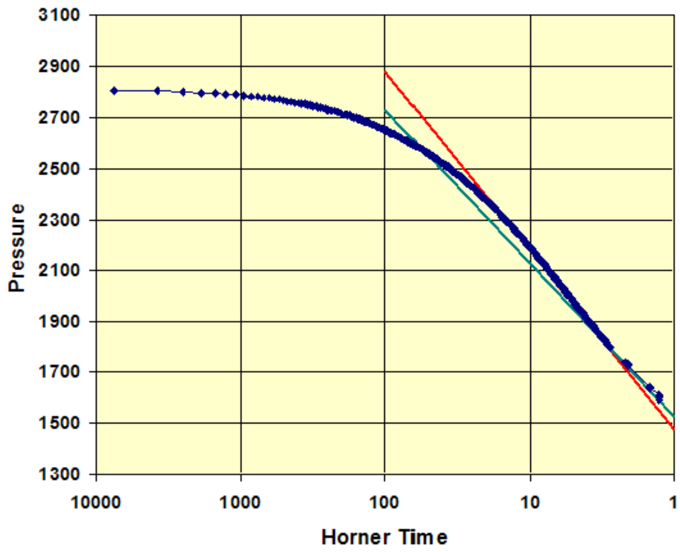

Figure 5.6. Horner plot of soak pressure decay.

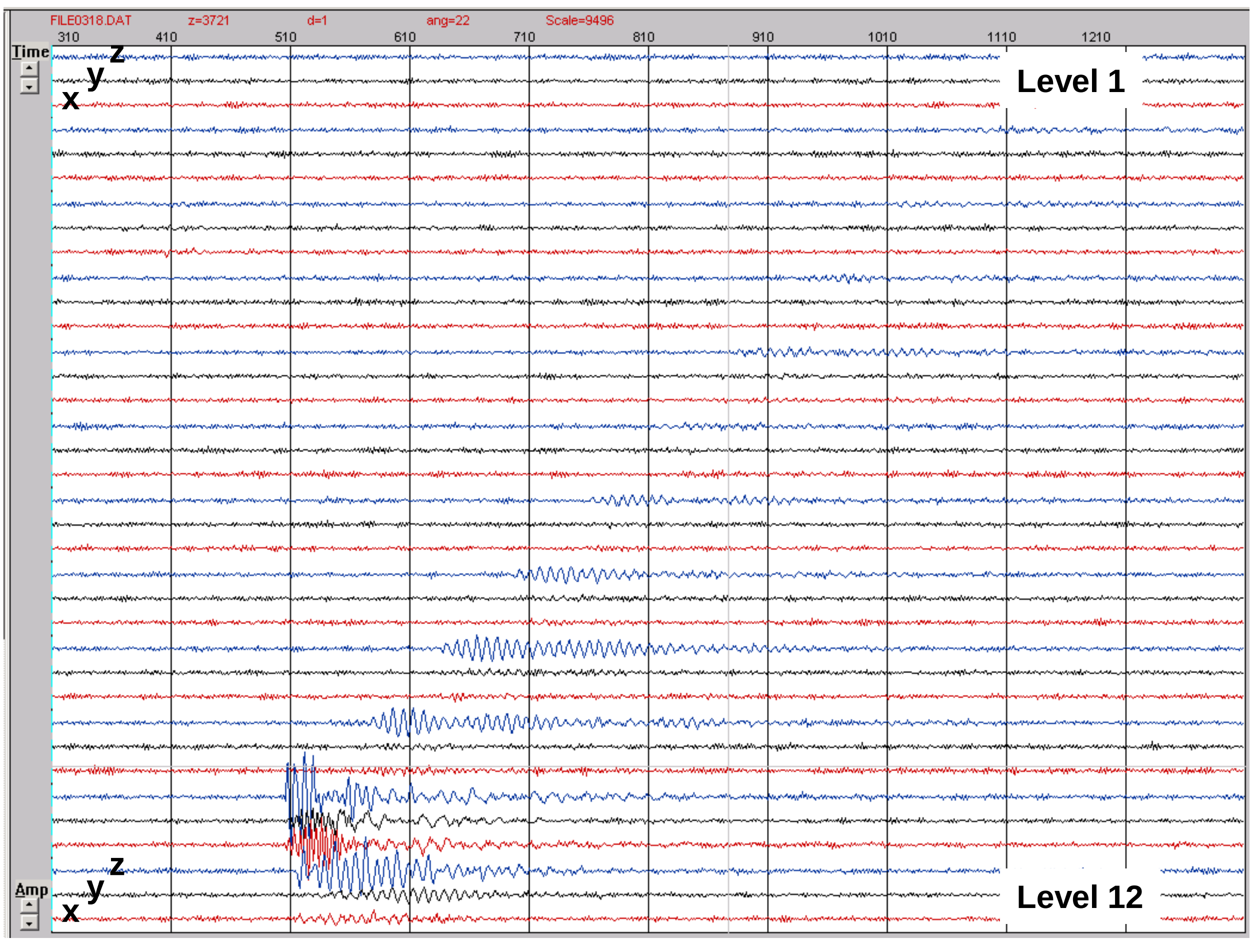

Figure 5.7. Waveforms of tube-wave generating event located near bottom of array.

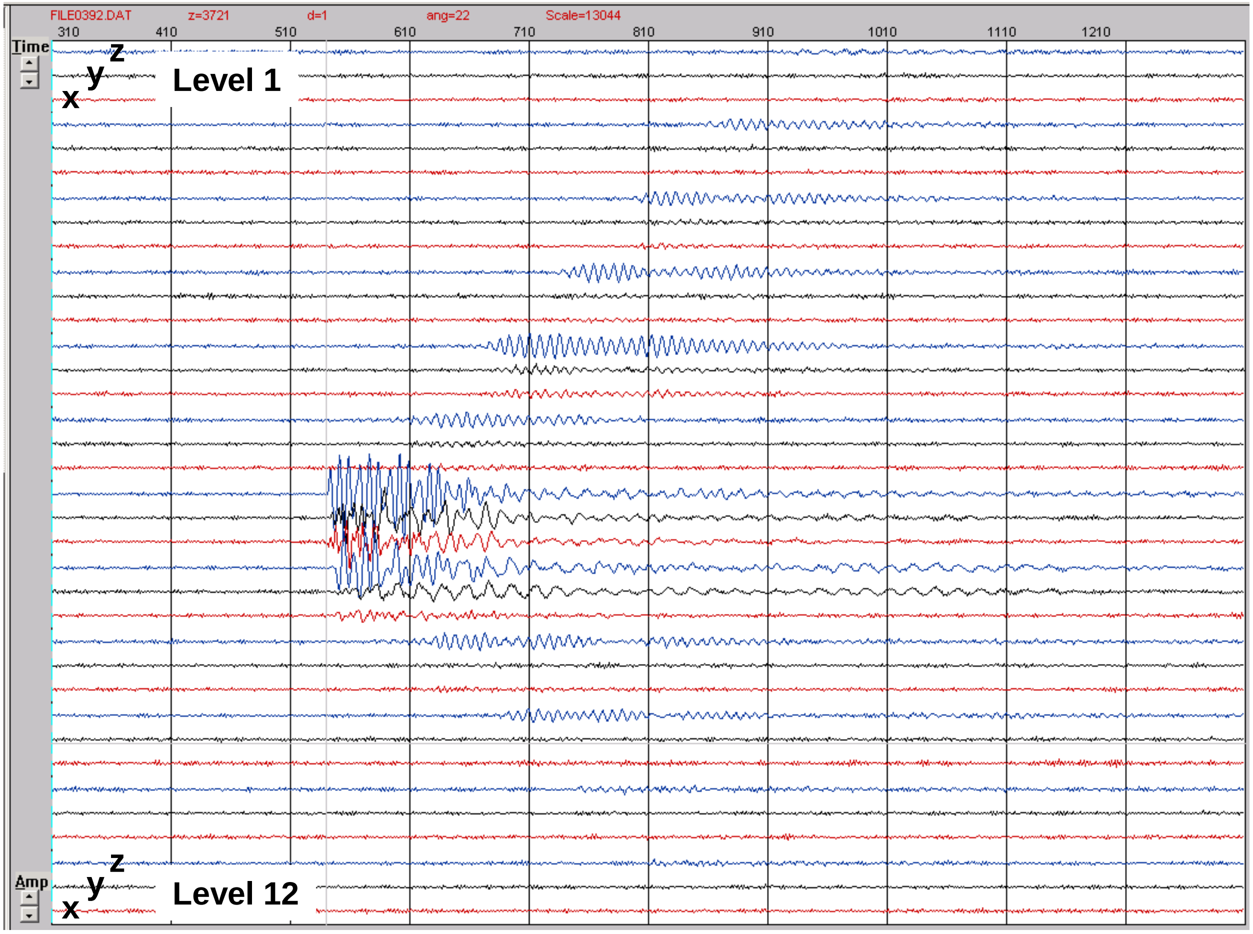

Figure 5.8. Waveforms of tube-wave generating event located near center of array.

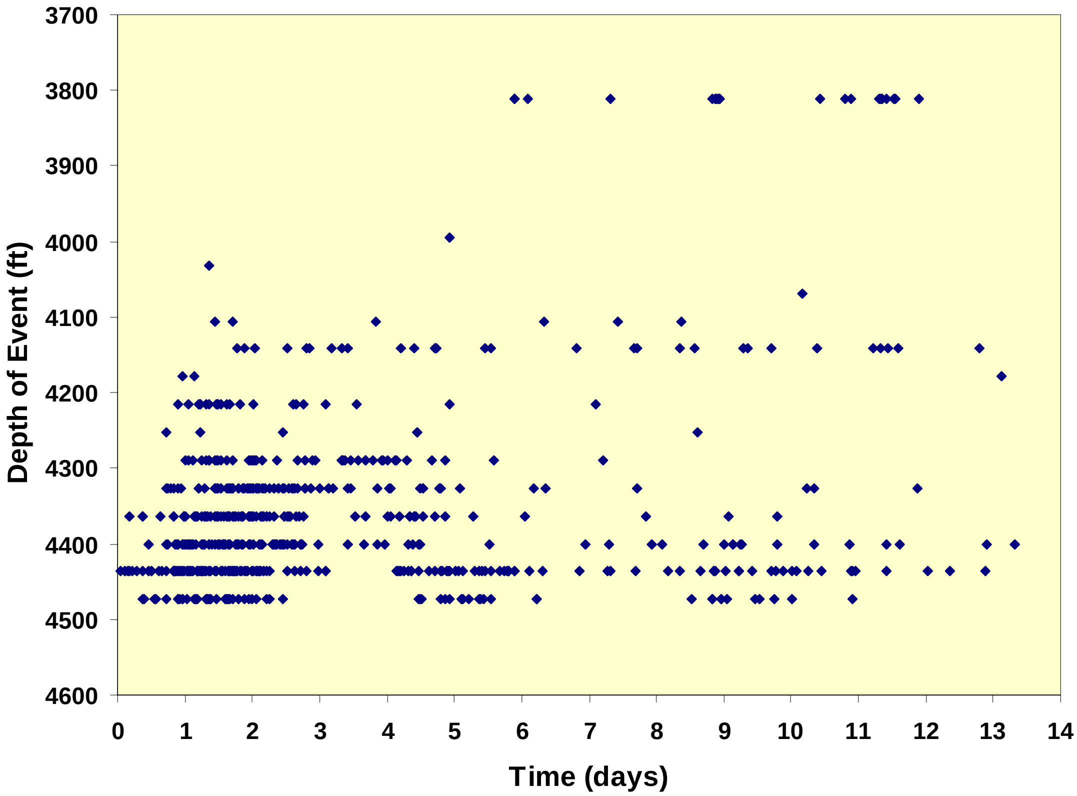

Figure 5.9. Location of origin of tube-wave generating events as a function of time.

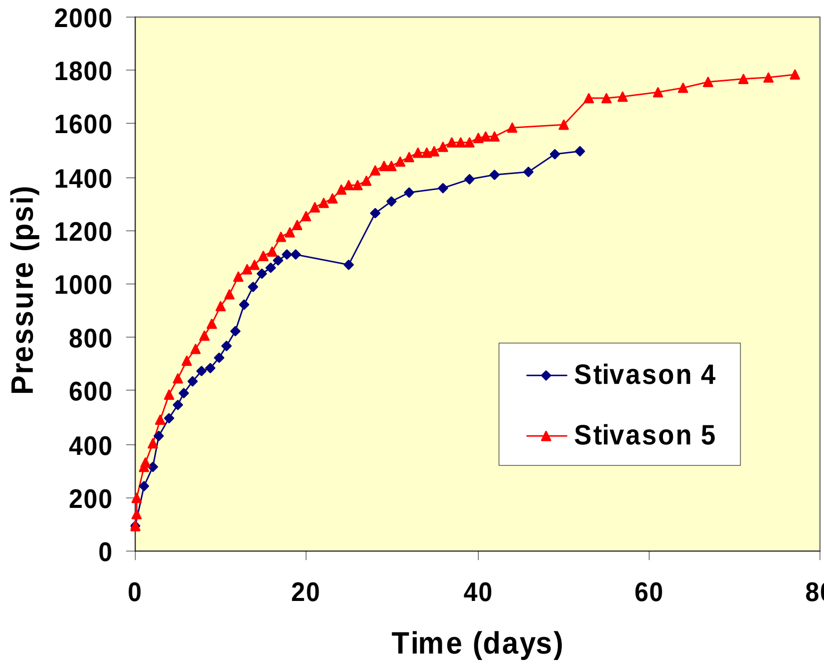

Figure 5.10. Pressure buildup after ~1.5 years of production.

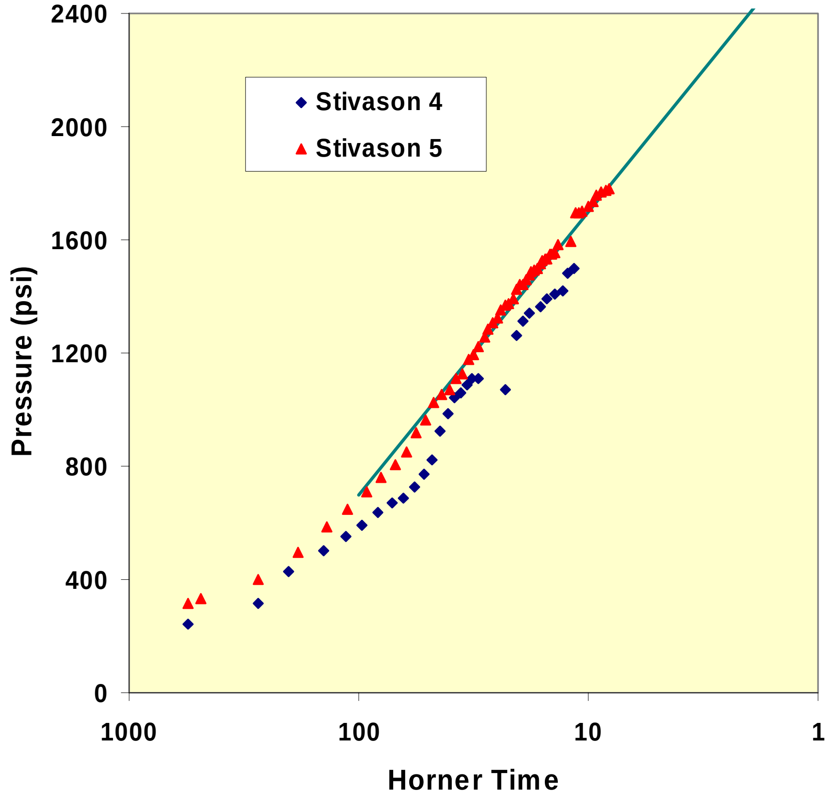

Figure 5.11. Horner plot of final pressure build up.

6.0 4D/9C SEISMIC ANALYSES

The primary monitoring technology applied to this experiment was a 4D/9C seismic reflection survey. The 4D refers to a 3D survey conducted more than once so that the fourth dimension is time, while the 9C refers to the use of three component receivers (one vertical and two horizontal) and three component sources (one vertical and two horizontal). The use of 9C technology allows for the development of S-wave reflection surveys, while the 4D obviously provides the potential for observing changes in the reservoir.

The overall management and analysis of the seismic surveying was performed by the Reservoir Characterization Project (RCP) at Colorado School of Mines. They provided the design of the survey, contracted for acquisition and basic processing, and then performed advanced analyses of the results.

6.1 DESIGN AND ACQUISITION

As shown in Figure 6.1, the survey was designed to cover an area of about one square mile centered over the Stivason #4 injection well. The survey parameters are given in Figure 6.2. There are approximately 1000 source and receiver locations, but with three different sources, there are around 3000 total source points. Frequency ranges are 8 to 120 for the P-wave source (vertical) and 6 to 80 Hz for the S (horizontals). Figure 6.3 shows a grid of the various locations, relative to the section lines, highway, and wells. The resulting fold coverage for the survey is shown in Figure 6.4. Every location within a two thousand ft radius of the survey center (the Stivason #4 well) has a fold coverage greater than 100, and in the immediate area of interest, the fold coverage approaches 300.

A photograph of the site location is shown in Figure 6.5. The acquisition trucks are to the left side of the photograph, and the general scrub oak and sand dune features of this area can be seen here. Two different source vehicles were employed for the shoot. Figure 6.6 shows an Industrial Vehicles TRI-AX unit, and Figure 6.7 shows an Input/Output Sidewinder unit. Both vehicles have capabilities to provide all three sources. A close up of the TRI-AX source as it is deployed is shown in Figure 6.8. The hydraulics lift the truck to provide the downward force for the vibrators when they are activated.

The baseline survey was performed in November and December of 2002, just prior to the start of injection. The second survey was conducted in August of 2003, just before the end of the six month soak period. Both surveys were performed in similar conditions (significant rains had soaked the site prior to both surveys, so the sand dunes were wet underneath). Good quality data were obtained.

6.2 BASELINE RESULTS

Figure 6.9 shows the P-wave reflectors observed on a west-to-east traverse of the site. The formations are very flat, and little structure can be discerned on this scale. The Shattuck Sandstone Member of the Queen Formation (sometimes referred to as the Queen Sandstone) is found at about 680 ms on the time scale. A time structure map of the top of the Shattuck Sandstone for the P wave is shown in Figure 6.10. The depth structure map at the top of the Shattuck for the P wave is shown in Figure 6.11. Of particular interest is the difference in the seismic structure compared to that estimated from well control (e.g., in Figure 6.1). The reservoir structure is considerably more complex than the simple elongated structure that was anticipated. There appears to be a slight structure feature separating the #4 and #5 wells, and there is a more significant feature to the northwest that separates the central part of the structure from the wells to the north. Otherwise, the structure does tail off to the northeast and southwest, as anticipated.

Similarly, the S-wave reflectors observed on the same east-west traverse as Figure 6.9 are shown in Figure 6.12, with very similar characteristics. Time structure and depth structure plots are also very similar and are not shown.

6.3 COMPARISON OF BASELINE AND POST-INJECTION P-WAVE SURVEYS

The overall results from the post-injection seismic survey are very similar to those shown above and are not shown again. However, with both surveys in hand, it is possible to compare the two and search for differences. To do this accurately, it is first necessary to match up the times because there are some subtle differences that can skew the results.

Figure 6.13 shows a comparison of east-west traverses of the P-wave reflections for the baseline survey and the post-injection monitoring survey when the times are unmatched and when they are matched. The differences between the two surveys are much smaller when the times are correctly matched.

Figure 6.14 shows the RMS amplitudes of the reflected P-wave energy for the baseline survey. These amplitudes are on the top of the Shattuck Sandstone. Figure 6.15 shows the RMS amplitudes of the reflected P-wave energy for the monitor survey. While the two data sets are very similar, there are subtle differences. The difference plot, found by subtracting the baseline amplitudes from the monitor amplitudes, is shown in Figure 6.16.

The zone around the injected CO_2 (around the Stivason #4 well in the center of the plot) shows an increase in the reflected energy, whereas the producing wells to the north show a decrease in the reflected energy. The water injection region to the southwest of the #4 well shows a slight increase in the reflected energy, although minimal water was injected during this period. The results shown in Figure 6.16 indicate that the CO_2 plume primarily migrated in three separate plumes, one to the south, one to the east, and one to the north. Figure 6.17 now shows the plume on top of the depth structure contours and presents a not unreasonable plume feature that is responding to structure, pressure (injection wells to southwest), and permeability.

A comparison of the reflection amplitudes for unmatched traverses of both the S1 and S2 waves (the vertical and horizontal shear waves) is shown in Figures 6.18 and 6.19.

The baseline RMS amplitude plot for the S1 waves is shown in Figure 6.20. The same feature to the northeast of the #4 well that shows up in the P-wave survey is also observed here. When the final S-wave matched data become available, an S-wave difference plot will also be prepared.

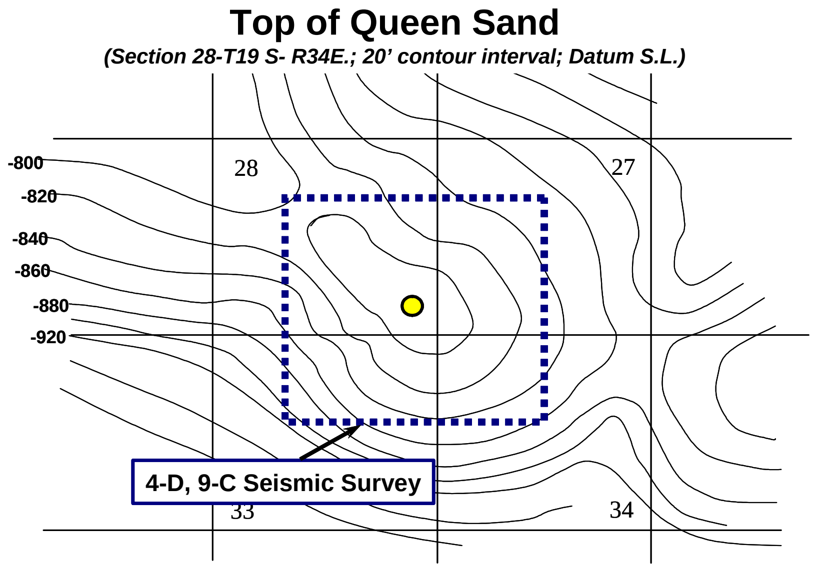

Figure 6.1. Aerial coverage for 4D, 9C seismic survey.

Type survey	**4-D, 9-C (time-lapse)**
Subsurface bin size	**55 feet X 55 feet**
Number of receiver locations	**986**
Number of source locations	**1057**
Total number of source points	**3171**
Type receiver spread	**Stationary: 6200' X 6200'**
Instrumentation	**I/O System II, 2 ms sample rate, 4 sec. record length**
Receiver array	**3, 3-C geophones – 3' inline spacing**
Source array (P-wave)	**Vertical vibrator: 8-120 hz linear sweep, 10 sec duration, 4 sweeps**
Source array (S-wave)	**Horizontal vibrator: 6-80 hz linear sweep, 10 sec duration, 3 sweeps, one source oriented N-S, one source oriented E-W**

Figure 6.2. Operational parameters for 4D, 9C seismic survey.

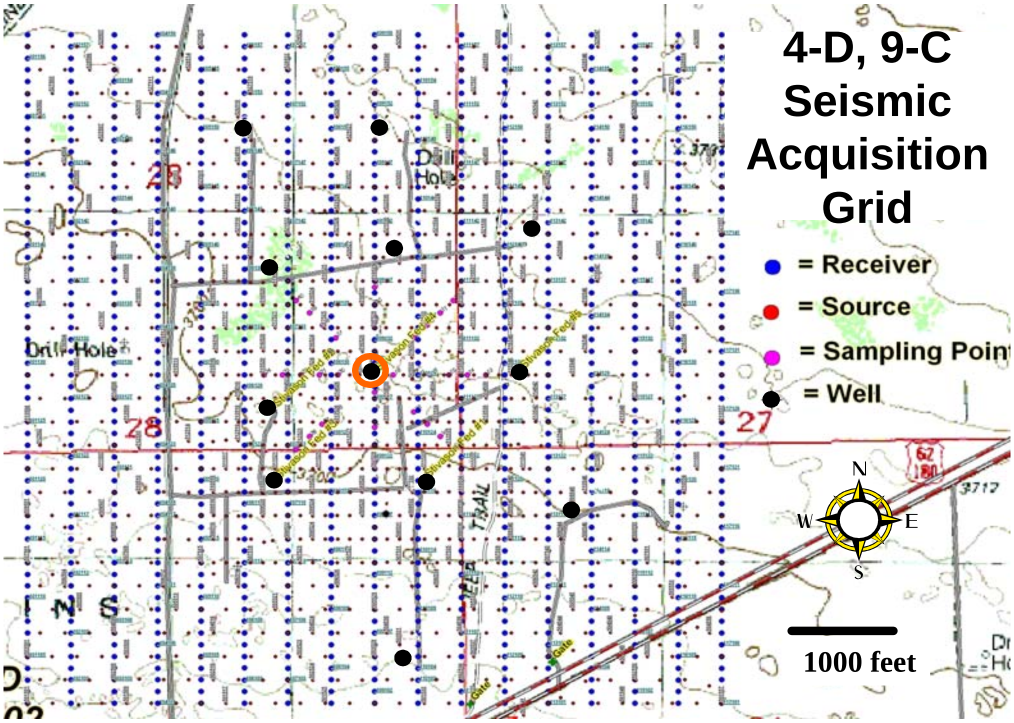

Figure 6.3. Source and receiver points for 4D, 9C seismic survey.

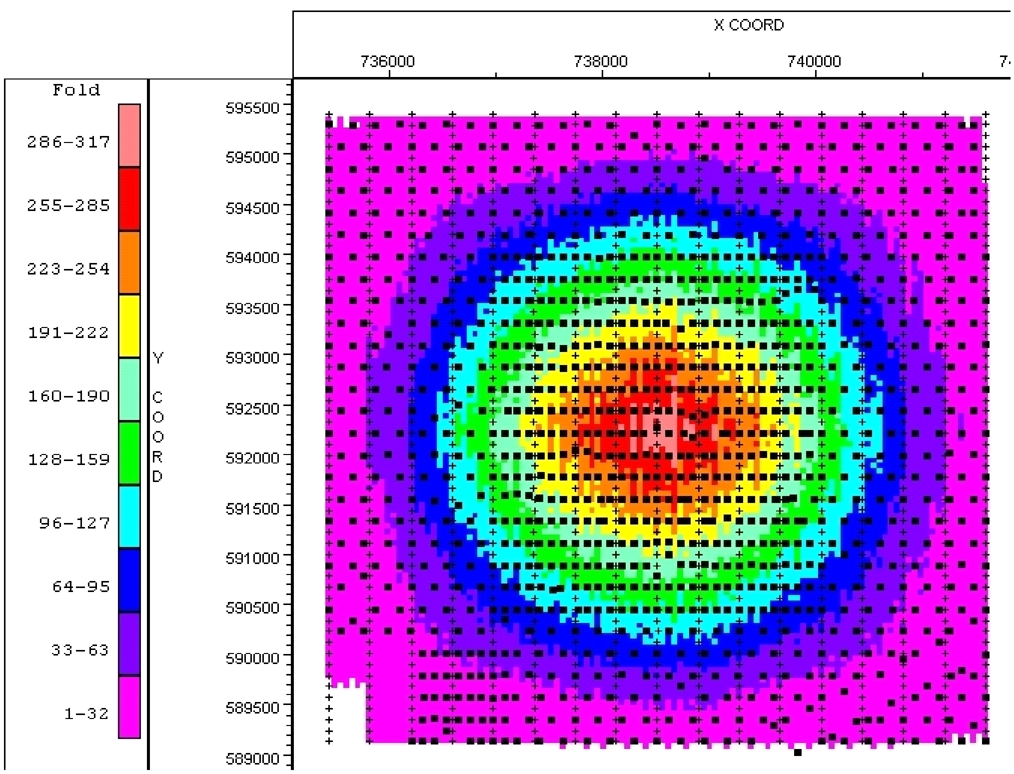

Figure 6.4. Fold coverage for 4D, 9C seismic survey.

Figure 6.5. Site with acquisition trucks at left.

Figure 6.6. Industrial Vehicles TRI-AX source truck.

Figure 6.7. Input/Output Sidewinder source truck.

Figure 6.8. Close-up of TRI-AX hydraulic foot.

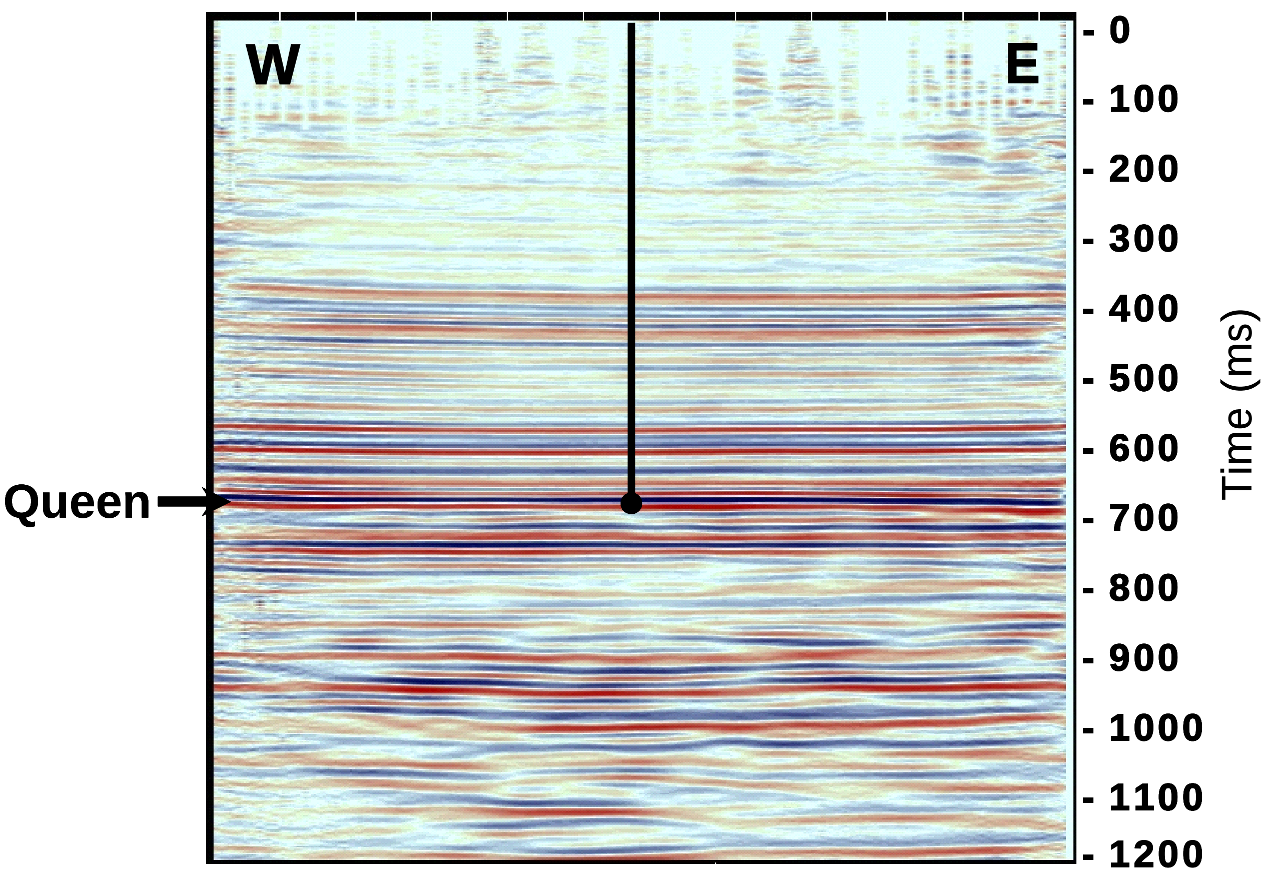

Figure 6.9. Observed reflections on east-west line through the Stivason #4 Well – P wave.

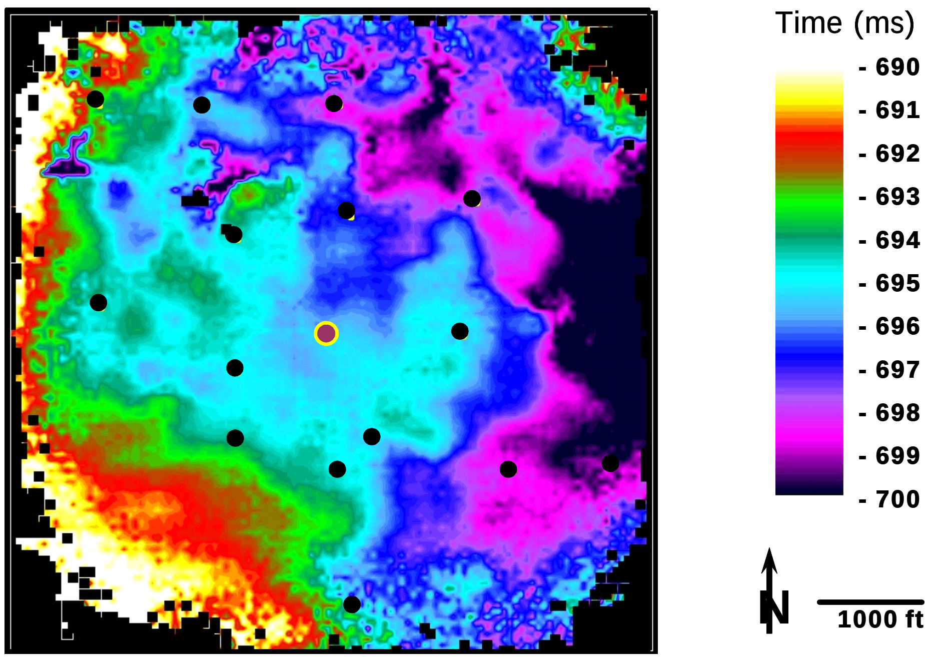

Figure 6.10. Time structure map on Queen Sandstone – P wave.

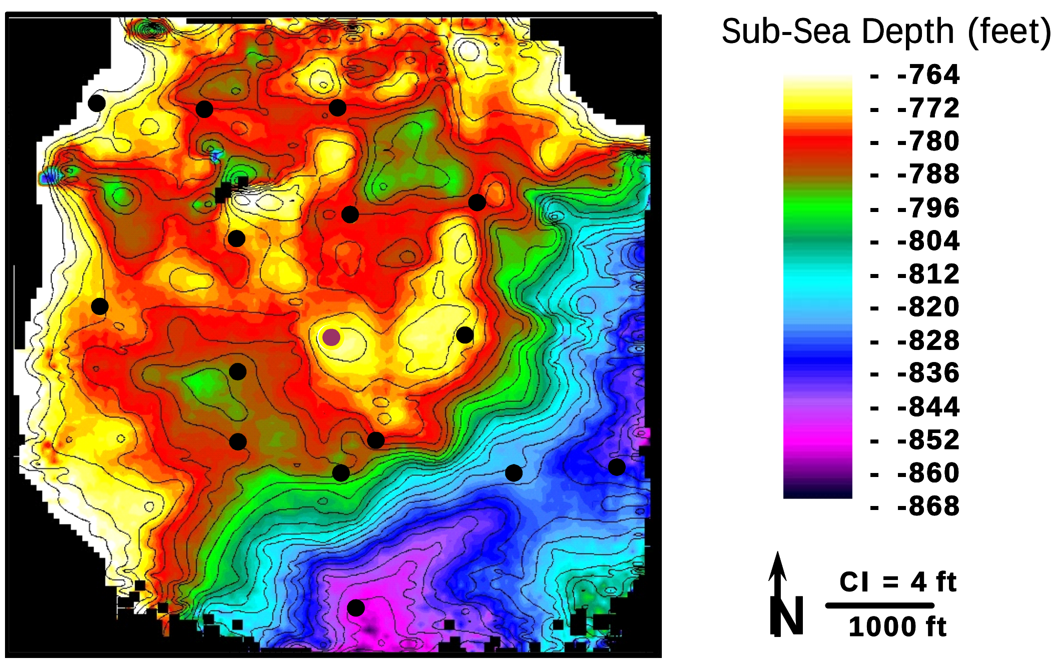

Figure 6.11. Depth structure map on Queen Sandstone – P wave.

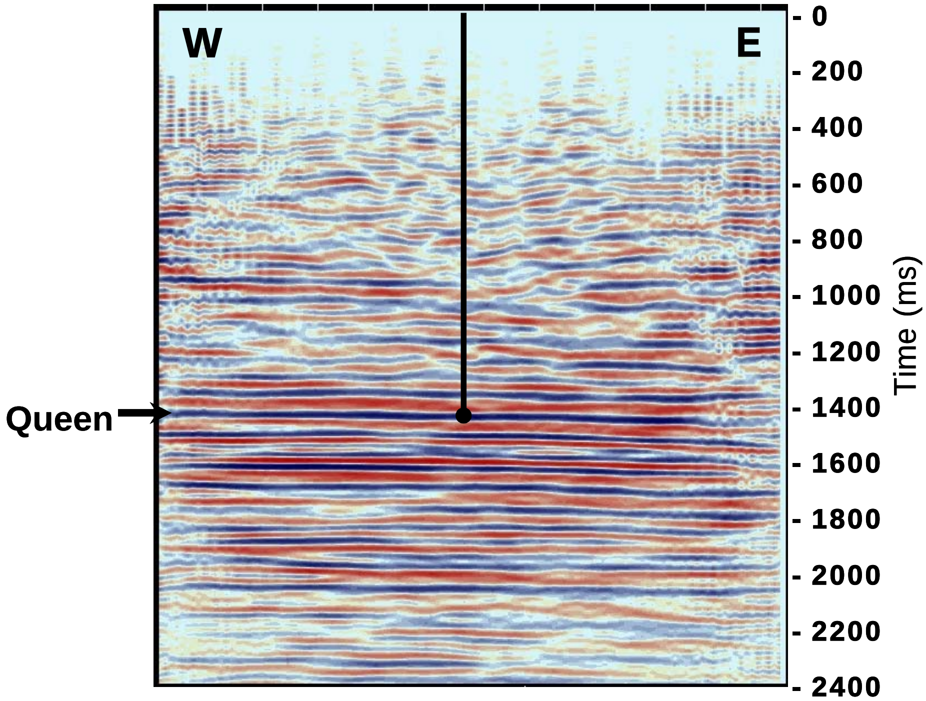

Figure 6.12. Observed reflections on east-west line through the Stivason #4 well – S wave.

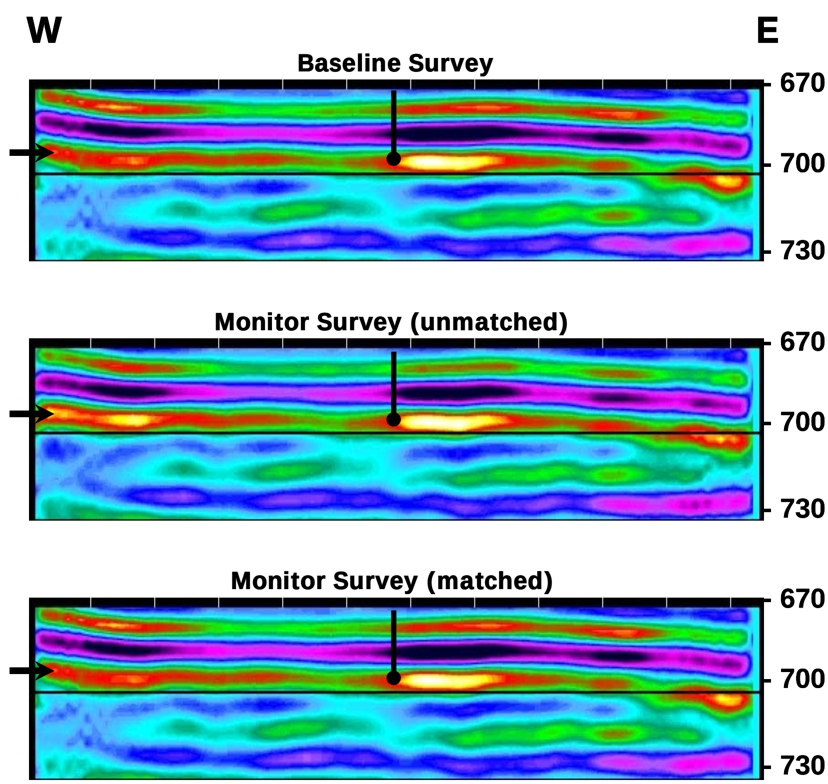

Figure 6.l3. Comparison of east-west, P-wave, reflection traverses for matched and unmatched data.

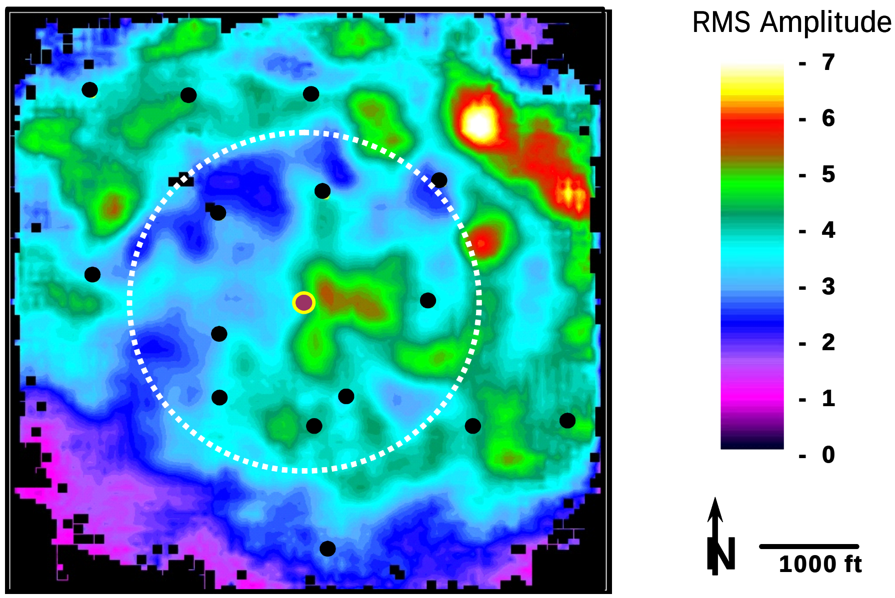

Figure 6.14. RMS reflection amplitude for baseline survey – P wave.

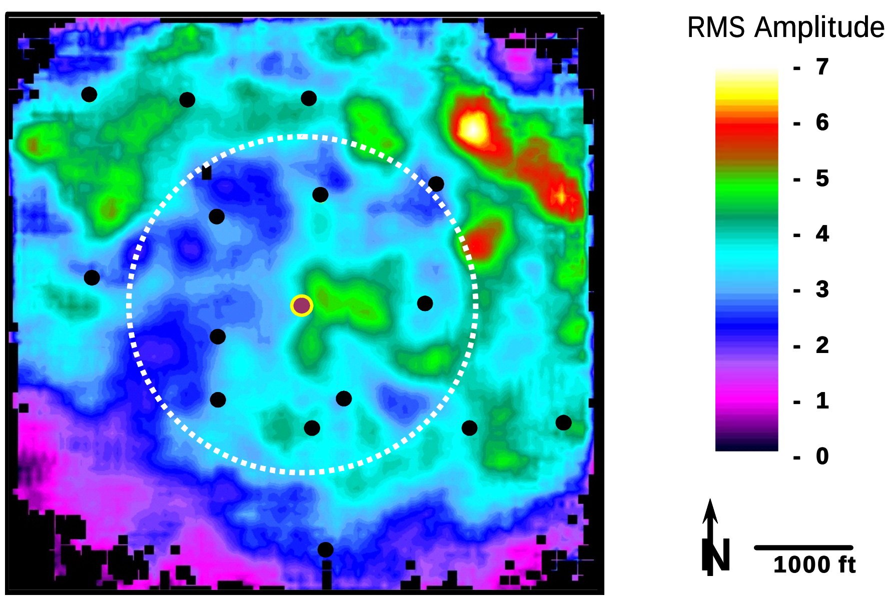

Figure 6.15. RMS reflection amplitude for monitor survey – P wave.

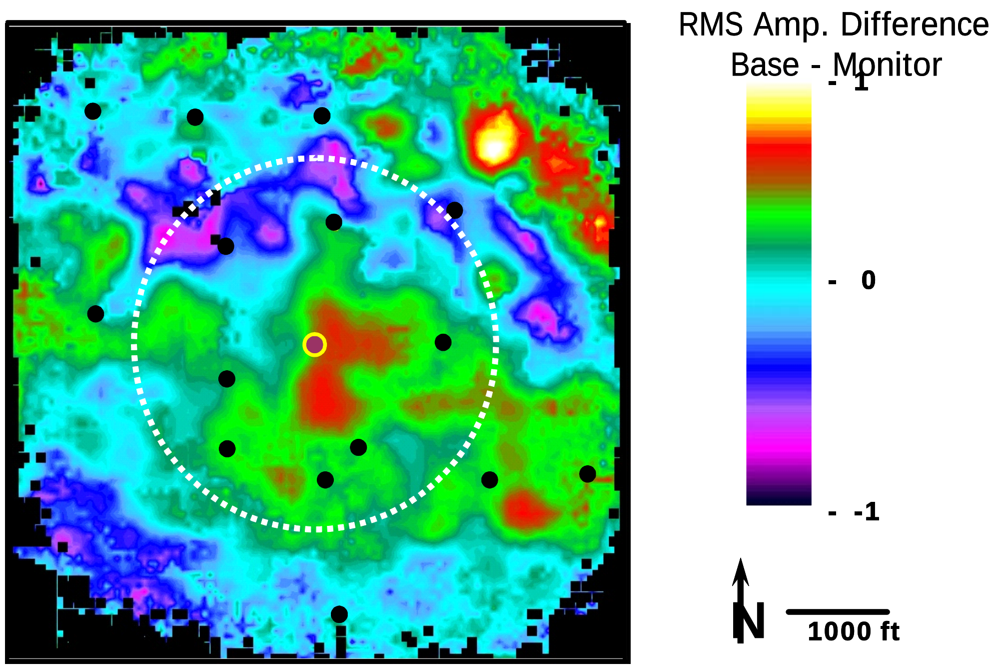

Figure 6.16. RMS reflection amplitude differences – P wave.

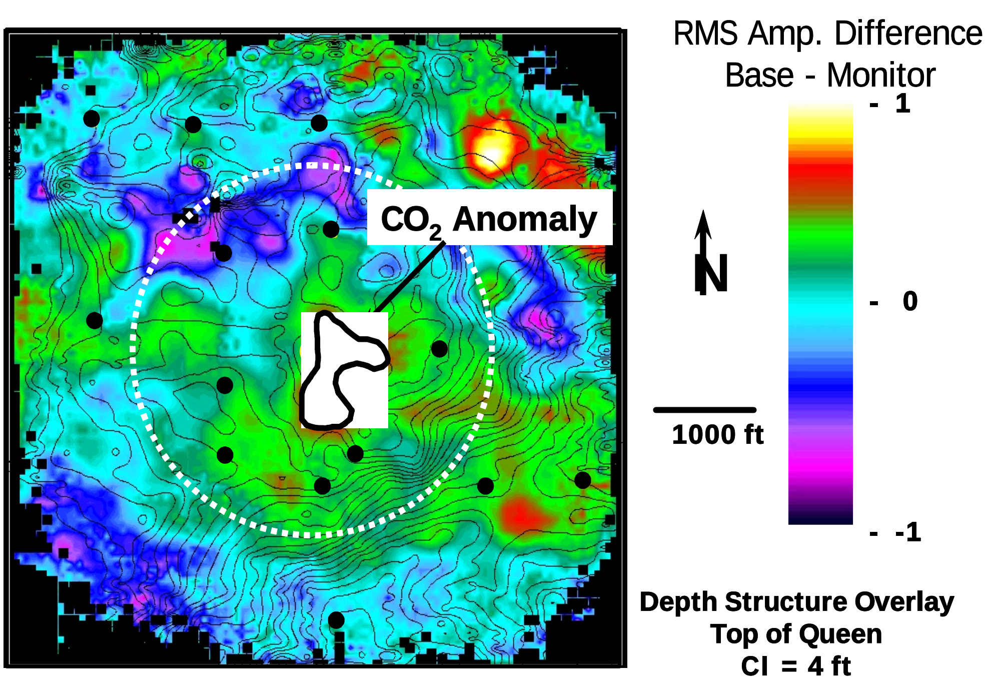

Figure 6.17. RMS reflection amplitude differences – P wave – along with depth structure contours and assume CO_2 plume.

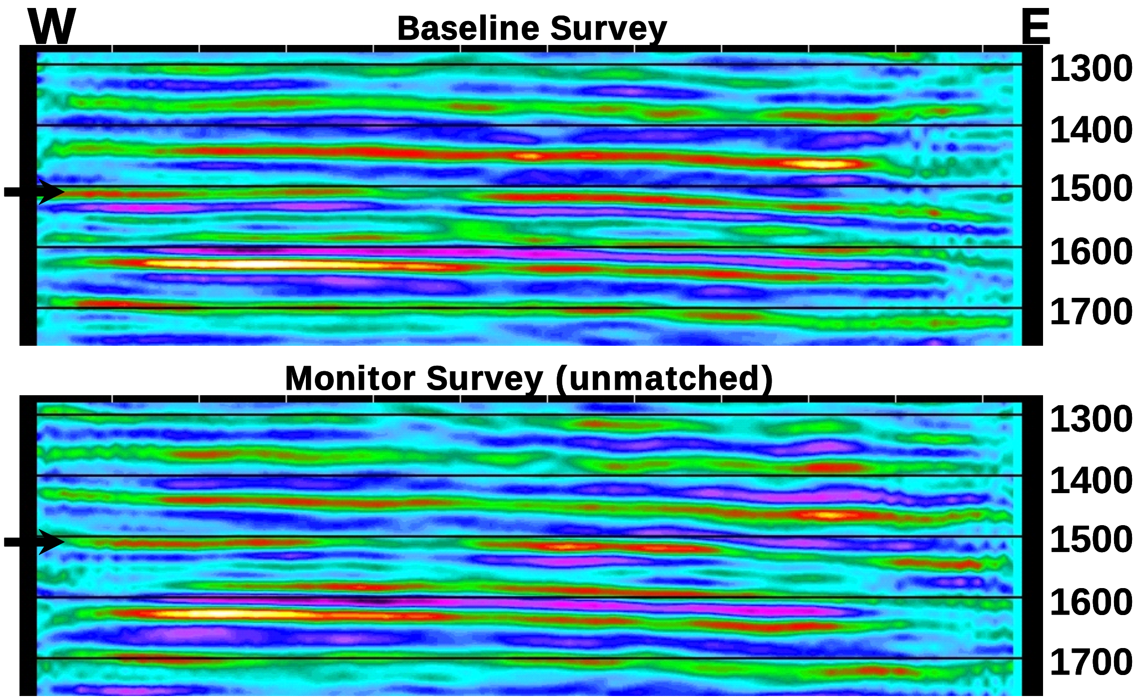

Figure 6.18. Comparison of the reflection amplitudes for unmatched traverses of the S1 waves (vertical shear wave)

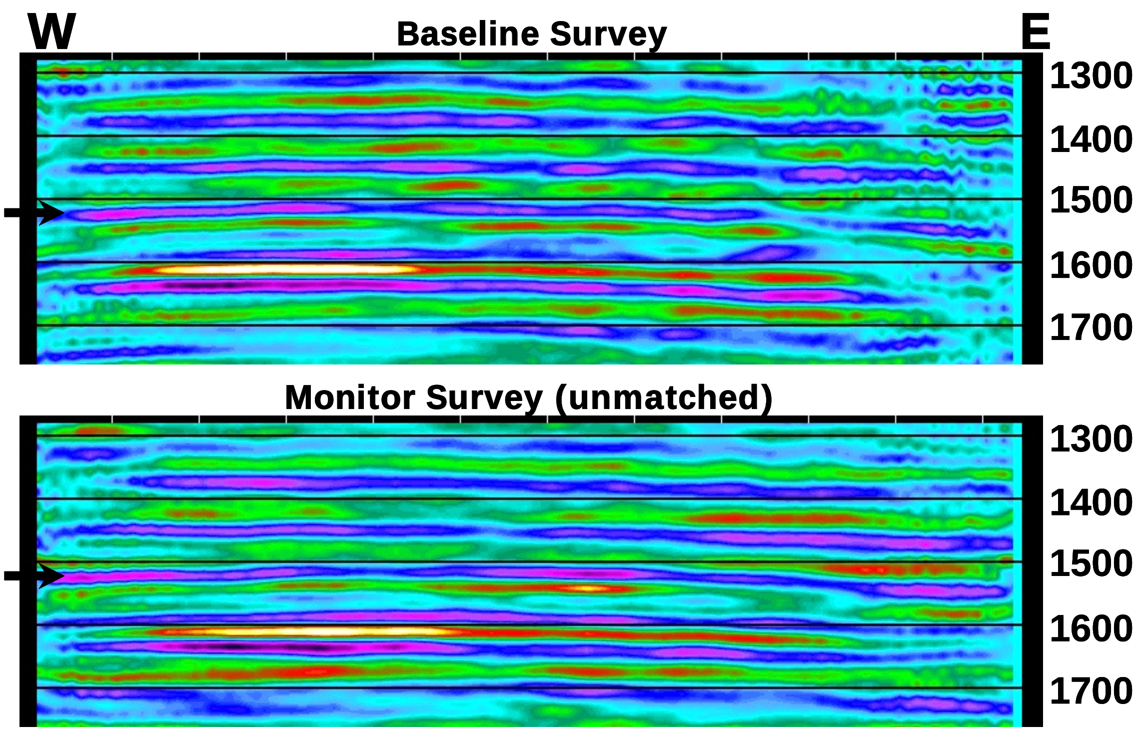

Figure 6.19. Comparison of the reflection amplitudes for unmatched traverses of the S2 waves (horizontal shear waves).

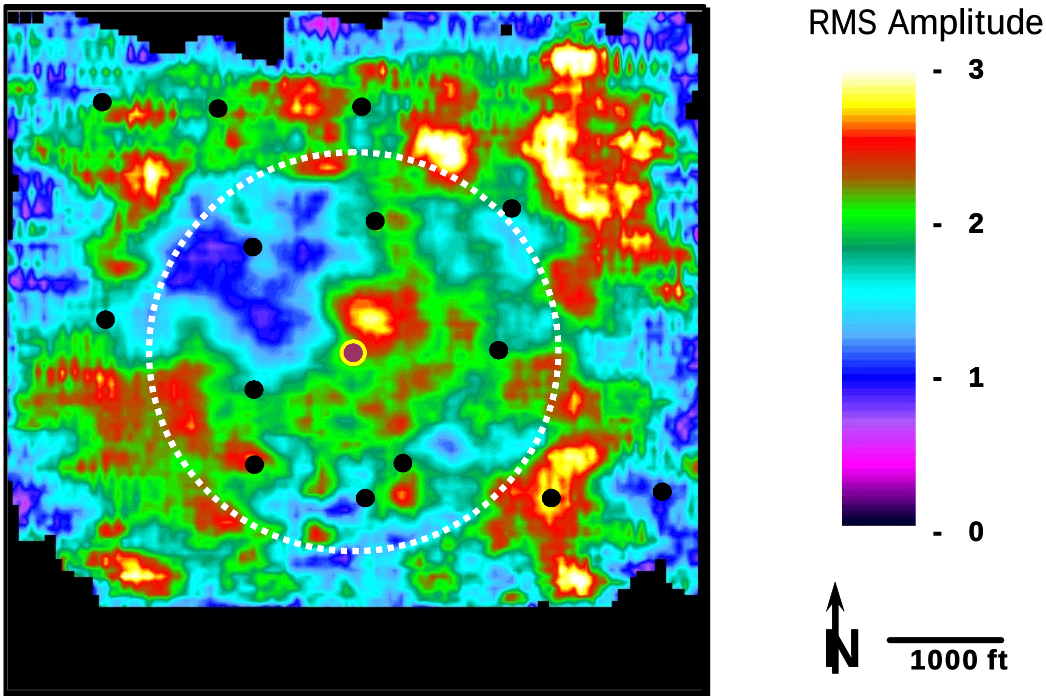

Figure 6.20. Baseline RMS amplitude plot for S1 waves

7.0 SUMMARY

Carbon dioxide (CO_2) sequestration in geological formations is the most direct carbon management strategy for reducing anthropogenic CO_2 emissions into the atmosphere and will likely be needed for continuation of the global fossil-fuel–based economy. Storage of CO_2 into depleted oil reservoirs may prove to be both cost effective and environmentally safe. However, injection of CO_2 into oil reservoirs is a complex issue, spanning a wide range of scientific, technological, economic, safety, and regulatory issues. Detailed studies about the long-term impact of CO_2 on the host reservoir are necessary before this technology can be deployed.

The main objectives of this project was (1) to characterize the oil reservoir and its sequestration capacity; (2) to better understand CO_2 sequestration-related processes; and (3) to predict and monitor the migration and ultimate fate of CO_2 after injection into a depleted sandstone oil reservoir. The project is focused around a field test that involved the injection of approximately 2090 tons of CO_2 into a depleted sandstone reservoir at the West Pearl Queen Field in southeastern New Mexico. Geophysical monitoring surveys, laboratory experiments, geophysical surveys, and numerical simulations were performed in support of the field experiment. Results show that the response of the West Pearl Queen reservoir during the field experiment was significantly different than expected based on the preinjection characterization data. Furthermore, results from a 19-month bench-scale experiments of CO_2 interaction with the Queen Sandstone were not able to be fully reproduced using the latest numerical modeling algorithms, suggesting that the current models are not capturing important geochemical interactions. Thus, the observations and experimental results show that extensive reservoir characterization is necessary to understand and predict the impact of CO_2 injection on storage reservoirs.

Geophysical monitoring using P-wave analysis of the three-dimensional, multicomponent seismic data shows an anomaly that may indicate the presence of CO_2. This study shows the applicability of the surface seismic method for detecting a CO_2 plume, although the amount of CO_2 injected was small and individual zones were thin.

The laboratory experiments also provided valuable results. Although dawsonite is a potential geochemical reaction product in sandstone reservoirs, this mineral was not formed during the laboratory experiments. Understanding the kinetics of dawsonite formation is critical for sequestration in sandstone reservoirs for two reasons. First, dawsonite is an important sink for CO_2, and second, its formation can also lead to irreversible and potentially damaging changes in reservoir properties such as permeability and porosity.

The methodologies developed during this study can be used in future studies to evaluate depleted oil reservoirs as a sequestration option. This work combined with future similar studies, should allow predictions on the long-term fate of CO_2 in depleted sandstone oil reservoirs.

8.0 REFERENCES

Bethke, C. M., *The Geochemist's Workbench (Release 3.0): A users software guide toRxn ,Act2, Tact, React, and Gtplot*, p. Pages, Hydrogeology Program, University of Illinois, (Urbana-Champaign) (1998).

Elkins, L. F., and Skov, A. M., 1960, Determination of fracture orientation from pressure interference: Petroleum Transactions, American Institute of Mining Engineers, v. 219, p. 301-304.

Greenberg, J. P.; and Møller, N. 1989. "The Prediction of Mineral Solubilities in Natural Waters: A Chemical Equilibrium Model for the Na-K-Ca-Cl-SO_4-H_2O System to High Concentration from 0 to 250 °C." *Geochimica et Cosmochimica Acta*, *53*, 2503–2518.

He, S.; and Morse, J. W. 1993. The Carbonic Acid System and Calcite Solubility in Aqueous Na-K-Ca-Mg-Cl-SO_4 Solutions from 0 to 90°C. *Geochimica et Cosmochimica Acta*, *57*, 3533–3554.

Hayes, P. T., and Koogle, R. L., 1958, Geology of the Carlsbad Caverns West Quadrangle, New Mexico-Texas: United States Geologic Survey Quadrangle Map GQ 112.

Krumhansl, J. L., R. Pawar, R. Grigg, H. Westrich, N. Warpinski, D. Zhang, C. Jove-Colon, P. Lichtner, J. Lorenz, R. Svec, B. Stubbs, S. Cooper, C. Bradley, J. Rutledge, and C. Byrer, "Geological Sequestration of Carbon Dioxide in a Depleted Oil Reservoir," in *Proceedings of the SPE/DOE 13th Symposium on Improved Oil Recovery*, Tulsa, OK, April 13-17, 2002.

Lorenz, J. C., and Finley, S. J., 1989, Differences in fracture characteristics and related production: Mesaverde Formation, Northwestern Colorado: Society of Petroleum Engineers Formation Evaluation, v. 4, p. 11-16.

Lorenz, J. C., Warpinski, N. R., and Teufel, L. W., 1996, Natural fracture characteristics and effects: The Leading Edge, v. 15, no. 8, p. 909-911.

Mazzullo, J., Malicse, A., and Siegel, J., 1991, Facies and depositional environments of the Shattuck Sandstone on the Northwest Shelf of the Permian Basin, *Journal of Sedimentary Petrology*, vol. 61, p. 940-958.

Nelson, R. A., 1985, Geologic analysis of naturally fractured reservoirs, Contributions in petroleum geology and engineering: Houston, Gulf Publishing Company, 360 p.

Pabalan, R. T., and Pitzer, K. S., 1987, Thermodynamics of concentrated electrolyte mixtures and the prediction of mineral solubilities to high temperatures for mixtures in the system Na-K-Mg-Cl-SO_4-OH-H_2O, *Geochimica et Cosmochimica Acta*, v. 51, p. 2429-2443.

Pitzer, K. S. 1991. "Ion Interaction Approach: Theory and Data Correlation." Pages 75–153 of *Activity Coefficients in Electrolyte Solutions*. 2nd Edition. Pitzer, K. S., ed. Boca Raton, Florida: CRC Press.

Tait, D. B., Ahlen, J. L., Gordon, A., Scott, G. L., Motts, W. S., and Spitler, M. E., 1962, *Artesia Group of New Mexico and west Texas*, American Association of Petroleum Geologists Bulletin, v. 46, no. 4, p. 504-517.

Westrich, H.R., J. Lorenz, S. Cooper, C. Jove Colon, N. Warpinski, D. Zhang, C. Bradley, P. Lichtner, R. Pawar, B. Stubbs, R. Grigg, R. Svec, C. Byrer, Sequestration of CO_2 in a Depleted Oil Reservoir: An Overview, *J. of Energy and Environmental Research*, v. 2, No. 1, p. 64-74, 2002.

APPENDIX A

Pawar, R.J., Warpinski, N.R., Lorenz, J.C., Benson, R.D., Grigg, R.B., Stubbs, B.A., Stauffer, P.H., Krumhansl, J.P., and Cooper, S.P., 2006, Overview of a CO_2 sequestration field test in the West Pearl Queen reservoir, New Mexico, American Association of Petroleum Geologists, *Environmental Geosciences*, v. 13, no.3, p. 163-180.

Overview of a CO_2 sequestration field test in the West Pearl Queen reservoir, New Mexico

Rajesh J. Pawar, Norm R. Warpinski, John C. Lorenz, Robert D. Benson, Reid B. Grigg, Bruce A. Stubbs, Philip H. Stauffer, James L. Krumhansl, Scott P. Cooper, and Robert K. Svec

ABSTRACT

Carbon dioxide (CO_2) sequestration in geological formations is the most direct carbon management strategy for reducing anthropogenic CO_2 emissions into the atmosphere and will likely be needed for continuation of the global fossil-fuel–based economy. Storage of CO_2 into depleted oil reservoirs may prove to be both cost effective and environmentally safe. However, injection of CO_2 into oil reservoirs is a complex issue, spanning a wide range of scientific, technological, economic, safety, and regulatory issues. Detailed studies about the long-term impact of CO_2 on the host reservoir are necessary before this technology can be deployed. This article provides an overview of a U.S. Department of Energy–sponsored project that examines CO_2 sequestration in a depleted oil reservoir. The main objectives of the project are (1) to characterize the oil reservoir and its sequestration capacity; (2) to better understand CO_2 sequestration-related processes; and (3) to predict and monitor the migration and ultimate fate of CO_2 after injection into a depleted sandstone oil reservoir. The project is focused around a field test that involved the injection of approximately 2090 tons (2.09 million kg) of CO_2 into a depleted sandstone reservoir at the West Pearl Queen field in southeastern New Mexico. Geophysical monitoring surveys, laboratory experiments, and numerical simulations were performed in support of the field experiment. Results show that the response of the West Pearl Queen reservoir during the field experiment was significantly different than predicted response based on the preinjection characterization data. Furthermore, results from a 19-month bench-scale experiments of CO_2 interaction with the Queen sand were not able to be fully

DOI:10.1306/eg.10290505013

AUTHORS

Rajesh J. Pawar ~ *Earth and Environmental Sciences Division, Los Alamos National Laboratory, MS T003, Los Alamos, New Mexico 87545; rajesh@lanl.gov*

Rajesh Pawar is a technical staff member at the Los Alamos National Laboratory. He received his Ph.D. from the University of Utah in chemical and fuels engineering. His primary research focus is fluid flow in porous media. He has served as the associate editor of *Reviews in Geophysics*.

Norm R. Warpinski ~ *Sandia National Laboratories, Albuquerque, New Mexico; present address: Pinnacle Technologies, Park North Technology Center, 219 Airtex Boulevard, Houston, Texas 77090; nrwarpi@sandia.gov*

Norm Warpinski is currently the chief technology officer for Pinnacle Technologies in Houston, Texas. He is in charge of developing new tools and analyses for hydraulic fracture mapping, reservoir monitoring, hydraulic fracture design and analysis, and integrated solutions for reservoir development. He previously worked at Sandia National Laboratories from 1977 to 2005 on various projects in oil and gas, geothermal, carbon sequestration, waste repositories, and other geomechanics issues. Norm has extensive experience in various types of hydraulic fracture mapping and modeling and has been involved in large-scale field experiments from both the hardware and software sides. He has also worked on formation evaluation, geomechanics, natural fractures, in situ stresses, rock behavior, and rock testing.

John C. Lorenz ~ *MS 0750, Sandia National Laboratories, Albuquerque, New Mexico 87185; jcloren@sandia.gov*

John Lorenz worked for the Peace Corps and the U.S. Geological Survey before joining Sandia National Laboratories in 1981, where he is presently a Distinguished Member of the Technical Staff. He received his Ph.D. from Princeton University, has been elected editor for AAPG, and has published widely on the sedimentology and natural fractures in hydrocarbon reservoirs.

Robert D. Benson ~ *Department of Geophysics, Colorado School of Mines, Golden, Colorado 80401-1887; rbenson@mines.edu*

Robert (Bob) D. Benson is a research associate professor in the Department of Geophysics at the Colorado School of Mines and is codirector of the Reservoir Characterization Project. Benson has more than 25 years of experience in seismic acquisition, processing, and interpretation. He holds B.S. and M.S. degrees and a Ph.D. in geophysics from the Colorado School of Mines. He is a past president of the Denver Geophysical Society.

Reid B. Grigg ~ *New Mexico Institute of Mining and Technology, 801 Leroy Place, Socorro, New Mexico 87801; reid@prrc.nmt.edu*

Reid Grigg is a senior engineer and section head at the New Mexico Petroleum Recovery Research Center and an adjunct professor at the New Mexico Institute of Mining and Technology. His research interests include high-pressure gas-flooding processes, phase behavior, and studies of the fluid properties of high-pressure injection gas and reservoir fluids related to improved oil recovery and carbon storage. He has authored more than 70 publications.

BRUCE A. STUBBS ~ *Strata Production Company, Roswell, New Mexico; pecos@lookingglass.net*

Stubbs is a consultant petroleum engineer, with 33 years of industry experience, for Pecos Petroleum Engineering, Inc., in Roswell, New Mexico. He has been a consultant since 1992 after spending 5 years with Hondo Oil and Gas Company. He holds a bachelor's degree in mechanical engineering from the New Mexico State University. He is the project engineer for Strata Production Company on the U.S. Department of Energy Class III Project at Nash Draw.

PHILIP H. STAUFFER ~ *MS T003, Los Alamos National Laboratory, Los Alamos, New Mexico 87545; stauffer@lanl.gov*

Phillip Stauffer is a technical staff member at the Los Alamos National Laboratory. His research involves code development, simulation, and assessment of subsurface multiphase transport in a variety of geological environments. His background in heat and mass transport includes work on the Yucca Mountain Project, the Ocean Drilling Program, and most recently, the Zero Emissions Research and Technology Program.

JAMES L. KRUMHANSL ~ *MS 0754, Sandia National Laboratories, Albuquerque, New Mexico 87185; jlkrumh@sandia.gov*

Jim is a principal member of the Sandia National Laboratories scientific staff, where he has worked since he received his Ph.D. in geology from Stanford University in 1976. His expertise is environmental and aqueous geochemistry, where he has applied numerous issues, including the Waste Isolation Pilot Project (WIPP) and the Yucca Mountain Project (YMP).

SCOTT L. COOPER ~ *MS 0750, Sandia National Laboratories, Albuquerque, New Mexico 87185; spcoope@sandia.gov*

Scott Cooper is a senior member of the technical staff at Sandia National Laboratories. He received his B.S. degree from the South Dakota School of Mines and Technology (1997) and his M.S. degree in geology from the New Mexico Institute of Mining and Technology (2000). His current research focuses on natural fracture systems and reservoir characterization.

ROBERT K. SVEC ~ *New Mexico Institute of Mining and Technology, 801 Leroy Place, Socorro, New Mexico 87801*

Bob Svec received his bachelor's degree in physics and his master's degree in geophysics from the New Mexico Institute of Mining and Technology. His current research interests lie in high-pressure experiments including CO_2 core flooding and reservoir characterization.

ACKNOWLEDGEMENTS

Funding for this work was provided by the U.S. Department of Energy. The authors also thank KinderMorgan CO_2 for donating the CO_2 used during field-injection experiments.

reproduced using the latest numerical modeling algorithms, suggesting that the current models are not capturing important geochemical interactions.

INTRODUCTION

Among the most direct methods to sequester CO_2 is its injection into geological formations. Deep saline aquifers, uneconomic coal seams, and depleted gas reservoirs are potential options; however, depleted oil reservoirs are available for immediate deployment of this technology. Depleted oil reservoirs have distinct advantages over other geological storage options.

- Knowledge base: A large number of oil reservoirs have already been extensively characterized. Most of the characterization information for oil fields in the United States and elsewhere is publicly available. Additionally, the use of CO_2 in enhanced oil recovery (EOR) operations for more than three decades has resulted in information on interactions between CO_2 and reservoir rock and fluids that could be useful in estimating capacity and predicting the long-term fate of CO_2.
- Infrastructure: A major advantage of oil and gas reservoirs is that numerous wells have been drilled in these fields. A large percentage of these wells have the potential to be converted to injection and/or monitoring wells. In addition, CO_2-EOR operations have also resulted in pipeline infrastructure for transporting CO_2, most extensively in the Permian Basin in west Texas.
- Economics: Depleted oil reservoirs have the potential for incremental oil recovery that can considerably improve the overall economics for CO_2 sequestration projects.

There are also some disadvantages to depleted oil reservoirs. Based on the initial estimates, these reservoirs have lesser capacity compared to saline aquifers. In addition to the existing wells, these reservoirs have a large number of abandoned wells. In some cases, the locations of these wells are unknown. Depending on the quality of abandonment, these wells may become potential future pathways for escape of CO_2 from the reservoir.

Before geological sequestration of CO_2 can be used on large scales, confidence in this technology needs to be ensured by addressing safety issues, developing a proper regulatory regime, and better evaluating the overall economics. Ensuring confidence requires undertaking projects with specific sequestration-related objectives. In the case of oil reservoirs, this would require projects that are not typical (e.g., oil production-driven) EOR projects. Current industrial EOR reservoir strategies, which include uniform flood sweep, optimized placement of wells, inhibition of viscous fingering, and minimizing CO_2 injection (Mungan, 1992), are based on economic goals that are not well aligned with sequestration goals.

Sequestration goals are targeted to enhance sequestration volume and duration of CO_2 in geological formations. In the past, there have been few economic incentives and minimal research-and-development support to understand the physical and chemical interactions and ultimate fate of injected CO_2 in oil-producing reservoirs during EOR sweeps.

Our project aims to provide important elements of the science and technology base that will be necessary to properly evaluate the safety and efficacy of long-term CO_2 sequestration in depleted oil reservoirs. The results and data generated in this project will be valuable in assessing other geological reservoirs. The ultimate goal of the project is to predict the migration and long-term fate of CO_2 in sandstone oil reservoirs. Although the ultimate goal of such studies is to improve our understanding of the main sequestration mechanisms and resultant reservoir processes, a complete assessment of geological sequestration will require several similar test programs to assess different geological settings. The project is a multiorganizational effort that includes United States national laboratories, academia, and industry. The primary partners include the Los Alamos National Laboratory, Sandia National Laboratories, Strata Production Company, the New Mexico Institute of Mining and Technology, and the Colorado School of Mines. The project combines a small-scale field-injection experiment with geophysical monitoring, numerical simulation, and laboratory experiments, with the following objectives:

- characterization of the oil reservoir and its capacity to sequester CO_2
- characterization of the interactions of CO_2 with reservoir fluids and rocks
- assessment of the ability of geophysical techniques to monitor

The project is divided into three phases:

- Phase I consisted of preinjection activities, including characterization of the reservoir, calculation of expected CO_2 injection and migration behavior, acquisition of baseline geophysical surveys, preparation of the injection well, and acquisition of legal permits for injection.
- Phase II consisted of activities pertaining to the injection and soaking of CO_2 in the reservoir; these included the design of the field-injection test, preparation of surface injection facilities, injection of CO_2, measurement of reservoir pressure changes, acquisition of geophysical surveys, postsoaking CO_2 production, and refinement of computer-simulation models.
- Phase III consisted of activities related to predicting CO_2 migration and its interaction with the reservoir rocks and fluids, including acquisition of postsoak geophysical surveys, venting of CO_2 from the reservoir, monitoring gas and liquid production, collection and analysis of gas and liquid samples, iteration of computer-simulation models, and integration of the results, analyses, and data from the project.

We are currently continuing work in phase III, monitoring CO_2 migration in the reservoir, and are integrating the data acquired to understand CO_2 migration. This study provides details of the preinjection characterization activities and the field experiments. Details of the integration of data and modeling results and CO_2 migration will be published at a later date.

FIELD SITE

We chose the West Pearl Queen depleted oil reservoir for the field test. It is located in southeastern New Mexico (Figure 1) and is operated by the Strata Production Company (SPC) of Roswell, New Mexico. This field had some distinct advantages, including

- no economic and technical restrictions of an EOR operation
- opportunity and freedom to observe the response of the reservoir without the concerns of early breakthrough or degradation of production reservoir features
- availability of offset wells for monitoring instead of production of oil
- ability of varying soak times beyond industry EOR standards

The field has produced about 250,000 bbl (39,746 m^3) of oil since 1984. Production from the field has slowed in recent years. No secondary or tertiary recovery operations have been applied in the field, which made this field an attractive field site because the interpretation of field experiment results would not have the complications related to the prior enhanced recovery operations.

Figure 2 shows a site map with the locations of wells in the field. The field is primarily located in Sec. 27, 28, and 33, T19S R34W. Strata Production Company has drilled five wells in the field. Of the

Figure 1. Location of the West Pearl Queen field, southeastern New Mexico. The reservoir strata are 4500 ft (1371 m) below the surface geology, which consists of poorly and unconsolidated Tertiary and Quaternary sediments.

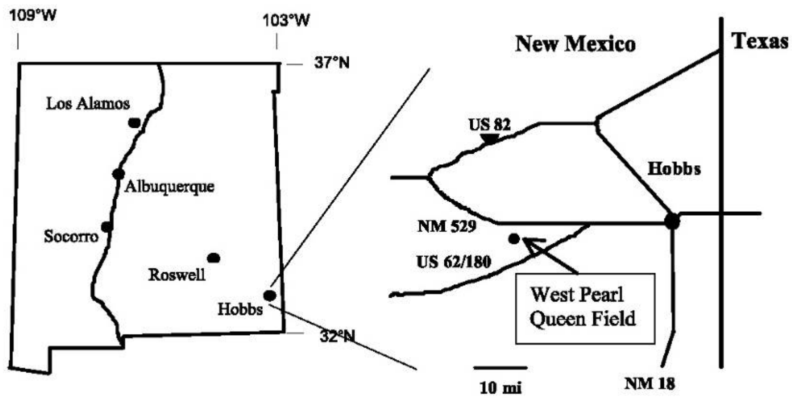

five wells, currently, only Stivason Federal 5 is actively produced. Wells Stivason Federal 1 and Stivason Federal 3 have been recently converted into produced-water disposal wells. Well Stivason Federal 2 has been shut in. Well Stivason Federal 4, which has been shut in since 1998, was chosen as the CO_2-injection well for the field experiment. Production from Stivason Federal 5 was stopped during the field experiment, and the well was available for monitoring and for cross-well surveys. Figure 2 also shows other wells in the area. Of these, only well Sun Pearl 2 is completed in the Queen Formation.

PREINJECTION CHARACTERIZATION

Preinjection characterization of the field included several activities. The goal was to characterize the reservoir geology, reservoir-flow dynamics, and the potential response of reservoir rock to CO_2 injection.

Geology

Several techniques and data sources were used to characterize reservoir geology. Prior to this project, data available to characterize the reservoir geology were

Figure 2. Structure-contour (subsea-depth) map of the West Pearl Queen field based on well picks at the top of the Shattuck Member of the Queen Formation. It is significantly different from the structure map based on seismic data presented later (Figure 8). This figure shows the locations of the wells pertinent to this study, including the production and water-injection wells, the central CO_2-injection well, and the monitor well.

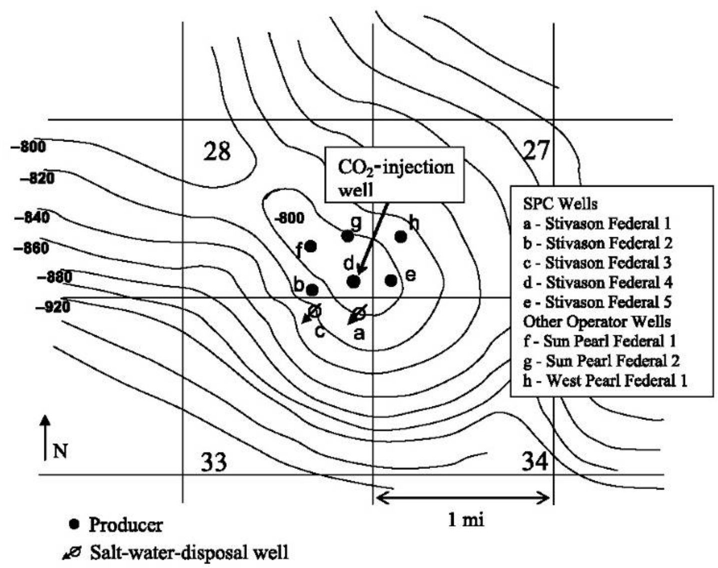

limited and primarily consisted of logs, including gamma ray, neutron porosity, density porosity, and dual laterologs (resistivity). In addition, results of core analyses, which consisted of porosity and permeability measurements for well Stivason Federal 1, were also available. No seismic surveys were acquired for the field prior to this project; hence, several activities were performed to further characterize the reservoir structure and geology. We were successful in obtaining actual core from the reservoir. A detailed analysis using the core, historic logs, and outcrop was performed. In addition, several geophysical surveys were acquired, including dipole sonic logs for wells Stivason Federal 4 and Stivason Federal 5; a cross-well survey between wells Stivason Federal 4 and Stivason Federal 5; and a high-resolution, three-dimensional, nine-component surface seismic survey. The surface seismic survey employed about 1000 source and receiver locations and covered an area of 1 mi^2 (2.6 km^2) around well Stivason Federal 4. The survey was repeated during the field experiment to monitor CO_2 migration. Both the repeat survey and the baseline survey were used to interpret the structure. The surveys had uniform azimuth and offset distribution and provided high-resolution coverage. Because time-lapse effects are subtle, the surveys were designed to maximize the signal-to-noise ratio of the data and its repeatability. In processing, surface-consistent linear processes were used, thereby preserving the integrity of the signal between the baseline and monitor surveys.

The West Pearl Queen field reservoir is in the Permian–age Shattuck Member of the Queen Formation. It is a sandy, shaly, and evaporitic unit deposited in ephemeral flood-plain fluvial environments at the margin of the Permian Basin (Holley and Mazzullo, 1988; Malicse and Mazzullo, 1990; Mazzullo et al., 1991). The average depth of the reservoir is about 4500 ft (1371.6 m). The average gross thickness of the reservoir is about 40 ft (12.2 m). Analysis of core shows three basic lithologies. About 80% of the available core consists of poorly cemented, oil-stained sandstone with 15–20% porosity and highly variable permeability up to 200 md (2×10^{-13} m^2). It is a cross-bedded to massive, arkosic, and fine- to very fine-grained sandstone. Oil staining and laboratory measurements indicate high porosity, and the three zones composed of this facies probably constitute the primary reservoirs. Several nonreservoir lithologies separate the zones of good reservoir properties. One common facies consists of thinly bedded sandstone to siltstone. The other common facies consists of laminated to massive, very fine-grained, light-gray sandstones.

Geophysical logs show that the reservoir is divided into three main high-porosity zones (Figure 3). In certain locations, one of the zones is further divided into two zones. Mineralogical analysis of the core shows that the good reservoir is a fine-grained, friable sandstone containing a preponderance of quartz, with lesser amounts of detrital K-feldspar and Na-rich plagioclase grains. The formation is cemented by prominent overgrowths of very pure euhedral, diagenetic K-feldspar and Mg-rich calcite (Figure 4). Any clays that may have been initially present were apparently obliterated by the diagenetic processes that gave rise to the K-feldspar and carbonate mineral overgrowths.

A P-wave tomogram from the cross-well survey is shown in Figure 5. In addition to the tomogram, derived velocity logs (red) and measured velocities using a dipole sonic log (black) are also shown. The West Pearl Queen Formation is the low-velocity zone between 4500- and 4600-ft (1371.6- and 1402.1-m) depth. The individual productive zones in the reservoir cannot be distinguished with the cross-well survey.

As mentioned earlier, both sets of three-dimensional surface seismic surveys were used to interpret the geological structure. Cross-equalization of the baseline and monitor seismic surveys was a critical part of the analysis. Figure 6 shows the reservoir interval on the baseline survey and both the matched and unmatched monitor surveys. Subtle differences are observed above the reservoir on the unmatched survey, and these differences were removed on the cross-equalized survey. The Queen Formation was interpreted as a trough between 740 and 758 ms, representing the Seven Rivers–Queen lithofacies change from carbonate to siliciclastic rocks. The time-structure map and edge-detection maps created from the P-wave seismic data on the reservoir interval characterize a sand-filled incised paleochannel and some paleohighs associated with the dome structure, as originally interpreted from the well data. The depth-structure map of the West Pearl Queen reservoir differs significantly from the time-structure map, showing an anticlinal structure to the east of the CO_2-injection well (Figure 7). Figure 8 shows the RMS (root-mean-squared) amplitude map. Both the cross-well survey and RMS amplitude map show that the reservoir is heterogeneous between wells Stivason Federal 4 and Stivason Federal 5.

Outcrops of the Shattuck Member sandstones approximately 50 mi (80 km) to the west but in the same position several miles landward of the Goat Seep reef contain two prominent and consistent fracture sets, but neither core nor well tests indicate the presence or

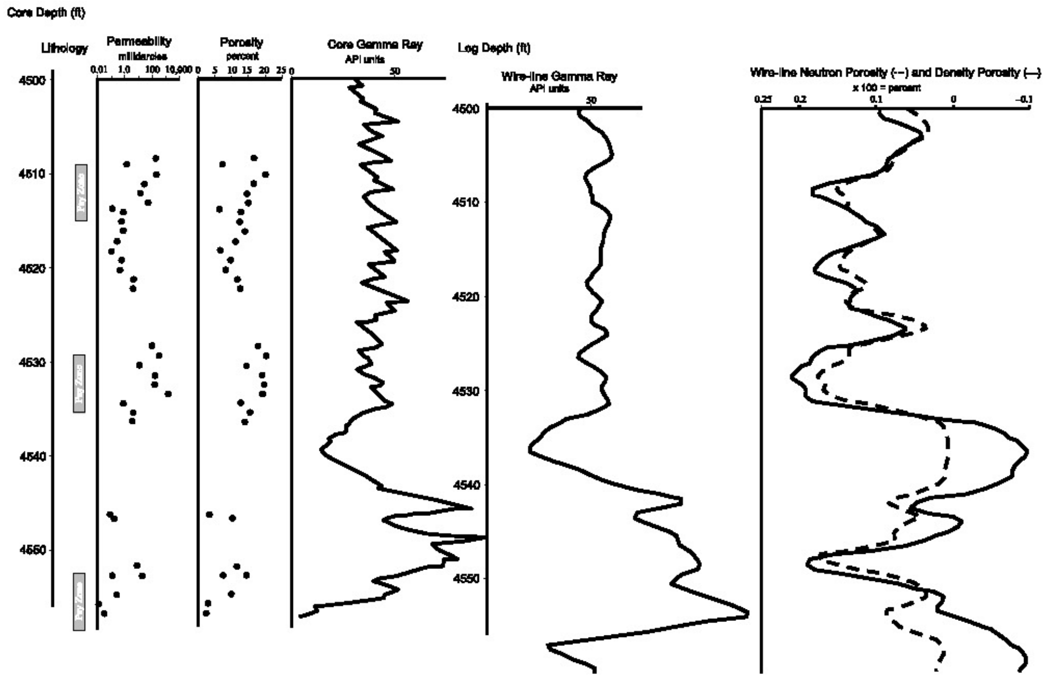

Figure 3. Comparison of core data and wire-line-log data for well Stivason Federal 1. Poor gamma-ray differentiation of units reflects the high potassium-feldspar content of the sandstones. Large sections of the core were missing by the time of this study, but records of the porosity and permeability data were found for some of the missing intervals. The three high-porosity zones depicted that both the neutron and density porosity logs (right scale) have been used in the modeling effort. A 10–12-ft (3–3.6-m) depth shift exists between the core and wire-line data.

influence of natural fractures in the subsurface reservoirs of the West Pearl Queen field. Similarly, the seismic data do not show the presence of any major faults in the reservoir, suggesting that there are no structural complications that would compartmentalize or divert injected CO_2.

Laboratory Experiments

To characterize the reservoir rock and fluids and to understand the impact of CO_2 on reservoir rock properties, two separate types of laboratory experiments were performed.

1. Static experiments: These experiments were performed to characterize the geochemical interactions between reservoir rock, formation brine, and CO_2. Injection of CO_2 leads to lowering the pH of formation brine and may initiate geochemical reactions. The geochemical reactions could either lower

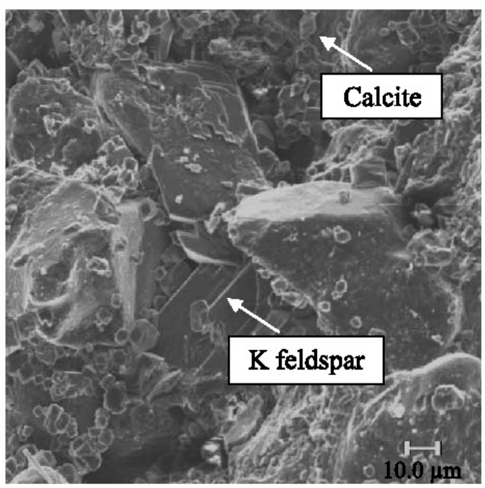

Figure 4. Scanning electron microscopy photograph of a West Pearl Queen reservoir rock sample prior to being exposed to CO_2. Calcite cements and potassium feldspars are fresh and unaltered.

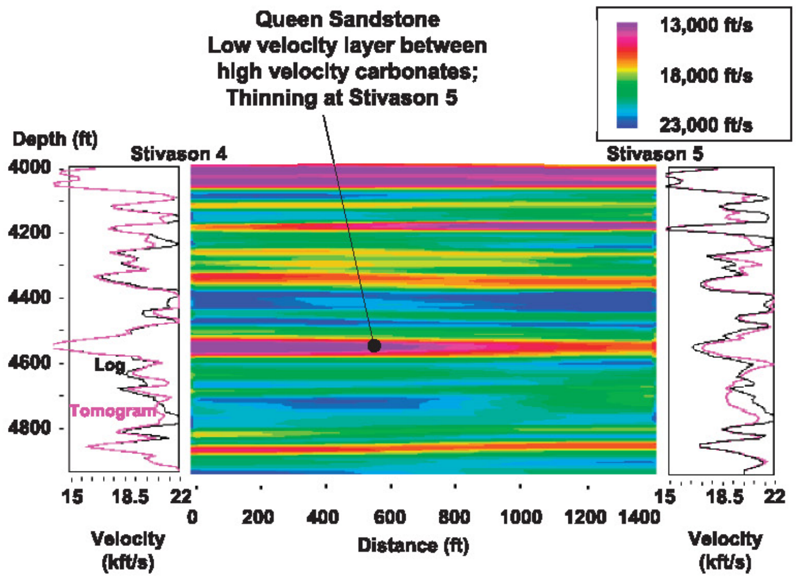

Figure 5. Tomogram of P-wave (center) and derived and measured log velocities (sides) for preinjection cross-well survey between wells Stivason Federal 4 and Stivason Federal 5.

formation porosity and permeability by precipitating new minerals or increase porosity and permeability by dissolving mineral phases. In the long term, geochemical interactions can lead to chemical fixation of CO_2 in the form of a stable mineral phase. It is crucial to determine what types of geochemical reactions are occurring as well as what the kinetics of the reactions are. These questions were addressed by a combination of laboratory experiments and numerical modeling. The laboratory experiments were relatively short term (months) and were most applicable to predicting what changes might have happened in the field experiment time frame. During the experiments, a few tenths of a gram of sandstone was placed in a stainless-steel autoclave with 3 mL of formation brine, and subjected to 700 psig (4.8 MPa) of CO_2 pressure at 40°C. After 19 months, both the fluid and rock samples were examined. The present-day indigenous brine is essentially a sodium (52 ppt)-chloride (109 ppt) brine, with lesser amounts of

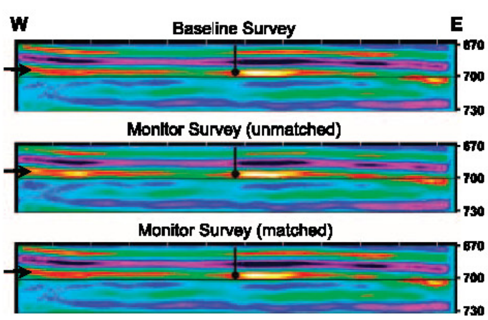

Figure 6. Cross section showing the West Pearl Queen reservoir based on the baseline and matched and unmatched monitor three-dimensional seismic survey.

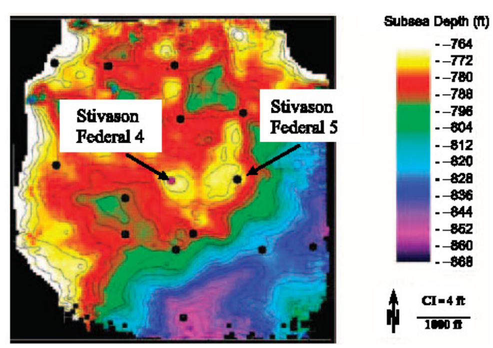

Figure 7. Depth-structure map of West Pearl Queen reservoir based on seismic two-way traveltimes converted to depth using the log-derived velocity model.

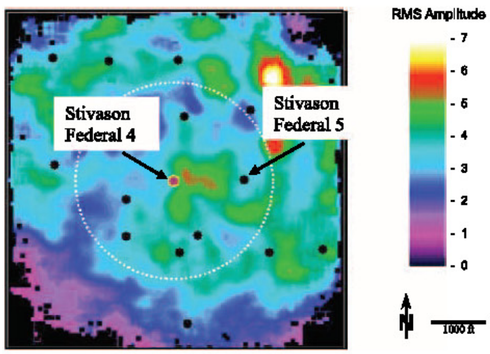

Figure 8. Root-mean-squared (RMS) amplitude map of the West Pearl Queen reservoir. Variability in the amplitude represents heterogeneity in the reservoir.

dissolved potassium (1.6 ppt), magnesium (3.1 ppt), calcium (also 3.1 ppt), sulfate (1.8 ppt), and bicarbonate (0.12 ppt). Post-test fluid analysis showed that the dissolved Ca levels had increased by 23%, and that of Mg had increased by 35%. Dissolved silicon (not silica) dropped from 12.3 to 3.6 ppm, whereas aluminum concentration increased from 0.05 to 0.33 ppm. Considering the amounts of alkali metals (Ca, Mg) initially present in the brine relative to the amounts of silicon and aluminum, it would be reasonable to surmise that most of the short-term changes in the formation chemistry would involve the removal of the carbonate minerals. In fact, all of the calcite and virtually all of the more Mg-rich dolomitelike phase were removed during the course of the experiment. Diligent examination of the samples, however, also revealed some etching of the plagioclase feldspars, as well the beginning of clay precipitation (Figure 9). The K-feldspars were not affected by the treatment. The laboratory experiments suggested that dawsonite might not form during the field test. Early formation of clays was relatively slow compared to the duration of the field test. These results indicate that the probable geochemical alterations during the field test will not affect reservoir transport properties.

2. Flowthrough experiments: These experiments were performed with samples from the reservoir core representing several possible producing zones (Table 1) to test for porosity, permeability to brine, and relative permeability to brine and CO_2 (the relative permeability measured in these experiments did not include three-phase relative permeability in the presence of oil). As can be seen from Table 1, the permeability varied from high to low within a short distance. Figures 10 and 11 represent the relative permeability curves for core plugs at 4510.5 ft (1374.8 m) depth. Each of these measurements was performed at 114°F (45.5°C) and at two pore pressures, 500 and 2000 psig (3.4 and 13.8 MPa). The differences in the two figures are primarily caused by differences in pressure. The difference in pressure results in large differences in the density of CO_2, solubility of water in CO_2 and CO_2 in brine, and surface tension between the phases. Figure 12 shows changes in porosity and permeability with time because of the effects of two-phase flow of brine and CO_2. The figure shows porosity and permeability versus pore volumes of fluid injected. It is interesting to note that, with time, porosity increased, whereas permeability decreased. A possible explanation for this could be that geochemical reactions with CO_2 have freed cemented fines that migrated and got stuck in pore throats, thus reducing the permeability. In each of the tests, the irreducible brine saturation was between 60 and 70% when using CO_2 to reduce brine saturation in a core 100% saturated with brine. Figure 13 shows the amount of brine

Figure 9. Scanning electron microscopy photographs of West Pearl Queen reservoir sandstone after 19 months exposure to high-pressure CO_2 gas. The potassium feldspars (left) have not been affected, whereas the sodium and calcium feldspars have started to etch (middle), and authigenic clays derived from dissolution of these components have started to form (right).

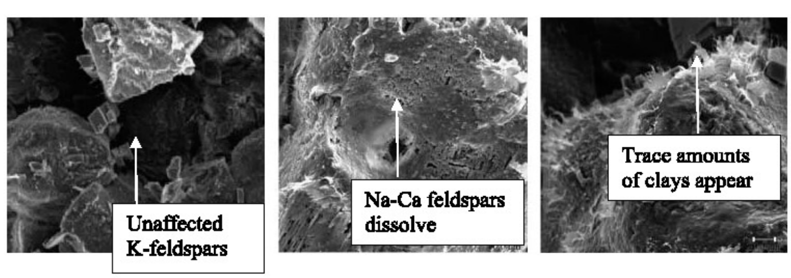

Table 1. Rock Properties from West Pearl Queen Reservoir Core Samples

Core Depth (ft)	Permeability to Brine (md)	Porosity (%)
4508.9	<<1	
4510.5	160	21.7
4511.2	15.8	18.1
4513.0	2.62	14.0
4532.5	117	20.5
4532.7	<1	

produced because of CO_2 injection during a laboratory core-flooding experiment. After 4000 cm^3 (244 $in.^3$) of CO_2 (at reservoir conditions) had been injected, 0.62 PV (pore volume) of brine was left behind in sample 4532.5.

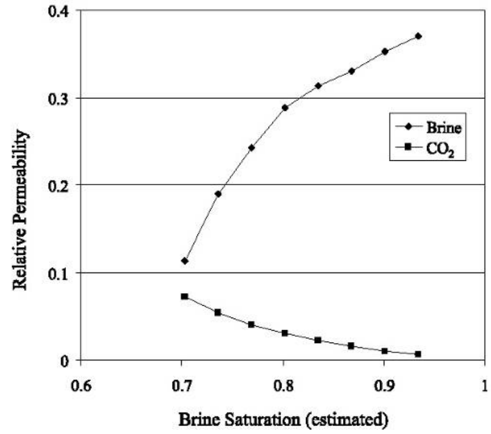

Figure 11. Relative permeability curve for core plug 4510.5 at 2000 psig (13.8 MPa). At higher pressures, the relative permeability to CO_2 decreases significantly as brine saturation increases.

Numerical Simulations

Two types of numerical simulations were performed, including flow simulations and geochemical reaction simulations. The overall goal of numerical simulations is to predict the long-term migration and the fate of CO_2 in the reservoir. The goal of the preinjection numerical simulations was to characterize the reservoir-flow dynamics, as well as the geochemical interactions. Results of these simulations were used to understand the laboratory experiment results and to predict field experiment behavior.

1. Reservoir-flow simulations. These simulations were performed to characterize the overall flow behavior of the reservoir. Preinjection simulations were also used to determine whether the proposed amount of CO_2 could be injected in the target interval given the operational and regulatory constraints. The regulation required the injection to be performed at a rate

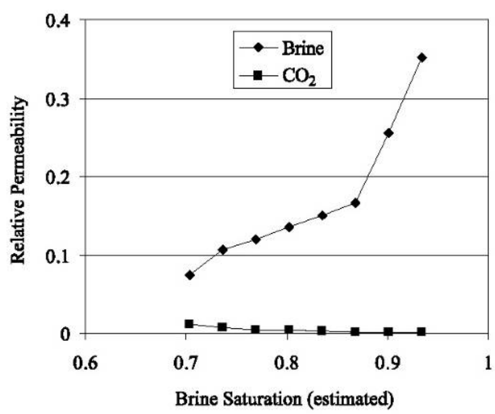

Figure 10. Relative permeability curve for core plug 4510.5 at 500 psig (3.45 MPa). The relative permeability to CO_2 decreases slightly as brine saturation increases.

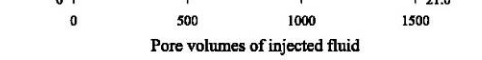

Figure 12. Change in core porosity and permeability during CO_2 injection in laboratory experiments. Permeability decreased by more than 50%, possibly because of growth and migration of clays, whereas porosity, initially increasing by several percent because of dissolution, stabilized.

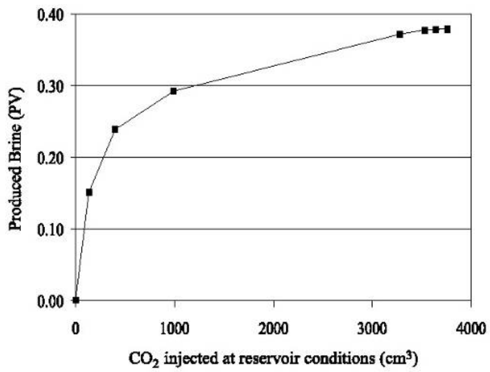

Figure 13. Amount of brine produced during CO_2 injection in laboratory experiment for core 4532.5 (20 cm^3 [1.22 $in.^3$] ~1 PV). The core was initially saturated with brine. Even after injection of almost 200 PV of CO_2, a significant amount of brine (~0.63 PV) is left behind in the core.

such that the bottom-hole pressure does not exceed the rock-fracturing pressure. Based on the prevailing lithostatic pressure gradient, 0.64 psi/ft (14.5 kPa/m), and depth of the injection interval, this pressure was determined to be about 2900 psi (19.9 MPa) at the bottom hole. In addition, the simulations were also used to determine the possible migration of CO_2 after injection. A numerical model for the reservoir was developed based on the geological characterization. At the time the preinjection simulations were performed, geophysical surveys were not acquired; hence, only the data based on log and core analysis were used to develop the flow model. The numerical simulations were run using Eclipse, Schlumberger's oil reservoir simulator. The flow model was validated through matching the historic production data and then used to perform CO_2-injection simulations. These simulations were performed using the compositional module. Compositional simulations consider thermodynamic interactions between the hydrocarbon components present in the reservoir. Several simulation runs were performed to characterize the reservoir response to varying injection conditions. The simulations were run to model the injection as well as subsequent soak and venting operations of the field experiments. The simulation results indicated that CO_2 could be injected in the reservoir at a rate of 100 t/day (100,000 kg/day) without exceeding the bottom-hole pressure constraint. It was also estimated that the CO_2 plume would reach the monitoring well (Stivason Federal 5) during the 6-month soak period. Simulation of the venting operation suggested that about half of the injected CO_2 could be produced from the reservoir in the first 6 months of venting.

2. Geochemical simulations. Two types of numerical models were used to characterize the geochemical interactions. The first model, REACT, was used to predict the most stable configuration of the system after equilibrium has been achieved along a reaction path with the steady addition of CO_2. The second numerical model, FLOTRAN (flow and transport simulator) (Lichtner, 2001), was used to explore both short- (months) and long (more than 1000-yr)-term geochemical behavior. The model REACT was used to study a system containing minerals and brine with compositions similar to the reservoir rock and brine and in proportions closer to what may be present in the reservoir (Table 2). Model predictions showed that this system could result in precipitation of large amounts of dawsonite [$NaAlCO_3(OH)$] (Figure 14). In addition, kaolinite would be formed from the reaction of albite. The brine-to-mineral ratio was varied to more closely reflect the conditions in the laboratory experiments mentioned earlier. This system predicted reaction products similar to the ones observed in the laboratory experiments, including the early appearance of some clay, the disappearance of calcite, and the partial early attrition of albite (Figure 15). However, the results of the model, having a more formationlike rock-to-brine ratio, suggest that the appearance of clays in the laboratory experiments should not be taken as a potential indicator that they would appear either throughout the long term in a sequestration setting or in the short term in a field test. The most important part of these calculations is the ubiquitous prediction that significant amounts of dawsonite will accompany the breakdown of feldspars.

Table 2. Proportion of Brine and Minerals Used for REACT Simulations

Component	Weight (kg)
Brine	1.0
K-feldspar	1.9
Quartz	10.3
Albite	2.5
Anorthite	12.5
Calcite	0.15
CO_2	0.6

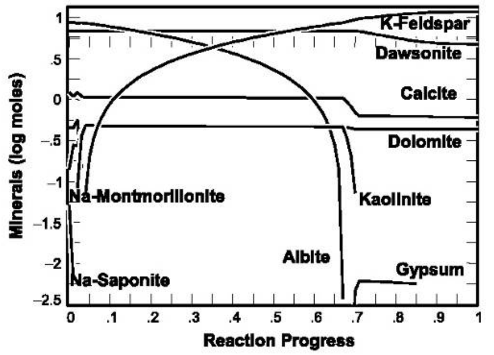

Figure 14. Calculation of minerals that would be formed because of CO_2 reaction with West Pearl Queen reservoir sandstone and brine using a mineral-to-brine ratio similar to that found in the actual reservoir.

Simulations with FLOTRAN were used to match observations of the laboratory experiment after 19 months. To match the experiment results, values of the kinetic constants at 25°C, k_{25} (mol/cm^2 s), and the mineral surface areas (m^2/g) were varied. Values of surface areas and the reaction parameters were obtained from literature (Rimstidt and Barnes, 1980; Knauss and Wolrey, 1986; Fetter, 1999; and Xu et al., 2003). Table 3 lists the allowed mineral phases and the associated variable parameters used to generate the best fit to the experiment. The initial water/rock ratio was set to 3.16. Similar to REACT simulations, this system also resulted in the formation of dawsonite. To match the laboratory observations, the formation of dawsonite and chalcedony had to be suppressed (to allow formation beidelite-Na, which may be the clay mineral observed in the SEM images in Figure 9), and the kinetic rate constant, k_{25}, for K-feldspar had to be reduced from 10^{-16} to 10^{-17} (mol/cm^2 s). Figure 16 shows the pre- and postexperiment major ion brine chemistry for both the laboratory experiment and the simulated experiment. Most of the experimental results are captured in this simulation; however, we were not able to lower the total Al^{3+} in solution to the levels seen in the experiment. In addition, the simulations predict slightly more aqueous SiO_2 than that seen in the experiment. This model was used to predict the long-term geochemical behavior by performing a 1000-yr simulation. For this model, the water/rock ratio was changed to 0.176, closer to that expected in the field. Figure 17 shows the time history of mineral formation and dissolution throughout 1000 yr. The results show that quartz, dolomite, and kaolinite precipitate. Initially, calcite precipitates, but after 50 yr, it dissolves slowly. Potassium-feldspar remains unaltered, whereas beidelite-Na initially precipitates until approximately 50 yr and then rapidly dissolves. Total porosity in the simulation dropped from 0.15 to 0.146, which implies that significant changes in the porous medium will not occur. The fugacity of CO_2 dropped from 48.26 to a value of 0.31 after 1000 yr. This means that the pure-phase CO_2 has been converted into both minerals (calcite, dolomite, and kaolinite) and aqueous carbonate species.

FIELD EXPERIMENT

The central part of the project was the characterization of field response to CO_2 through a field experiment. The field experiment consisted of three steps: injection, soak, and venting. The total duration of the test from the beginning of the injection to the initial venting was about 11 months. Details of each of these steps follow.

Injection

The injection consisted of 2090 t (2.09 million kg) of CO_2 throughout a period of 50 days, between December 20, 2002, and February 11, 2003. As mentioned earlier, CO_2 was injected through well Stivason Federal 4. Based on preinjection characterization, the expected rate of injection was about 100 t/day (100,000 kg/day). This rate was estimated based on the bottom-hole pressure upper-limit constraint of 2900 psi (19.9 MPa).

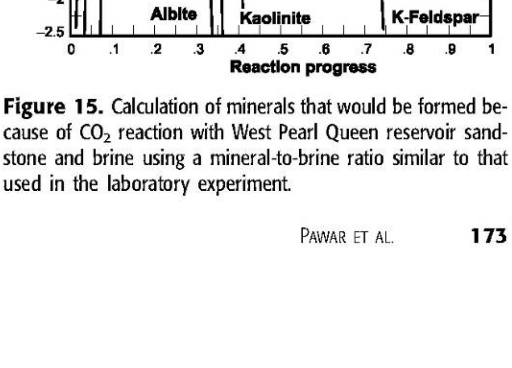

Figure 15. Calculation of minerals that would be formed because of CO_2 reaction with West Pearl Queen reservoir sandstone and brine using a mineral-to-brine ratio similar to that used in the laboratory experiment.

Table 3. Best-Fit Parameters Used for FLOTRAN Simulations of the Bench-Scale Experiment for All Mineral Phases Allowed in the Simulation

	Surface Area (cm^2/g)	Log k_{25} (mol/[cm^2 s])	Initial Volume Fraction Bench Scale	Initial Volume Fraction Field Scale	Final Volume Fraction Field Scale (pH = 6.6)
Albite	6×10^2	10^{-16}	0.07	0.136	0.125
Anorthite	6×10^2	10^{-16}	0	0.007	0.0
Quartz	5×10^2	$10^{-17.9}$	00.129	0.587	0.591
SiO_2 amorphous	1×10^5	$10^{-15.6}$	0	0	0
K-feldspar	3×10^2	10^{-17}	0.042	0.118	0.119
Magnesite	3×10^4	10^{-15}	0	0	0
Kaolinite	3×10^5	10^{-17}	0	0	1.18×10^{-2}
Dolomite-dis	3×10^4	$10^{-18.2}$	0.0001	4.25×10^{-4}	1.85×10^{-3}
Calcite	3×10^3	$10^{-12.8}$	0.00043	1.53×10^{-3}	3.82×10^{-3}
Beidelite-Na	3×10^5	10^{-17}	0	0	0
Gypsum	1×10^5	10^{-13}	0	0	0

During injection, the surface injection pressure quickly reached 1400 psi (9.6 MPa). Based on the surface pressure, the bottom-hole pressure was estimated to be about 2900 psi (19.9 MPa), and the surface injection pressure was not increased above this value. The injection rate was about 200 bbl/day, which translated to 40 t/day (40,000 kg/day). This rate was significantly lower than the preinjection estimates. The surface injection pressure remained constant throughout injection, and the rate of injection could not be increased. Figure 18 shows the pressure, injection rate, and cumulative injected CO_2 during the experiment. We also deployed a passive seismic monitoring technique during injection. A receiver array was deployed in well Stivason Federal 5, and the microseisms generated during injection were recorded. Analysis of the data did not show any significant microseismic events, suggesting that the injection rate was not high enough to cause any significant fracturing. The lower-than-expected injection rate suggests that the reservoir permeability was lower than estimated, and that the reservoir pressure was higher than expected.

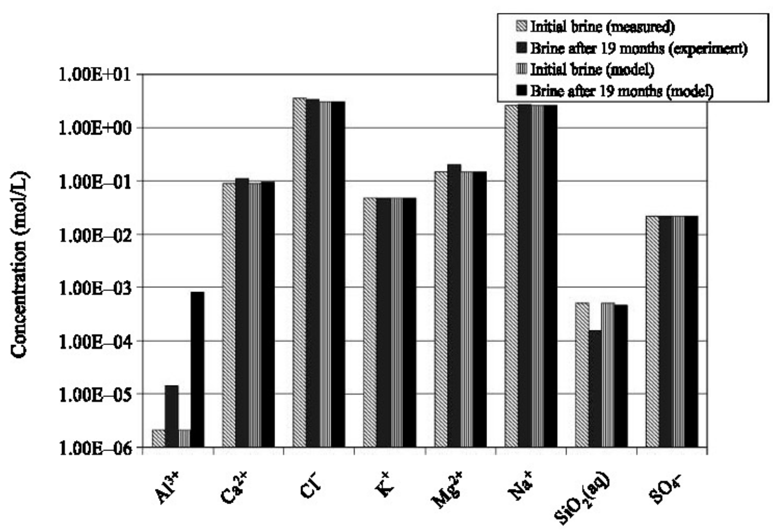

Figure 16. Comparison of FLOTRAN results with geochemical laboratory experiment results after 19 months. Dawsonite and chalcedony formation had to be suppressed to make the model ("model") match the laboratory results ("measured" and "experiment").

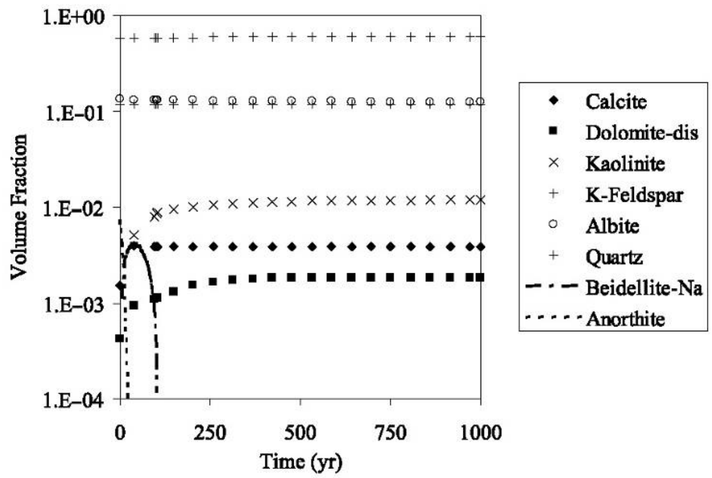

Figure 17. FLOTRAN predictions of geochemical reaction products after 1000 yr. Most changes occur within the first 150–200 yr, when kaolinite and dolomite precipitate while anorthite dissolves. Beidellite-Na initially precipitates but then dissolves.

Soak

At the end of injection, a downhole pressure monitor was deployed in the injection well, and the well was shut in for 6 months. The pressure in the reservoir was monitored intermittently. The measured reservoir pressure is shown in Figure 19. As can be seen from the figure, the pressure near the injection well did indeed reach 2900 psi (19.9 MPa). The pressure reached an asymptotic value after the initial drop-off, indicating that steady state was reached. The equilibrium pressure value was about 1700 psi (11.7 MPa), which was significantly higher than earlier predictions. Carbon dioxide was allowed to soak for 6 months, at the end of which, another three-dimensional, multicomponent seismic survey was acquired. As mentioned earlier, this monitoring survey had the same attributes as the baseline survey.

Venting

After acquisition of the postinjection seismic survey, CO_2 was vented from well Stivason Federal 4. The well was connected to a separator and a fluid collection

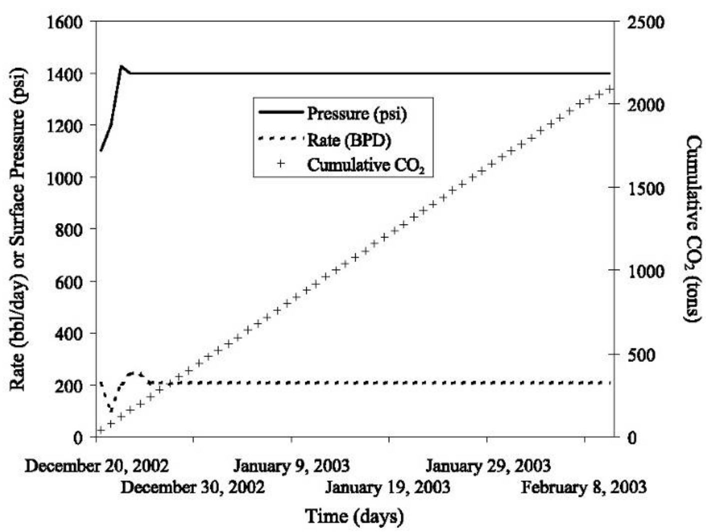

Figure 18. CO_2-injection parameters during field injection experiment. The injection rate stabilized at 40 tons/day (200 bbl/day), well below the expected 100 tons/day, because injection pressures were much higher than expected.

Figure 19. Bottom-hole pressure in well Stivason Federal 4 during the post-injection soak period, showing that the reservoir pressure was nearly stabilized at equilibrium 2 months after shut-in.

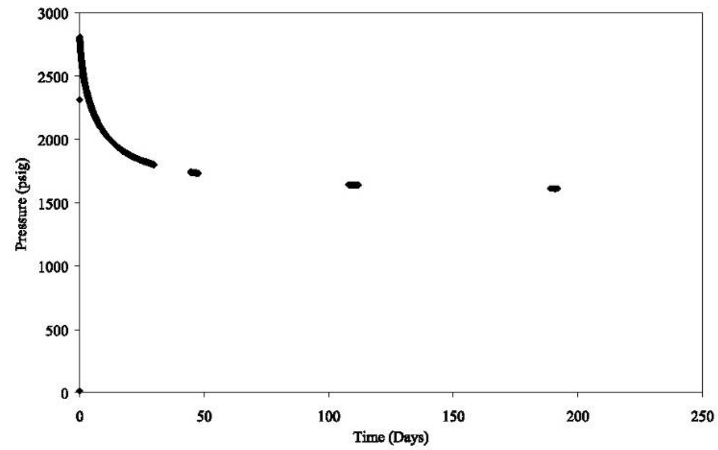

facility to monitor the amounts of fluids produced, as well as to collect periodic samples for chemical analyses. In addition, gas samples from well Stivason Federal 5 were also collected for chemical analyses. During the initial venting period, well Stivason Federal 4 produced fluids (gas and liquids) without any pumping. This period lasted for 9 days. After 9 days, the well stopped flowing, at which point a pumping unit had to be installed to produce the well further. The well has been on continuous production since that time and is currently on production. Figure 20 shows the amount of gas produced from the well for the first 3 months of venting and production. The daily rates of production of oil and water for the first 3 months of production are plotted in Figure 21. The gas production rates were significantly lower than the CO_2-injection rates. During the first 3 months of venting, only 17% of the total injected CO_2 was produced. The amounts of oil and water produced during venting and subsequent production phase were similar to production from the well during the pre-experiment days when it was actively produced. Figure 22 is a plot of the overall gas compositions of the samples collected from well Stivason Federal 4 during the venting and subsequent production operations. Figure 23 shows the trend in % CO_2 in the gas produced from Stivason Federal 4 until December 2004. Similarly, Figure 24 shows a plot of the gas composition of the samples collected from well

Figure 20. CO_2 production from well Stivason Federal 4 during the postsoak venting operation. Open-flow rates diminished rapidly during the first 200 h or 9 days of venting, after which, it would not flow. A pump was subsequently installed on the well, and production reached near equilibrium about 1 month after venting first began.

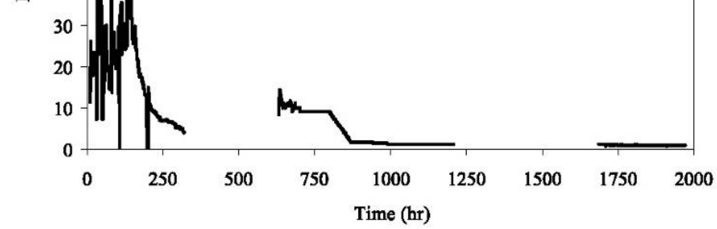

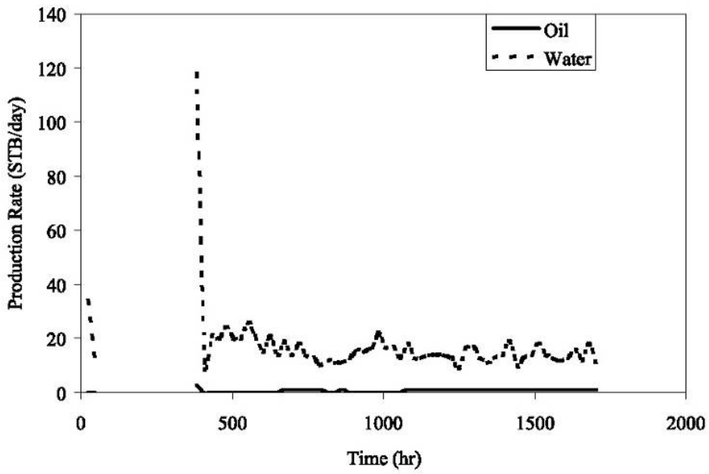

Figure 21. Water and oil production from well Stivason Federal 4 during the postsoak venting operation. The jump in water production subsequent to the installation of pump is caused by the accumulation of water during the shut-in period, during which the pump was installed.

Stivason Federal 5. The pre-CO_2-injection gas from the reservoir had less than 1% CO_2, whereas the gas samples collected from well Stivason Federal 4 during the venting operation was in the range of 95–99 mol% CO_2 through June 2004. The last two samples taken in October and December 2004 had 87.9 and 89.9 mol% CO_2, respectively. Samples from well Stivason Federal 5 do not show any presence of CO_2, which indicates that CO_2 had not migrated to well Stivason Federal 5 until December 2004. The oil and water production data from well Stivason Federal 5 and Sun Pearl 2, which are the only two actively producing wells from the West Pearl Queen reservoir interval, indicate that production from these wells has not been affected after the CO_2-injection experiment.

Geophysical Monitoring

As mentioned earlier, we used a time-dependent, three-dimensional seismic survey to monitor the CO_2 plume in the reservoir. So far, only the P-wave data have been processed, whereas interpretation of the S-wave data is still in progress. The P-wave seismic difference volume shows time-lapse amplitude anomalies in the reservoir interval east and southeast of the injection well. Figure 25 is a map of the RMS amplitude difference between the baseline and matched monitor survey over the West Pearl Queen reservoir interval. The contours that are overlain are the West Pearl Queen reservoir depth structure with a contour interval of 4 ft (1.22 m). The interpreted CO_2 distribution is highlighted and

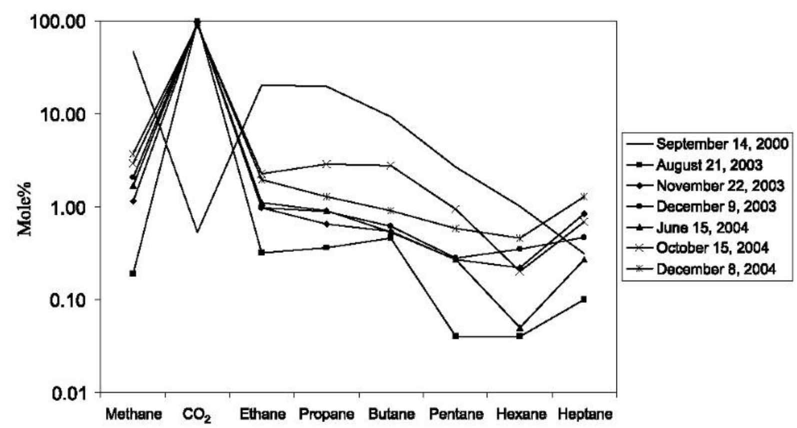

Figure 22. Composition of gas produced from well Stivason Federal 4 during CO_2 venting operation, showing the dramatic increase in CO_2 over the original gas compositions prior to injection.

Figure 23. CO_2% in the gas produced from well Stivason Federal 4 decreased with time during CO_2 venting operation.

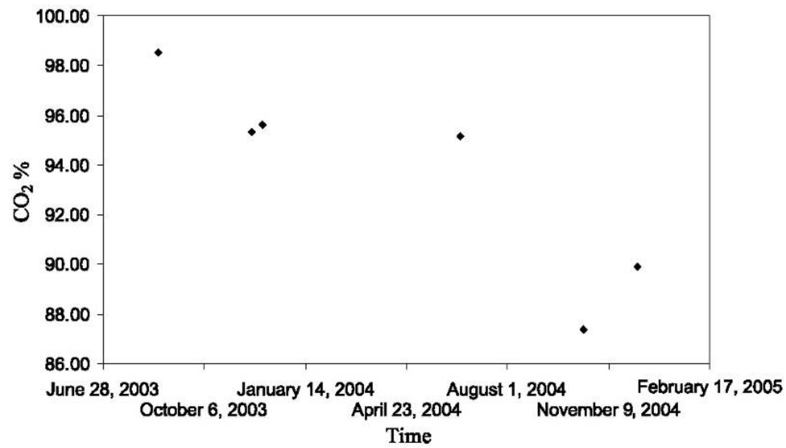

contained in the thicker, higher quality sands near the crest of the subtle anticline. The extent of the CO_2 plume as shown in the figure is consistent with observed CO_2 migration, based on production response from the wells in the vicinity, as well as the gas composition analyses from well Stivason Federal 5. The plume is also consistent with the reservoir structure and sand continuity between wells Stivason Federal 4 and Stivason Federal 5. Analysis of seismic data also shows that CO_2 has not migrated to formations other than the West Pearl Queen reservoir.

SUMMARY AND CONCLUSIONS

The observations and experimental results show that extensive reservoir characterization is necessary to understand and predict the impact of CO_2 injection on storage reservoirs. The response of the West Pearl Queen reservoir during the field experiment was significantly different than expected based on the preinjection characterization.

First, the observed CO_2-injection rate was much lower than the estimates based on earlier characterization work. This indicates that the permeability of the reservoir to CO_2 injection is significantly different than the laboratory values measured on core samples prior to this project. The static and dynamic laboratory experiments showed that geochemical interaction between CO_2 and West Pearl Queen sandstone could result in the migration of fines and decreased permeability, although more research is necessary to confirm that permeability changes observed in cores and in the field are the result of the same process. Second, the log analyses indicated that West Pearl Queen reservoir is continuous between the injection well (Stivason Federal 4) and the monitoring well (Stivason Federal 5). Numerical simulations with models based on the log analyses

Figure 24. Composition of gas produced from well Stivason Federal 5. Mole % of CO_2 in the produced gas from this well indicates that injected CO_2 has not migrated to the well until at least December 8, 2004, approximately 2 yr after CO_2 injection began in well Stivason Federal 4.

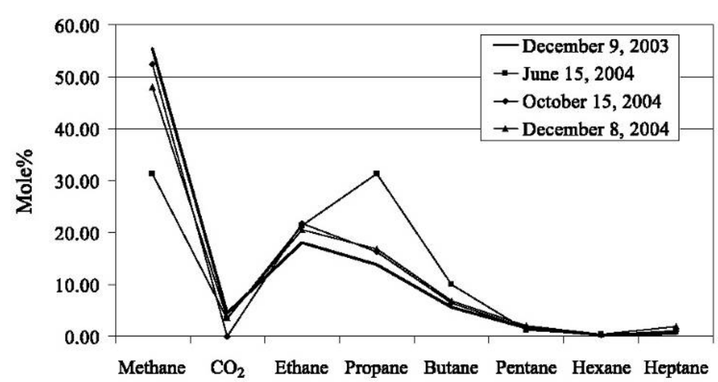

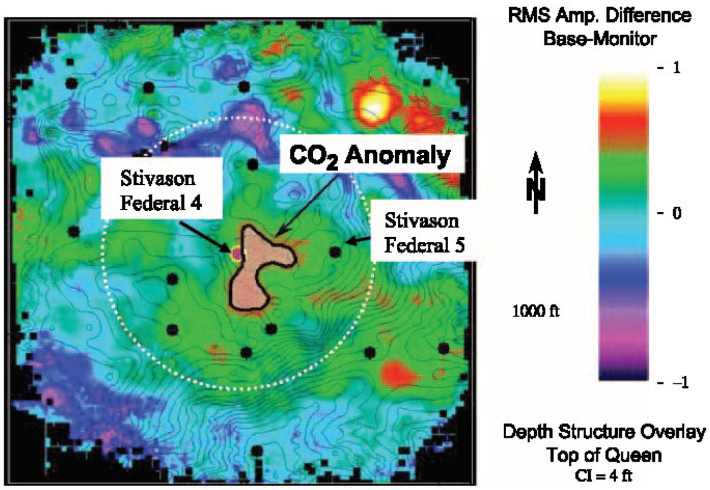

Figure 25. A map of RMS (root-mean-squared) amplitude difference between baseline and monitor three-dimensional, multidimensional surveys. The difference between the pre- and postinjection maps is taken as an indication of the probable location of the injected CO_2.

indicated that response of CO_2 injection in well Stivason Federal 4 would be observed in well Stivason Federal 5 in about 6 months. However, the observed production response during the field experiment as well as the geologic interpretation based on the seismic data imply that the reservoir is not continuous between the two wells. Comparison of the structure contours in Figure 2 (which were generated from well-log picks) and the structure interpreted from geophysical data (Figure 7) suggests that the reservoir geologic heterogeneity is not completely captured with analyses based on the log data alone. This project clearly demonstrates the importance of capturing the interwell heterogeneity for monitoring purposes. Third, the rate of production and the cumulative production during the initial 3 months of venting were significantly lower than expected. This indicates possible formation damage near the wellbore. It is also possible that the injected CO_2 dissipated away from the wellbore during the soak period into porosity not connected to the monitoring and production well.

Geophysical monitoring using P-wave analysis of the three-dimensional multicomponent seismic data shows an anomaly that may indicate the presence of CO_2. We are currently analyzing S-wave data to support this conclusion. This study shows the applicability of the surface seismic method for detecting a CO_2 plume, although the amount of CO_2 injected was small and individual zones were thin.

The laboratory experiments also provided some valuable results. Although dawsonite is a potential geochemical reaction product in sandstone reservoirs, this mineral was not formed during the laboratory experiments. Understanding the kinetics of dawsonite formation is critical for sequestration in sandstone reservoirs for two reasons. First, dawsonite is an important sink for CO_2, and second, its formation can also lead to irreversible and potentially damaging changes in reservoir properties such as permeability and porosity.

The results described in this study provide a basis that can be used to perform further studies to evaluate depleted oil reservoirs as a sequestration option. Our conclusions, combined with those of additional observations in this and other similar studies, should allow predictions on the long-term fate of CO_2 in depleted sandstone oil reservoirs.

REFERENCES CITED

Fetter, C. W., 1999, Contaminant hydrogeology: Upper Saddle River, New Jersey, Prentice-Hall, 171 p.

Holley, C., and J. Mazzullo, 1988, The lithology, depositional environments, and reservoir properties of sandstones in the Queen Formation, Magutex North, McFarland North, and McFarland fields, Andrews County, Texas, *in* B. K. Cunningham, ed., Permian and Pennsylvanian stratigraphy, Midland Basin, west Texas: Studies to aid hydrocarbon exploration: Permian Basin Section-SEPM Research Seminar No. 1, Publication 88-28, p. 55–63.

Knauss, K. G., and T. J. Wolrey, 1986, Dependence of albite dissolution kinetics on pH and time at 25°C and 70°C: Geochimica et Cosmochimica Acta, v. 50, no. 11, p. 2481–2497.

Lichtner, P. C., 2001, FLOTRAN user manual. LA-UR-01-2349: Los Alamos, New Mexico, Los Alamos National Laboratory, 172 p.

Malicse, A., and J. Mazzullo, 1990, Reservoir properties of the desert

Shattuck Member, Caprock field, New Mexico, *in* J. H. Barwis, J. G. McPherson, and J. R. J. Studlick, eds., Sandstone petroleum reservoirs: Casebooks in earth science: New York, Springer-Verlag, p. 133–152.

Mazzullo, J., A. Malicse, and J. Siegel, 1991, Facies and depositional environments of the Shattuck Sandstone on the northwest shelf of the Permian Basin: Journal of Sedimentary Petrology, v. 61, p. 940–958.

Mungan, N., 1992, Carbon dioxide flooding as an enhanced oil recovery process: Journal of Canadian Petroleum Technology, v. 31, p. 13–15.

Rimstidt, J. D., and H. L. Barnes, 1980, The kinetics of silica-water reactions: Geochimica et Cosmochimica Acta, v. 44, no. 11, p. 1683–1699.

Xu, T., J. A. Apps, and K. Pruess, 2003, Reactive geochemical transport simulation to study mineral trapping for CO_2 disposal in deep arenaceous formations: Journal of Geophysical Research, v. 108, no. B2, p. 2071.

APPENDIX B

Benson, R. D. (Colorado School of Mines) and Davis, T. L. (Colorado School of Mines), 2006. Multicomponent Seismic Monitoring of a CO_2 Sequestration Pilot, West Pearl Queen Field, U.S.A., R.D. Benson (Colorado School of Mines) & T.L. Davis (Colorado School of Mines) EAGE 68th Conference & Exhibition - Vienna, Austria, 12-15 June 2006.

Multicomponent Seismic Monitoring of a CO_2 Sequestration Pilot, West Pearl Queen Field

R.D. Benson (Colorado School of Mines) & T.L. Davis (Colorado School of Mines)

Summary

This paper describes an experiment in West Pear Queen Field, Lea County, New Mexico, to measure differences in the Queen Formation sandstone reservoir before and after an injection of 2090 tons of CO_2 into the reservoir. Time-lapse (4-D), multicomponent (9-C) seismic data were used to monitor the thin sandstone and provides an improved understanding of the subtle structural and stratigraphic framework of the reservoir. Interpretation of the multicomponent seismic data volumes demonstrate that it is possible to detect and monitor injected CO_2 in this reservoir interval and reveals that the CO_2 migrates structurally up dip from the injection well.

Introduction

West Pearl Queen Field is located in the Permian Basin west of Hobbs, New Mexico, USA (Figure 1). The field has been selected as the site of a field test for geologic sequestration of CO_2. The field is currently on the economic limit of primary production, is pressure depleted, and the operator has no plans for an Enhance Oil Recover (EOR) project. Production from this reservoir is a recent development, with the wells and infrastructure of the reservoir being in good repair. These factors allow the research project access to the field with little interference to the current operations of the field, and allows the field to be a controlled environment with few changes to the reservoir except the CO_2 injection and storage that is being studied.

The reservoir is the Shattuck Sandstone member of the Permian Queen Formation (Figure 2). The reservoir, at an approximate depth of 1370 m (4500 ft), consists of irregularly bedded sandstones and siltstones containing irregular anhydrite beds and nodules. The net reservoir interval is 7 m (23 ft), with a gross thickness of approximately 12 m (40 ft). The productive interval has a porosity of 18% and a permeability of 5-30 md. The reservoir is interpreted as a structural dome with the CO_2 injection well, the Strata Stivason Federal #4, located on the apex of the structure (Figure1).

Methodology

To assist in monitoring the CO_2 in the reservoir, a time-lapse (4-D), multicomponent (9-C) seismic monitoring project was implemented. Its purpose is to demonstrate the ability of repeated (time-lapse) 3-D, 9-C seismology to detect and monitor changes in rock/fluid properties associated with the CO_2 injection and "soak" process. The initial 3-D, 9-C seismic survey was collected from December 3 - 16, 2002. The injection of CO_2 began on December 18, 2002, and lasted until February 11, 2003. Approximately 2090 tons of CO_2 were injected into the reservoir during this period. The CO_2 remained in the reservoir until after a monitor 3-D, 9-C seismic survey was acquired in August 2003.

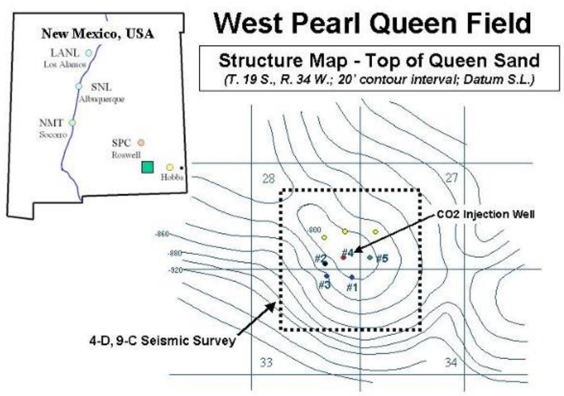

Figure 1. Location map of the West Pearl Queen field and depth structure map on the top of the Queen sandstone.

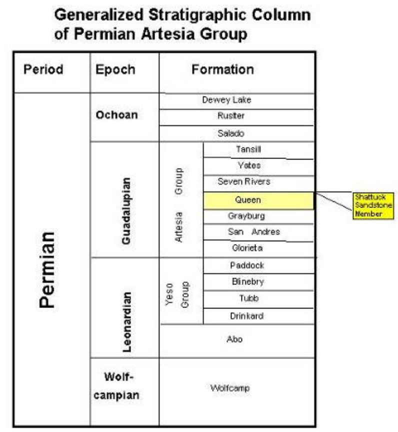

Figure 2. Generalized Stratigraphic Column of the Permian Artesia Group.

Time-lapse effects are subtle, so baseline and monitor surveys are designed to maximize the signal-to-noise ratio of the data and its repeatability. The surveys have uniform azimuth, offset distribution, and provide high-resolution coverage over the center of the West Pearl Queen field. In processing, linear processes are used that are surface consistent, thereby preserving the integrity of the signal between the baseline and monitor surveys. P-wave, S-wave, and Converted-wave data were processed through final migrated volumes with the baseline and monitor surveys being cross-equalized to minimize differences in acquisition and random noise levels.

Static Reservoir Characterization

Initial interpretation of the reservoir utilizes the baseline P-wave seismic data. The Queen Formation sandstone reservoir is contained within a single seismic wavelet trough between 740 and 758 ms. The Queen Formation time structure map (Figure 3) does not correspond to true structural depth. A depth structure map (Figure 4) has been generated from the time structure map constrained by the existing well control and velocity information available within the field area. This depth structure map shows much greater reservoir detail than the original depth map generated from the well control alone (Figure 1), and delineates a structural high east of the original interpreted structural high.

High P-wave seismic amplitudes extracted from the reservoir interval correspond to greater net sand thickness and better reservoir quality (Figure 5). The thickest net sand interval is interpreted to be located to the east of the CO_2 injection well and corresponds with the structural high delineated by the depth structure map. S-wave amplitude maps also confirm the location of the higher net sand interval (Figure 6).

Dynamic Reservoir Characterization

Baseline and monitor seismic surveys are cross-equalized based on a "static" interval above the reservoir where there has been no know production processes occurring. P-wave seismic data matching results are shown in Figure 7, for an east-west seismic line extracted through the CO_2 injection well. The top panel of the figure is the baseline survey, the middle panel is the unmatched monitor survey, and the bottom panel is the matched monitor survey. The matching process is critical due to the extremely subtle reservoir changes caused by the CO_2 injection process. Figure 8 is a difference map of the reservoir interval RMS amplitudes extracted form the baseline and matched monitor surveys, showing a clear time-lapse anomaly in predominantly east to the CO_2 injection.

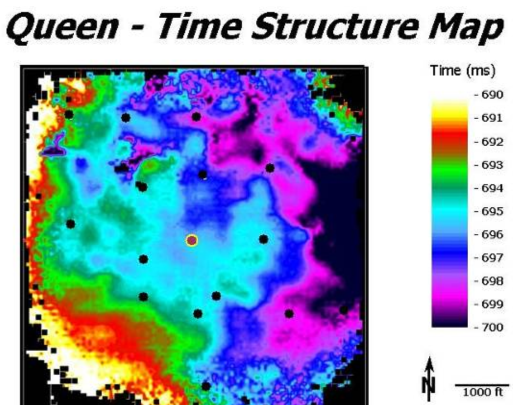

Figure 3. Top of Queen – Time Structure Map.

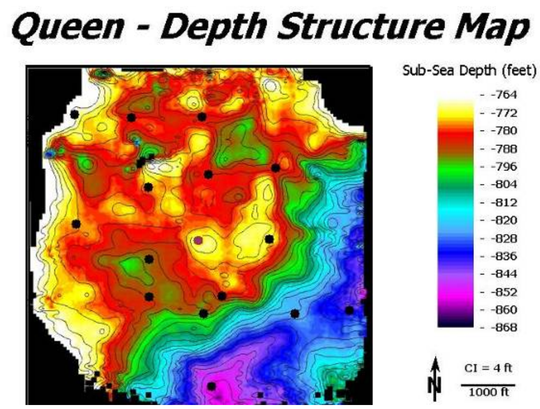

Figure 4. Top of Queen – Depth Structure Map

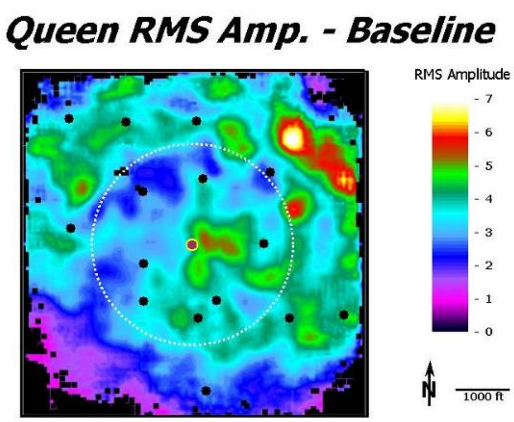

Figure 5. P-wave RMS amplitude map generated around the reservoir interval – Baseline survey.

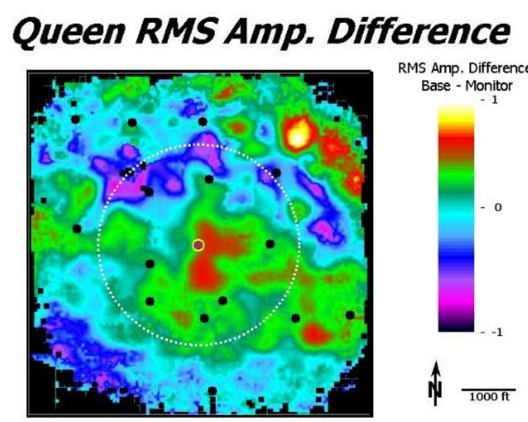

Figure 6. S-wave RMS amplitude map extracted from the reservoir interval.

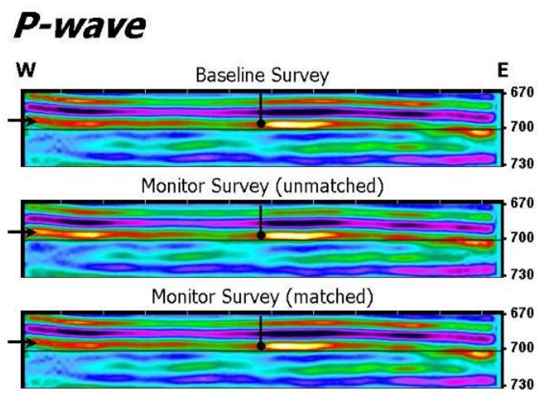

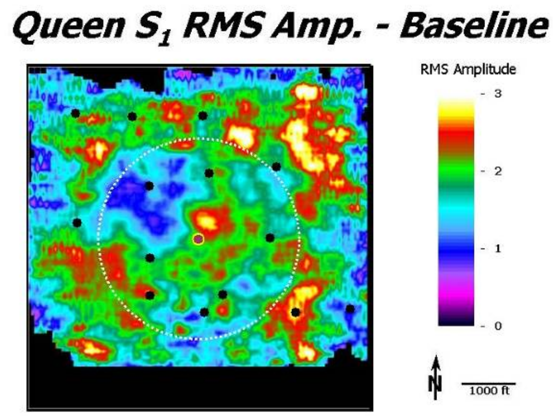

Figure 7.P-wave seismic line across the CO_2 injection well showing the baseline survey, unmatched monitor survey and the match monitor survey

Figure 8. P-wave, time-lapse RMS amplitude difference map.

Conclusions

This research project conducted a time-lapse, multicomponent (9-C), 3-D seismic study of geologic sequestration of CO_2 in an economically depleted oil reservoir. The detailed seismic information provides and an improved structural image of the reservoir and moves the crest of the anticline east of the original interpreted location. Seismic attributes delineate the higher net sand locations within the reservoir, with one of the thickest net sand zones coincident with the structural high east of the CO_2 injection well. After detailed processing of the 3-D multicomponent data, the application of cross-equalization achieves a high quality amplitude difference image of the reservoir interval. It is interpreted that the injected CO_2 migrated east, and structurally up dip, from the injection well, while being contained in higher net sand area of the reservoir (Figure 9).

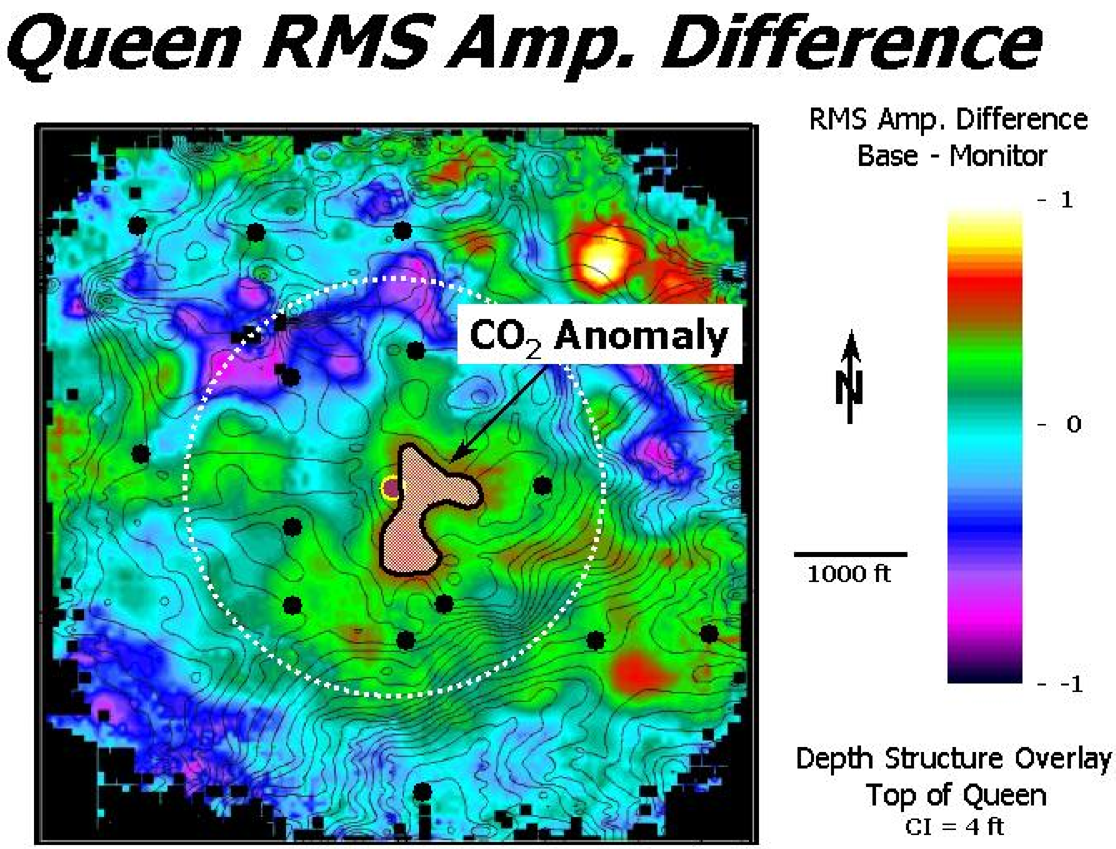

Acknowledgements

The authors gratefully acknowledge Colorado School of Mines, Sandia National Laboratories, Los Alamos National Laboratories, New Mexico Tech, Strata Production Company, Kinder Morgan, and the U.S. Department of Energy's National Energy Technology Laboratory (NETL) for their collaboration and support of this research. The authors would also like to thank Landmark Graphics Corporation and Hampson-Russell Software Services for the use of their software.

APPENDIX C

Westrich, H.R., J. Lorenz, S. Cooper, C. Jove Colon, N. Warpinski, D. Zhang, C. Bradley, P. Lichtner, R. Pawar, B. Stubbs, R. Grigg, R. Svec, C. Byrer, Sequestration of CO_2 in a Depleted Oil Reservoir: An Overview, *J. of Energy and Environmental Research*, v. 2, No. 1, p. 64-74, 2002.

Sequestration of CO_2 in a Depleted Oil Reservoir: An Overview

H. Westrich (hrwestr@sandia.gov; 505-844-9092)
J. Lorenz (jcloren@sandia.gov; 505-3695)
S. Cooper (spcoope@sandia.gov; 505-844-3977)
C. Jove Colon (cfjovec@sandia.gov; 505-284-5494)
N. Warpinski (nwarpi@sandia.gov; 505-844-3640)
Geoscience and Environment Center
Sandia National Laboratories
Albuquerque, NM 87185-0750

D. Zhang (dongzhang@lanl.gov; 505-667-3541)
C. Bradley (cbradley@lanl.gov; 505-665-6713)
P. Lichtner (lichtner@lanl.gov; 505-667-3420)
R. Pawar (rajesh@lanl.gov; 505-665-6929)
Earth & Environmental Sciences Division
Los Alamos National Laboratory
Los Alamos, NM 87545

Bruce Stubbs (pecos@lookingglass.net; 505-624-2800)
Pecos Petroleum Engineering, Inc.
Roswell, NM 88202

R. Grigg (reid@baervan.nmt.edu; 505-835-5403)
R. Svec (bsvec@prrc.nmt.edu; 505-835-6142)
Petroleum Recovery Research Center
New Mexico Tech University
Socorro, NM 87801

C. Byrer (cbyrer@netl.doe.gov; 304-285-4547)
Fuel Resources Division
National Energy Technology Lab
Morgantown, WV 26507-0880

Abstract

Geologic sequestration of CO_2 in depleted oil reservoirs, while a complex issue, is thought to be a safe and effective carbon management strategy. This paper provides an overview of a NETL-sponsored R&D project to predict and monitor the migration and ultimate fate of CO_2 after being injected into a depleted oil reservoir as part of a micropilot scale field experiment. The Queen Formation sandstone, located in the West Pearl Queen field in SE NM, was identified as the CO_2 injection site for this project. Core samples of this formation were obtained for lithologic analysis and laboratory experimentation. Preliminary flow simulations were run using this data and suggest that at least 2000 tons of CO_2 can be injected into the reservoir over a period of one month. Our planned suite of computer simulations, laboratory tests, field measurements and monitoring efforts will be used to calibrate, modify and validate the modeling and simulation tools. Ultimately, the models and data will be used to predict storage capacity and physical and chemical changes in oil reservoir properties. Science or technology gaps related to engineering aspects of geologic sequestration of CO_2 also will be identified in this study.

Introduction

Carbon dioxide sequestration in geologic formations is the most direct carbon management strategy for long-term removal of CO_2 from the atmosphere, and is likely to be needed for continuation of the US fossil fuel-based economy and high standard of living. Subsurface injection of CO_2 into depleted oil reservoirs is a carbon sequestration strategy that might prove to be both cost effective and environmentally safe. Part of this confidence is due to an extensive knowledge base about site-specific reservoir properties and subsurface gas-fluid-rock processes from the mining and petroleum industries, including those from recent EOR CO_2 flooding activities (Morris, 1996). However, CO_2 sequestration in oil reservoirs is a complex issue spanning a wide range of scientific, technological, economic, safety, and regulatory concerns, requiring more focused R&D efforts to better understand its cost and consequences (DOE Offices of Science and Fossil Energy report, 1999).

Objective

Our project, "Sequestration of CO_2 in a Depleted Oil Reservoir: A Comprehensive Modeling & Site Monitoring Project," is funded by the DOE/NETL Carbon Sequestration program. One of the program's stated goals is to provide the science and technology basis to properly evaluate the safety and efficacy of long-term CO_2 sequestration in geologic formations. The specific objective of our project is to better understand CO_2 sequestration processes in a depleted oil reservoir. Because of the nature of an oil reservoir and the presence of multiple phases, CO_2 sequestration mechanisms can include hydrodynamic trapping, aqueous solubility or mineralization. Viscous fingering, gravity separation, miscible fluids, reaction kinetics, and possible leakage through fractures are but a few of the processes that also can affect geologic sequestration effectiveness. Broad project goals include computer simulations and laboratory measurements of fluid flow and reaction, as well as a field experiment in order to better understand the complex nature of geosequestration processes. The micropilot field experiment calls for injection of several thousand tons of CO_2 into a depleted oil reservoir. An ideal site for this project would be located in a geologically simple setting in porous and permeable sandstone, having a recent development and production history, and where no secondary water or enhanced CO_2 treatments have been used. These site parameters allow for simplified modeling and easier interpretations of field results. Specific R&D objectives for this project include:

This project utilizes a suite of computer simulations, laboratory tests, field measurements and monitoring efforts to understand those physical and chemical processes governing geologic sequestration of CO_2 in oil reservoirs. The micropilot demonstration calls for injection of several thousand tons of CO_2 into the Queen Formation, followed by a comprehensive suite of geophysical field surveys to monitor the advance of the CO_2 plume and lab experiments to measure geochemical changes in reservoir mineralogy and permeability. Specific field and lab observations will be used to calibrate, modify and validate the modeling and simulation tools. The field demonstration, however, will be the ultimate test of our computer simulations.

Project Description

This field demonstration project has three phases: I) baseline characterization, II) CO_2 injection and soaking, and III) post-injection characterization. Phase I includes compilation of a geologic model for the depleted reservoir, evaluation of available flow and reaction simulators, well preparation, acquisition of legal permits, collection of reservoir fluids, and baseline geophysical surveys of the reservoir. Phase II of this project involves the design of the micropilot field test, preparation of surface injection facilities, refinement of computer simulation models, injection of 2000-4000 tons of CO_2 over a one month period, measurement of fluid pressure changes or plume breakthroughs and geophysical surveys of the plume. Phase III of the project includes wellhead venting of the injected CO_2, and downhole pumping of residual fluids and final geophysical surveys. Our project combines geologic, flow and reaction path modeling and simulations, injection of CO_2 into the oil-producing formation, geophysical monitoring of the advancing CO_2 plume and laboratory experiments to measure reservoir changes with CO_2 flooding. The field data will provide a unique opportunity to test, refine and calibrate the computer model(s) that will simulate those subsurface interactions. Iteration of modeling, laboratory and field data is crucial to the improvement of simulation tool methodologies.

<u>Modeling and Simulation</u>

Our ability to accurately predict the migration and fate of CO_2 in oil reservoirs is limited by inadequate reservoir characterization as well as the lack of a comprehensive simulator to model coupled chemical, hydrological, mechanical and thermal (CHMT) processes. However, existing commercial and research codes, such as ECLIPSE and FLOTRAN, are available and will be used to simulate some of the important geoprocesses involved during CO_2 sequestration (e.g., three-phase flow and geochemical reactions). The goal of this task is to choose one or more codes that have the ability to simulate the coupled processes that occur during injection and migration of CO_2 in the depleted oil reservoir. These codes will be evaluated based on availability, cost, ease of use, robustness and flexibility to modification. With the selected code(s) and input data from a geologic model, a computer model will be built for a depleted oil reservoir, which will incorporate site-specific information and previous characterization results. This model will be used to aid in designing a micropilot field study of high-flow CO_2 injected in the depleted oil reservoir. The geologic model will integrate available data on stratigraphy and reservoir rock properties, including wireline logs, structure-contour and isopach maps, core samples from the Stivason-Federal well #1, and appropriate regional geologic data.

Geophysical Monitoring

State of the art geophysical techniques are one of the few ways to remotely characterize oil reservoir properties and changes due to injection of CO_2. Remote geophysical sensing techniques will be used prior to, during and after CO_2 injection, consisting of borehole geophysics, surface to borehole surveys, and surface reflection seismic surveys. These surveys will identify and characterize formation changes due to saturation and injection effects (Knight et. al., 1998; Withers and Batzle, 1997). The borehole geophysics will include dipole sonic logs, limited microseismic surveys during injection and multi-level, 3C crosswell seismic surveys. The surface to borehole seismic surveys will include a Vertical Seismic Profile (VSP) in which receivers are placed in the injection wellbore to detect arrivals from surface shots (e.g., Lizarralde and Swift, 1999). The 4D, 9C seismic surveys will be run before and after injection, as well as a third survey conducted after flow-back of the injected CO_2.

Field Demonstration

Our micropilot demonstration calls for injection of several thousand tons of CO_2 into the Queen Formation at a depth of about 4500 feet using the Stivason-Federal well #4 as the injection well. This reservoir is geologically simple and consists of a small structural dome of thinly bedded sandstones. Although the reservoir is pressure depleted (<3.0 MPa), it has not been subjected to secondary oil recovery treatment with water or CO_2, and is therefore an ideal site to study the effects of CO_2 injection in a depleted oil reservoir. Strata Production Company will coordinate all field preparations, surveys and injection operations.

Laboratory Tests

Mineralization is the geochemical interaction of CO_2 with sedimentary minerals to form stable and environmentally benign carbonate phases, and is a desired sequestration end stage. However, the nature and kinetics of CO_2-dominated fluid/mineral interactions is not well understood. This knowledge is essential for the prediction of carbonation reactions and the formation of carbonate minerals that will be responsible for the long-term confinement of CO_2 into the reservoir. Our project will examine static and non-static flow experiments of pure CO_2 and CO_2-H_2O mixtures interacting with plugs of Queen Formation sandstone for time periods up to 15 months at reservoir conditions (P=4.5 MPa, T=40°C). Static tests will explore the effects of fluid chemistry and flow on mineral dissolution and precipitation reactions. Non-static flow (percolation) tests will elucidate the effects of fluid-mineral interaction on rock porosity and permeability. Solid and liquid samples from these tests will be analyzed for chemical, structural and morphological changes using standard geochemical techniques. These results should provide critical information on the mechanisms and rates of CO_2-mineral interactions in a depleted oil reservoir.

Results

Geology

Approximately 30 ft of discontinuous, four-inch diameter core of the Queen Formation (Shattuck Sandstone Member) from the Stivason Federal #1 well was available for study and to develop a geologic model. This well is approximately 1200' from our injection well and its core should be representative of the reservoir. No natural fractures are present in this core, although it is not precluded for the rest of the reservoir. In general, the Shattuck Sandstone consists of irregularly bedded sandstones, siltstones, and sandy siltstones, containing irregular anhydrite beds and nodules. The sandstones are a heterogeneous mix of oxidized detrital sands and siltstones, with detrital and authigenic cements of dolomite, gypsum, anhydrite, and halite. The main reservoir lithology (lithology C in Figure 2) is a poorly cemented, oil stained sandstone exhibiting between 15-20% porosity and irregular permeabilities up to 200 millidarcies (Figure 2). The percentage of the reservoir represented by this lithology is unknown due to missing core, although about a third of the core available consists of this facies. The upper parts of the core represent the confining strata rather than the reservoir rock. The likely reservoir sandstone represents about

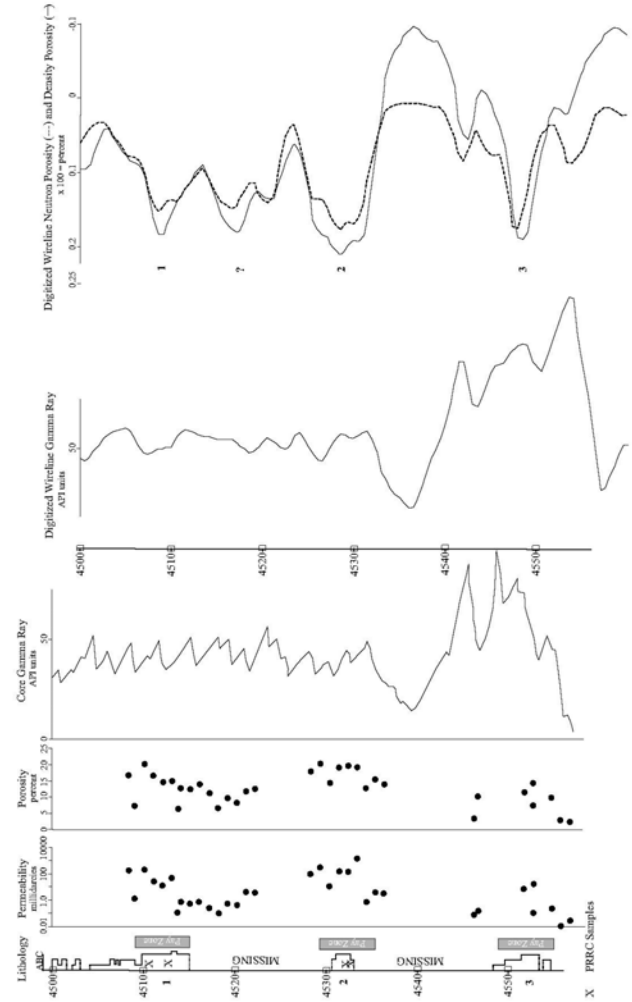

Figure 2. Chart showing the lithologic and geophysical properties of the Stivason Federal well #1 core with depth, and correlated to permeability, porosity and gamma ray logs; shaded intervals are oil stained and are likely sequestration zones.

80% of the core available from the designated main reservoir intervals. Oil staining suggests high porosities and that they will be the primary hosts for injected CO_2 as long as local hydrofracture pressure is not exceeded during injection. The variability in oil staining and measured permeability shown by this lithology suggests that some of the residual oil may be difficult to displace during CO_2 injection.

Non-reservoir strata contain more pore-lining illite and chlorite, as well as illite/smectite and anhydrite cements (Mazzullo, et al., 1991). Mineralogic changes caused by CO_2 injection into these heterogeneous strata would probably occur in the cementing mineral phases, most likely in the carbonates and sulfates. The heterogeneity of the cements suggests that a thorough base-line characterization prior to injection would be necessary in order to fully understand and document any changes caused by injection.

Flow Modeling

Porous media flow simulations were used to match the historic production data. Values of a number of unknown reservoir rock and fluid properties had to be determined by trial and error due to lack of appropriate data. The reservoir model was subsequently used to determine feasibility of injecting CO_2 over a period of one month. A number of injection scenarios were tested to determine the response of the reservoir over a wide range of operating conditions and regulatory operational constraints. The preliminary injection studies indicate that the injected CO_2 plume can be dispersed in the Shattuck Formation sandstones to such an extent that it can be characterized through a variety of proposed monitoring techniques. More details of the geologic and flow modeling can be found in Pawar, et al. (2001).

Pearl Queen Brine Chemistry

Brine samples taken from wells Stivason Federal #4 and Stivason Federal #5 (see Figure 1) were analyzed for cations and anions using Direct Current Plasma (DCP) spectroscopy and ion chromatography (IC); pH was measured using a pH electrode. The chemical analyses (Table 1) show that these oil-field brines are mainly composed of Na and Cl with an ionic strength of ~2.4 Molar. There is a charge imbalance of about 0.3 Molar (due to an excess of negative charges), and the Al concentrations in the brines are suspiciously high, perhaps due to the presence of colloids. Additional chemical analyses should resolve these concerns, and will allow for subsequent calculation of equilibrium mineral phases. We suspect that the Pearl Queen brine is close to equilibrium with gibbsite, kaolinite, dolomite, calcite and quartz. Total carbon analyses are scheduled soon. Preliminary reaction path modeling of CO_2 mixing with the brine shows an initial sharp decrease in pH as expected. Preliminary modeling of low pH fluid interactions with the estimated major modal mineralogy of the Shattuck Member sandstone (75% quartz, 10%-15% K-feldspar, and 5%-10% dolomite cement), and for several modal fractions of initial dolomite, shows the resulting fluid pH ranges from 4-5 after reaction with these minerals. This preliminary result is an indication of the potential buffering capacity of the reservoir when the low pH CO_2-brine reacts with the Queen Formation during injection. Further modeling trials are needed when considering different CO_2 fugacities and initial mineral fractions.

Table 1. Chemical analyses of brines from Stivason Federal wells # 4 and #5[1]

Well #	pH	Al[2]	Si	Na	K	Mg	Ca	Cl	Br	SO_4
#5	6.786	0.000414	0.00014533	2.085	0.00268	0.123	0.056	2.99	0.0041	0.0208
#5	6.852	0.000410	0.00013823	2.044	0.00307	0.122	0.056	3.12	0.0040	0.0220
#4	7.181	-	-	1.797	0.00264	0.110	0.049	-	-	-

[1] Analyses performed at the NMBMMR, Socorro, NM on same samples yielded similar results.

[2] Elemental compositions reported as molarity (moles/L)

Geophysical Monitoring

Negotiations are underway to schedule pre-injection geophysical surveys, including dipole sonic logs, a deviation survey and a 3 component crosswell survey. We are planning to have the 3C Vertical Seismic Profile survey and the 3D, 9C surface seismic surveys completed by the end of FY01, immediately prior to CO_2 injection.

Application

Ultimately, the models and data resulting from this CO_2 sequestration project will be used to predict geologic storage capacity and physical and chemical changes in reservoir properties, such as fluid composition, porosity, permeability and phase relations. Development of accurate monitoring tools will also permit validation of the computer simulations that will be needed for future performance and risk assessments. Science or technology gaps related to engineering aspects of CO_2 sequestration will be identified in the course of this study. In addition, a better understanding of CO_2-reservoir interactions resulting from this project should improve industrial EOR flooding practices.

Future Activities

Current geologic and preliminary flow simulation results indicate the feasibility of CO_2 injection in a depleted oil reservoir. These results also provide guidelines for upcoming geophysical monitoring (e.g., spacing of seismic sources and receivers). Geochemical lab experiments with Shattuck Member sandstones have been initiated to evaluate mineralization reaction kinetics. Preparation for CO_2 injection and acquisition of geophysical surveys has begun and should be completed by the end of FY01. CO_2 injection is scheduled for the beginning of FY02. Final characterization and modeling efforts will be completed in FY03. Upon completion of this project, the West Pearl Queen reservoir will be one of the most completely characterized oil reservoirs, setting the stage for follow-on DOE/NETL CO_2 sequestration experiments. This field site could be used for field demonstration experiments of greater scope and duration, including injection of larger volumes of CO_2, soaking of CO_2 for a duration significantly longer than a month, drilling of additional observation wells or sampling of the reservoir for actual core analysis.

Acknowledgements

The authors wish to acknowledge the financial support from the Department of Energy's National Energy Technology Laboratory, as well as the overall support of Mark Murphy from Strata Production Company.

References

Department of Energy, Carbon Sequestration: Research and Development, Officesof Science and Office of Fossil Energy report, December 1999.

Knight, R., Dvorkin, J. and Nur, A., Acoustic Signatures of Partial Saturation, Geophysics, 63(1), 132-138, 1998.

Lizarralde, D. and Swift, S., Smooth Inversion of VSP Traveltime Data, Geophysics, 64(3), 659-661, 1999.

Mazzullo, J., Malicse, A., and Siegel, J., 1991, Facies and depositional environments of the Shattuck Sandstone on the Northwest Shelf of the Permian Basin: Journal of Sedimentary Petrology, vol. 61, p. 940-958.

Morris, G., More CO_2 floods start up in West Texas. Oil & Gas Journal, 87-88, 1996.

Pawar, R., Zhang, D., Stubbs, B., and Westrich, H., Preliminary Geologic Modeling and Flow Simulation Study of CO_2 Sequestration in a Depleted Oil Reservoir,, NETL Carbon Sequestration Conference Proceedings, May 15-17, 2001.

Withers, R.J. and Batzle, Modeling Velocity Changes Associated with a Miscible Flood in the Prudhoe Bay Field, Geophysics, 62(5), 1442-1455, 1997.

Distribution

25	MS 0750	Gregory J. Elbring	06314
10	MS 0750	Scott P. Cooper	06314
1	MS0899	Technical Library	9536 (electronic copy)

Sandia National Laboratories